UNIVERSIDAD DE CHILE
FACULTAD DE CIENCIAS FÍSICAS Y MATEMÁTICAS
DEPARTAMENTO DE INGENIERÍA DE MINAS

GEOSTATISTICAL MODELING OF GEOTECHNICAL VARIABLES CONSIDERING DIRECTIONAL DEPENDENCE

TESIS PARA OPTAR AL GRADO DE DOCTOR EN INGENIERÍA DE MINAS
EN COTUTELA CON LA UNIVERSITE PARIS SCIENCES & LETTRES (MINES PARISTECH)

LIZETH KATHERINE SANCHEZ CABALLERO

PROFESOR GUÍA:
DR. XAVIER EMERY

PROFESOR CO-GUÍA:
DR. JACQUES RIVOIRARD

MIEMBROS DE LA COMISIÓN:

DR. DENIS MARCOTTE
DR ROBERTO BRUNO
DRA. CHANTAL DE FOUQUET
DR. JOSÉ MUNIZAGA ROSAS

SANTIAGO DE CHILE

2022

RESUMEN: MODELAMIENTO GEOSTADÍSTICO DE VARIABALES GEOTÉCNICAS CONSIDERANDO LA DEPENDENCIA DIRECIONAL

Junto con el modelamiento geológico y geometalúrgico, el modelamiento geotécnico es uno de los componentes esenciales para la planificación y desarrollo de proyectos mineros a rajo abierto y subterráneos. Una característica particular de muchas variables geotécnicas es su dependencia direccional, es decir, la medición de una muestra de sondaje depende no solo de su posición geográfica sino también de su orientación. La práctica común en el modelamiento geotécnico no considera esta característica y extrapola o promedia la información del soporte de muestra (sondaje o línea de exploración) a soportes de bloques tridimensionales o a todo el macizo rocoso, asumiendo que este macizo rocoso es un medio continuo e isótropo. Para considerar la dependencia direccional, se propone regionalizar las variables geotécnicas en un espacio de cinco dimensiones correspondiente al producto del espacio geográfico tridimensional y la esfera bidimensional, de modo que cada medición se indexe por su este, norte, elevación, azimut e inclinación. En lugar de hacer predicciones y simulaciones condicionadas a una dirección particular, este nuevo paradigma permite interpolar variables geotécnicas en cualquier lugar del espacio geográfico, para cualquier dirección. La estructura de correlación espacial se puede inferir y modelar utilizando covarianzas separables o combinaciones de covarianzas separables, bajo un supuesto de estacionaridad en el espacio geográfico e isotropía en la esfera. Además, la simulación condicional se puede realizar mediante métodos espectrales o de bandas rotantes, basados en productos de campos aleatorios estacionarios básicos en el espacio geográfico y campos aleatorios isotrópicos en la esfera.

La metodología propuesta se ilustra con tres casos de estudio. El primero presenta las bases teóricas para el modelado 5D de correlaciones espaciales, propone un algoritmo novedoso para la simulación condicional e ilustra los conceptos anteriores con una aplicación al modelamiento de la frecuencia de discontinuidad lineal (P10) en una base de datos del depósito de cobre El Teniente (Chile). La comparación entre los resultados de la simulación en ausencia o presencia de componente direccional permite visualizar la variabilidad espacial esperada en terreno para una dirección dada. Se puede ser consciente de las variaciones de las variables geotécnicas no solo en el espacio geográfico sino también en el espacio direccional. El segundo caso de estudio se centra en el problema del escalamiento o cambio de soporte, es decir, la extensión de una muestra a un bloque más voluminoso, para la Designación de Calidad de la Roca (RQD). Se propone una estrategia de escalamiento basada en el promedio de los valores RQD correspondientes a la misma dirección que evita mezclar valores RQD medidos en diferentes direcciones o restringir el estudio a una sola dirección. Además de la definición de un RQD de bloque dependiente de la dirección, proponemos derivar un RQD no direccional (mínimo), que cuantifica el grado de fractura en un bloque, y un índice de anisotropía (AI) del grado de fracturamiento para macizos rocosos, indicando cuánto varía el RQD entre una dirección y otra. El tercer caso de estudio extiende las metodologías anteriores al escenario multivariante, con la definición de modelos de covarianza directas y cruzadas en el espacio 3D cruzado con la esfera 2D, mediante el análisis de una base de datos del yacimiento cuprífero Radomiro Tomic (norte de Chile) para estimar la calidad del macizo rocoso. En concreto, el Slope Mass Rating (SMR) se obtiene a partir del Rock Mass Rating (RMR) básico añadiendo un ajuste factorial en función del talud del rajo y la máxima orientación local de fracturamiento que aflora en el talud. El modelado geoestadístico conduce a un criterio de aceptación de constructibilidad de taludes para el diseño de minas a rajo abierto.

Los resultados de la tesis destacan las ventajas de considerar el espacio direccional al modelar variables geotécnicas y sustentan el impacto beneficioso de este enfoque en la zonificación geotécnica, el conocimiento del comportamiento espacial de los macizos rocosos y el manejo de incertidumbres en proyectos de minería a rajo abierto o subterránea. Complementariamente a las herramientas estándar utilizadas para la representación tridimensional de variables regionalizadas, también propone nuevas herramientas de visualización que pueden ser de interés para geólogos estructurales y geotécnicos, tales como proyecciones azimutales regionalizadas que mapean las variaciones direccionales de las propiedades del macizo rocoso en ubicaciones determinadas en el espacio geográfico.

ABSTRACT

Together with geological and geometallurgical modeling, geotechnical modeling is one of the essential components for the planning and development of open pit and underground mining projects. A particular characteristic of many geotechnical variables is to be direction-dependent, i.e., the measurement of a core sample depends not only on its geographical position but also on its orientation. The common practice in geotechnical modeling overlooks this characteristic and extrapolates or averages sample-support information (from boreholes or scanlines) to three-dimensional block supports or to the entire rock mass by assuming that this rock mass is a continuum and isotropic medium. To account for direction-dependence, it is proposed to regionalize geotechnical variables in a five-dimensional space corresponding to the product of the three-dimensional geographical space and the two-dimensional sphere, so that each measurement is indexed by its easting, northing, elevation, azimuth, and dip. Instead of making predictions and simulations conditioned to a particular direction, this new paradigm allows geotechnical variables to be interpolated at any place in the geographical space, for any direction. The spatial correlation structure can be inferred and modeled by using separable covariances or combinations of separable covariances, under an assumption of stationarity in the geographical space and isotropy on the sphere. Also, conditional simulation can be performed by turning bands or spectral methods, based on products of basic stationary random fields in the geographical space and isotropic random fields on the sphere.

The proposed methodology is illustrated with three case studies. The first one presents the theoretical basis for the 5D modeling of spatial correlations, proposes a novel algorithm for conditional simulation, and illustrates the previous concepts with an application to the modeling of the linear discontinuity frequency (P10) in a dataset from El Teniente copper deposit in Chile. The comparison between the simulation results in the absence or the presence of a directional component allows visualizing the spatial variability to be expected in the field for a given direction. One can be aware of the variations of geotechnical variables not only in the geographical space but also in the directional space. The second case study focuses on the problem of upscaling or change of support, i.e., the extension from a sample to a more voluminous block, for the Rock Quality Designation (RQD). An upscaling strategy to large blocks is proposed, based on block-averaging the RQD values corresponding to the same direction that avoids mixing RQD values measured along different directions or restricting the study to a single direction. In addition to the definition of an upscaled direction-dependent RQD, we propose to derive a non-directional (minimum) RQD, which quantifies the degree of fracturing in a block, and an anisotropy index (AI) of jointing degree for rock masses, indicating how much RQD is likely to vary between one direction and another. The third case study extends the previous methodologies to the multivariate setting, with the definition of direct and cross covariance models in the 3D space crossed with the 2D sphere, through the analysis of a dataset from the Radomiro Tomic copper deposit (northern Chile) to estimate the rock mass quality. Specifically, the Slope Mass Rating (SMR) is obtained from the basic Rock Mass Rating (RMR) by adding a factorial adjustment in function of the pit slope and the maximum fracturing local orientation that outcrops at the slope. The geostatistical modeling leads to a slope constructability acceptance criterion for Open Pit Mine design.

The results of the thesis highlight the advantages of considering the directional space when modeling geotechnical variables and hold up the beneficial impact of this approach in the geotechnical zoning, knowledge of spatial behavior of rock masses, and management of uncertainties in open pit and underground mining projects. In complement to the standard tools used for the three-dimensional representation of regionalized variables, it also proposes new visualization tools that can be of interest to structural geologists and geotechnicians, such as regionalized azimuthal projections that map the directional variations of the rock mass properties at given locations in the geographical space.

RÉSUMÉ

Avec la modélisation géologique et géométallurgique, la modélisation géotechnique est l'une des composantes essentielles de la planification et du développement de projets miniers à ciel ouvert et souterrains. Une caractéristique particulière de nombreuses variables géotechniques est d'être dépendante de la direction, c'est-à-dire que la mesure d'une carotte de sondage dépend non seulement de sa position géographique mais aussi de son orientation. La pratique courante de la modélisation géotechnique néglige cette caractéristique et extrapole ou fait la moyenne des informations au support d'échantillon (provenant de sondages ou de lignes de mesure) à des supports de blocs tridimensionnels ou à l'ensemble de la masse rocheuse en supposant que cette masse rocheuse est un milieu continu et isotrope.

Pour tenir compte de la dépendance directionnelle, il est proposé de régionaliser les variables géotechniques dans un espace à cinq dimensions correspondant au produit de l'espace géographique à trois dimensions et de la sphère à deux dimensions, de sorte que chaque mesure soit indexée par ses coordonnées est, nord, élévation, azimut et pendage. Au lieu de faire des prédictions et des simulations conditionnées à une direction particulière, ce nouveau paradigme permet d'interpoler des variables géotechniques à n'importe quel endroit de l'espace géographique, et pour n'importe quelle direction. La structure de corrélation spatiale peut être inférée et modélisée en utilisant des covariances séparables ou des combinaisons de covariances séparables, sous une hypothèse de stationnarité dans l'espace géographique et d'isotropie sur la sphère. De plus, une simulation conditionnelle peut être effectuée par des méthodes spectrales ou de bandes tournantes, basées sur des produits de champs aléatoires stationnaires dans l'espace géographique et de champs aléatoires isotropes sur la sphère.

La méthodologie proposée est illustrée par trois études de cas. Le premier présente les bases théoriques de la modélisation 5D des corrélations spatiales, propose un nouvel algorithme de simulation conditionnelle et illustre les concepts précédents avec une application à la modélisation de la fréquence de discontinuité linéaire (P10) sur un jeu de données du gisement de cuivre d'El Teniente au centre du Chili. La comparaison entre les résultats de la simulation en l'absence ou en présence d'une composante directionnelle permet de visualiser la variabilité spatiale à attendre sur le terrain pour une direction donnée, minimisant le risque de biais pouvant apparaître lors de l'extrapolation des informations d'échantillonnage d'une direction à une autre. On peut être conscient des variations des variables géotechniques non seulement dans l'espace géographique mais aussi dans l'espace directionnel. Ce dernier est en outre utile pour définir quantitativement les conditions favorables à l'avancement de l’excavation d'un point de vue non qualitatif, comme cela se fait actuellement dans la classification RMRM de Bieniaswski.

La deuxième étude de cas porte sur le problème de changement d'échelle ou de changement de support, c'est-à-dire l'extension d'un échantillon à un bloc plus volumineux, pour la désignation de la qualité de la roche (RQD). Une stratégie de mise à l'échelle physiquement significative vers de grands blocs est proposée, basée sur la moyenne des valeurs RQD correspondant à la même direction. Cette stratégie évite de mélanger les valeurs de RQD mesurées dans différentes directions ou de restreindre l'étude à une seule direction pour (a) mesurer et (b) régulariser au support de bloc les valeurs de RQD. En plus de la définition d'un RQD de bloc dépendant de la direction, nous proposons de dériver un RQD non directionnel (minimum), qui quantifie le degré de fracturation dans un bloc, et un indice d'anisotropie (AI) du degré de jointure de la masse rocheuse, indiquant de combien RQD est susceptible de varier d'une direction à l'autre. De cette manière, il est possible de connaître la variabilité directionnelle du RQD dans chaque bloc, reflétant l'anisotropie du massif rocheux et donnant un aperçu de la géométrie des fragments formés par l'intersection des joints dans un massif rocheux.

La troisième étude de cas étend les méthodologies précédentes au cadre multivarié, avec la définition de modèles de covariances directes et croisées dans l'espace 3D croisé avec la sphère 2D, à travers l'analyse d'un jeu de données du gisement de cuivre de Radomiro Tomic (nord du Chili) pour estimer la qualité du massif rocheux. Plus précisément,

le Slope Mass Rating (SMR) est obtenu à partir du Rock Mass Rating (RMR) de base en ajoutant un ajustement factoriel en fonction de la pente de la fosse et de l'orientation locale de fracturation maximale qui affleure à la pente. La modélisation géostatistique permet de construire des cartes de qualité géomécanique des pentes et conduit à un critère d'acceptation de la constructibilité des pentes pour la conception de la mine à ciel ouvert.

Les résultats de la thèse mettent en évidence l'intérêt de considérer l'espace directionnel lors de la modélisation des variables géotechniques et soutiennent l'impact bénéfique de cette approche dans la zone géotechnique, la connaissance du comportement spatial des massifs rocheux et la gestion des incertitudes dans les projets miniers à ciel ouvert ou souterrains. En complément des outils standards utilisés pour la représentation tridimensionnelle des variables régionalisées, la thèse propose également de nouveaux outils de visualisation qui peuvent intéresser les géologues structuralistes et les géotechniciens, tels que les projections azimutales régionalisées qui cartographient les variations directionnelles des propriétés du massif rocheux à des endroits donnés de l'espace géographique.

ACKNOWLEDGMENTS

Firstly, I would like to express my sincere gratitude to Xavier Emery, thesis director, and friend, for his support and guidance provided throughout these years, as well as my thesis advisors in France Dr Jacques Rivoirard and Dr Serge Séguret, who gave me the possibility and tools necessary to develop this thesis. I am also grateful to Dr Eleonora Widzyk-Capehart for welcoming me into her project during the beginning of this process.

I would like to acknowledge the funding of the National Agency for Research and Development of Chile (ANID), through grants AFB180004 PIA CONICYT and CONICYT / FONDECYT / REGULAR / N°1170101, and of the CSIRO-Chile International Center of Excellence in Mining and Mineral Processing. Also, I am grateful to ANID for the postgraduate study scholarship CONICYT-PFCHA/Doctorado Nacional/2019-21190855, and to Universidad de Chile, ARMINES and Mines ParisTech for the support in the supervision of my thesis work. I thank the Postgraduate School of the FCFM at Universidad de Chile for the tuition scholarship to pursue my studies. Likewise. I extend my thanks to the International Association of Mathematical Geosciences (IAMG) for the Computers & Geosciences Research Scholarship granted in the first year of the doctoral thesis, and to Codelco for the "Piensa Minería" funding granted in the last year of the doctoral thesis.

I thank my dear colleagues from the AMTC-Csiro Chile project and from the Center of Geosciences at MINES ParisTech, for welcoming me to the group, for helping answer questions and for all the good times shared. It was great to have an opportunity to work in your team.

It is extremely difficult to make the appropriate thanks to the enormous number of people who were involved in this process, making it possible that, at this moment, I am finishing an important stage of my life. This achievement is definitely for Sarai, the engine of my life who drives me to be a better version of myself every day. Without a doubt, the protagonists of this are my family, especially my parents who, throughout these years, have given me their love and unconditional support and have planted in me beautiful teachings that guide my steps day by day. If you walk alone, you will go faster, but if you walk accompanied you will go further.

I cannot fail to mention the friends I met when I arrived in France and those left behind in Chile, who made my stay more enjoyable, thank you for being present during this stage, which became a huge challenge, to those who are and to those who have gone, thank you for listening to me ramble and complain, for your support in difficult times and for making a space in your life for me. I intentionally try to avoid mentioning specific names because I might forget some, but I make a written commitment that once this process is finished, I will personally thank you for your valuable friendship.

TABLE OF CONTENTS

LIST OF FIGURES

LIST OF TABLES

CHAPTER I.

INTRODUCTION

1.1. Spatial characterization of a rock mass

The identification of the mechanical, hydraulic and engineering properties of a rock mass is a crucial task for the development of open pit and underground mining operations, tailings tanks, hydrocarbon and geothermal reservoirs, aquifers and underground nuclear waste disposals (National Research Council, 2006; Bonnet et al., 2001). The management of costs in geotechnical engineering is critical but must be balanced with a detailed and comprehensive characterization of the subsurface, so as to reduce uncertainty and increase workers' safety at the lowest cost possible. To achieve an optimal characterization of the rock mass, it is necessary to know the rock mass quality to adequately design the underground infrastructures or to define the slope geometry in the case of open-pit mining.

Geological phenomena in the subsurface often present spatial heterogeneities, showing a high contrast at a short scale, e.g., transitions between zones of greater or lesser strength and rigidity. Accordingly, it is difficult to predict without any error the mechanical properties of the rock mass by means of deterministic approaches. Then, other methodologies must be considered to model the geotechnical behavior. In this context, the use of probabilistic techniques has increased in recent decades (Fenton, 1997; Christian and Baecher, 2003; Le Goc et al., 2014; Popescu et al., 2005; Sejnoba et al., 2007), aiming to obtain ranges of values and safety factors instead of deterministic values. One of the practical limitations to implement these approaches is that they do not account for the fact that the variables under consideration are regionalized and spatially structured. Spatial variability can mean adverse conditions not detected in the design phase that bring about accidents in the construction phase (Karim et al., 2007).

The complexity of geotechnical and hydrogeological problems requires the use of methods that significantly reduce the uncertainty associated with geological and geotechnical variability to avoid the problems generated by open pit and underground

excavations (Lei, 2016). The deterministic models and probabilistic techniques traditionally implemented in the characterization of the rock mass have in common the limitation in the identification of natural heterogeneities, because they assume that the variables are normally distributed and their values are independent from sample to sample, which is not the case in the earth sciences where regionalized data usually do not satisfy these assumptions (Chilès and Delfiner, 2012). Instead, geostatistics is capable of integrating spatial variability and heterogeneities in the modeling of the rock mass. In this respect, geostatistics offers tools that take into account the spatial behavior of the variables, contrarily to traditional probabilistic techniques, and methods that provide an accurate prediction of these variables, accompanied by uncertainty measures, contrarily to deterministic approaches.

The application of geostatistical methods in geotechnics is a recent topic, so the number of works published in this field is not as voluminous as it might be expected when considering the potential of this technique in the modeling of regionalized phenomena. In the past decades, several authors have been using geostatistics to predict or to simulate lithological properties, such as the works developed by Rosenbaum et al. (1997), Mao and Journel (1999), Emery et al. (2008). Regarding the classification of rock mass using empirical methods and some geotechnical parameters, the number of published works increases, and it is essential to highlight the following:

- Rock Quality Designation (RQD): this is a measure of the degree of jointing or fracturing of a rock mass, consisting of 100 times the ratio between the total length of core pieces larger than 100 millimeters and the total core run length (Deere et al., 1966). Ozturk and Nasuf (2002) applied cokriging to predict RQD using correlated covariates. In a more recent work by Ozturk and Simdi (2014), kriging techniques are also used to predict the intact rock and rock mass elastic modulus. Madani and Asghari (2013) simulated RQD values to detect failures in 3D blocks (RQD <20 interpreted as fault zones). Séguret and Guajardo (2015) argued that RQD, as well as the fracture frequency (FF), are actually direction-dependent variables and proposed to predict them by accounting for sampling direction classes. Séguret and Emery (2019) suggested that a solution to direction

dependence is to consider the regionalization space as a 5D space, three for the usual coordinates and two for the space crossed by the dip and the azimuth, which is a key idea developed in this thesis.

- Rock Mass Rating (RMR), an index of rock mass quality that combines the most significant geologic parameters of influence: uniaxial compressive strength, rock quality designation, spacing of discontinuities, conditions of discontinuities, groundwater conditions and orientation of discontinuities (Bieniawski, 1989). The number of publications about this classification method is significant. Since 2002, Choi et al. (2002), Ryu et al. (2003), You (2003), Oh et al. (2004), Stavropoulou et al. (2007) and Exadaktylos and Stavropoulou (2008) applied kriging techniques to map RMR values. Some of the abovementioned works (Stavropoulou et al., 2007 and Exadaktylos and Stavropoulou, 2008) used the prediction obtained in the numerical analysis of underground works (tunnels). Jeon et al. (2009), Egaña and Ortiz (2013), Ferrari et al. (2014) and Pinheiro et al. (2016a, b) presented some applications to the simulation of RMR, with algorithms such as the sequential Gaussian or the turning bands that consider RMR as a continuous random field, or the truncated Gaussian algorithm that considers the different parameters underlying the definition of RMR as discrete random fields.

- Geological Strength Index (GSI), a parameter that accounts for both the rock structure and block surface conditions (Hoek, 1994). The prediction of GSI can be obtained by applying a correlation function with the RMR system, therefore all the works mentioned above can be included. However, it is worth mentioning works such as Deisman et al. (2013) or Ozturk and Simdi (2014) about the direct simulation of GSI.

- Fracture frequency (FF), consisting of the number of observed fractures or discontinuities per unit length of borehole. The research of Ellefmo and Eidsvik (2009) used kriging techniques to predict the spatial frequency of discontinuities and the associated variability in an iron ore located in

Norway. Besides, Etminan and Seifi (2008) combined sequential Gaussian and sequential indicator simulation to build a fractured rock mass model considering its azimuth, depth, and density integrated with the porosity and permeability of the rock mass. Séguret et al. (2014) also used kriging techniques to predict the fracture frequency to assess its relationship with the crushed length and the number of fractures in a core sample, suggesting including in the RMR evaluation the probability or proportion of crushing.

- Fracture intensity (P_{xy}, where *x* is the dimension of the sampling space and *y* the dimension of the sample measure): several recent developments focused on stochastic methods (Jing, 2003; Chilès, 2005; Dershowitz et al., 2004; Dowd et al., 2007). The consistency between models and field observations is achieved by restricting 3D density and orientation maps derived from seismic attributes (Dershowitz, 1984; Maerten et al., 2000; Will et al., 2004; Freudenreich et al., 2005) and/or deformation analysis (Priest and Hudson, 1976; Kloppenburg et al., 2003). The works of Chilès et al. (2008) and Hekmatnejad et al. (2016, 2017) suggest studying the three-dimensional fracture intensity P_{32} (fractured area per unit rock volume) instead of the one-dimensional intensity (linear fracture frequency P_{10} observed along boreholes) or the two-dimensional intensity (P_{21}) observed in areal samples (such as outcrops), since P_{32} is an additive and non-directional variable, characteristics that P_{10} and P_{21} do not share.

These works confirm the advantages of using geostatistical techniques to model geotechnical parameters, but most are limited to applying prediction techniques such as kriging. However, simulation is the most effective and robust technique to identify the spatial variability of geotechnical properties and the existence of heterogeneities. Based on this fact, more works, and practical applications must be developed in the context of geostatistical simulation of geotechnical variables. Also, except for Séguret et al. (2014, 2015, 2019), no author has accounted for the direction dependence of geotechnical parameters such as the linear fracture frequency or the RMR, a key property that makes traditional prediction or simulation methods inadequate when

used directly in the three-dimensional Euclidean space without accounting for the azimuth and dip of the measurements. Therefore, the developed models lack this essential feature in the characterization of rock masses.

1.2. Limitations of Geostatistics in Geotechnics

The application of geostatistical techniques in the modeling of geotechnical parameters faces several challenging issues, such as the ***lack of additivity*** of most regionalized variables, which complicates the change of support (extension from a sample to a more voluminous block), as well as the ***direction dependence*** (the measurement depends on the sampling direction). In the following, these difficulties found in the implementation of geostatistics in the modeling of geotechnical variables are analyzed into detail.

1.2.1. Direction dependence (directionality)

Unlike other variables that studied in geosciences, such as the grade of a metal or the thickness of a vein, several of the geotechnical parameters have some peculiar characteristics that complicate working with them, such as the direction dependence. Direction dependence means that the measured value depends on the sampling direction. In practice, what is generally done is averaging all the sampled values that belong to a given geotechnical domain without discriminating in directional terms, which amounts to indiscriminately mixing different populations of data. For example, the RQD is direction dependent because its value depends on the angles between the direction of the sample and the fractures. Figure 1.1 shows three extreme examples where the RQD has values 0 and 100 for the same type and degree of fracturing, due to the change in the core direction. RQD refers to intact rock lengths and is related to the number of discontinuities (Fracture Frequency, FF). In addition, the measurements of the separations between the fractures are also subject to a directional bias depending on the type of fracture network (Séguret et al., 2014).

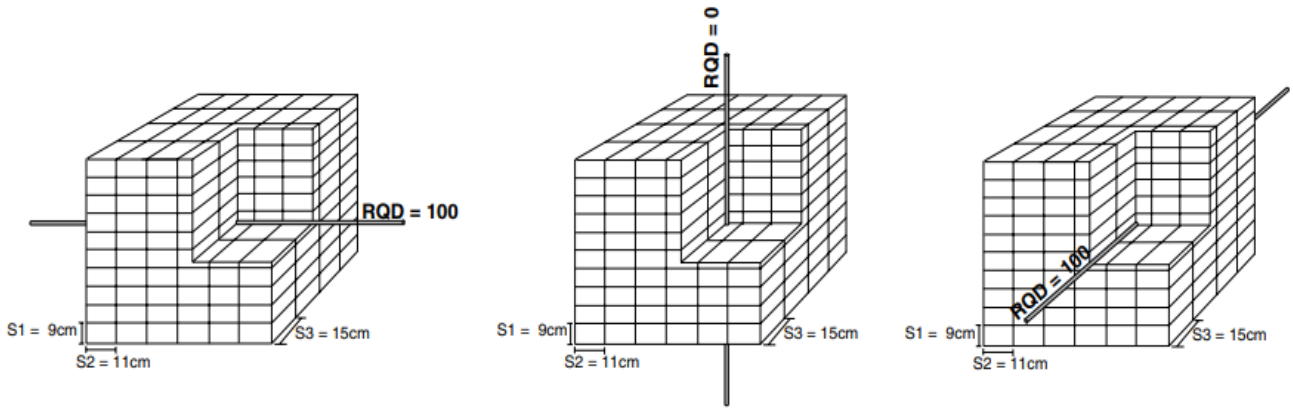

Figure 1.1. Three boreholes in different directions in the same rock mass, where RQD is 0 or 100 (Palmstrom, A., 2005).

FF is also a directional variable since the fracture count varies depending on the angle between the fracture network and the sampling direction. In practice, one can assess FF without bias by calculating the fracture frequency in the direction of the measurement and correcting by a factor equal to the sine of the angle between the fracture direction and the sampling direction (Terzaghi, 1965). Such an operation is not possible with RQD. One solution to study directional variables such as RQD is to classify the samples according to the sampling directions (Séguret and Guajardo 2015), but this is not enough, since it only allows predicting RQD in these directions, without any interpolation between them. These authors suggest that a solution to account for direction dependence is to consider the real space of regionalization as the usual geographical 3D space crossed by the 2D space of dip and azimuth, meaning that RQD measurements should be assigned five coordinates. It is worth mentioning that, with the exception of Séguret et al. (2014, 2015, 2019), very few authors have considered the direction dependence of geotechnical parameters such as fracture frequency, RQD or RMR, so that the models developed lack this essential feature in the characterization of rock masses.

The direction dependence of the geotechnical variables suggests that a regionalized variable can be defined not only in the 3D Euclidean space (with east, north and elevation coordinates), but also in the 2D sphere (with the spherical coordinates corresponding to the azimuth and the inclination of the measurement), which gives rise to a space of five dimensions: east, north, elevation, azimuth, inclination. This idea will be crucial in this thesis. Let us develop and exemplify this

idea by focusing on the fracture frequency (FF). FF corresponds to the number of fractures or any discontinuity per unit length measured in the core (see Figure 1.2). The core contains discontinuities of various structural sets, each of which has a different geometry, dip, and azimuth. Thus, FF will depend on the borehole direction, from which it follows that this variable depends on the direction of the measurement, i.e., it is directional.

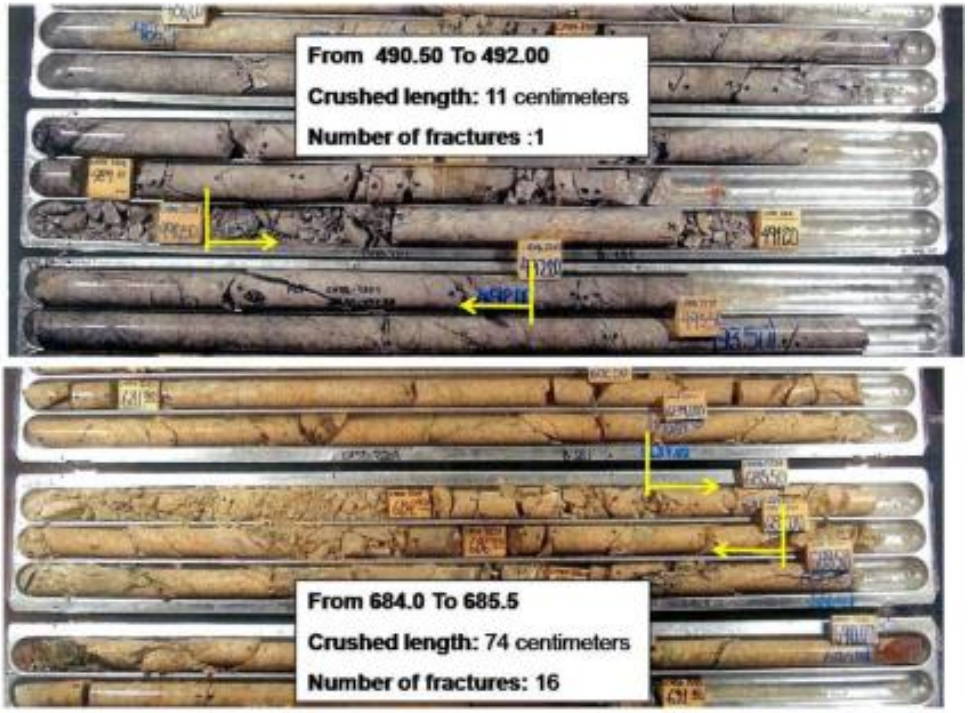

Figure 1.2. Two samples of cores that present fracturing and crushing, considered for the prediction of the fracture frequency (FF). Séguret et al., 2014

To illustrate this statement, let us consider a network of parallel fractures. The "intrinsic" fracture frequency can be defined as the one measured along the direction orthogonal to the fracture plane (**¡Error! No se encuentra el origen de la referencia.**). According to the correction proposed by Terzaghi (1965), the fracture frequency at a point **x** of the Euclidean space along the direction α (with α a point of the unit sphere $\mathbb{S}^2$ embedded in $\mathbb{R}^3$) is:

$$\mathrm{FF}(\mathbf{x},\boldsymbol{\alpha}) = \underbrace{\mathrm{FF}(\mathbf{x},\boldsymbol{\theta})}_{\substack{\text{Intrinsic}\\ \text{fracture}\\ \text{frequency}}} |<\boldsymbol{\theta},\boldsymbol{\alpha}>| \qquad (1)$$

where <, > is the scalar product and $\boldsymbol{\theta}$ is a point of $\mathbb{S}^2$ that indicates the direction orthogonal to the fracture plane (fracture pole); $<\boldsymbol{\theta}, \alpha>$ represents the cosine of the angle between $\boldsymbol{\theta}$ and α. Now, if the intrinsic fracture frequency $\mathrm{FF}(\mathbf{x}, \boldsymbol{\theta})$ has a non-centered covariance function $C_\theta(\mathbf{h})$ in the 3D Euclidean space, which only depends on the spatial separation (assumption of second-order stationarity), then the non-centered covariance function of FF is:

$$C_{FF}(\mathbf{x}, \boldsymbol{\alpha};\ \mathbf{x}', \boldsymbol{\alpha}') = \underbrace{C_{\boldsymbol{\theta}}(\mathbf{x} - \mathbf{x}')}_{\substack{\text{spatial} \\ \text{component}}} \underbrace{|<\boldsymbol{\theta}, \boldsymbol{\alpha}><\boldsymbol{\theta}, \boldsymbol{\alpha}'>|}_{\substack{\text{directional} \\ \text{component}}} \quad (2)$$

which involves the product of a stationary spatial covariance (defined in the 3D space with east, north, elevation coordinates) depending on the geographical separation **x** – **x'** between the measurements, and a directional component that depends on the orientations α and α' of the measurements taken at **x** and **x'**, respectively. This directional component has a periodicity of 2π for the azimuth and the dip of the measurements.

The previous example is voluntarily simplistic, and things are more complex in practice, in particular the fracture network rarely consists of parallel fractures, reason for which the covariance model (2) is probably unsuitable in most cases. However, the idea of constructing covariance models by multiplying a covariance function that only depends on the geographic separation in the 3D space by another covariance function that only depends on the orientations of the measurements on the 2D sphere will be kept, as a way to obtain a flexible class of covariance models for data regionalized in a 5D space.

As for covariance models on the sphere, there have been several recent developments in such a space intended to represent phenomena on the surface of the Earth (e.g., in climatology or environmental sciences) or in the sky (e.g., in astronomy), mostly restricted to isotropic, i.e., rotation-invariant, models (Gneiting, 2013; Emery et al., 2022).

1.2.2. Lack of additivity

A regionalized variable is said to be additive when the value in the union of several domains is equal to the arithmetic mean of its values over each of them. This restriction is necessary so that the calculation of the average value in a support larger than the support of the measurements has a physical sense. Geotechnical variables such as RMR, Mining Rock Mass Rating (MRMR), GSI and Rock Tunneling Quality Index (Q), present a non-linear scale (Carrasco et al., 2008), so that these variables are non-additive. The practical limitations of non-additive variables when applying geostatistical techniques are (Egaña, 2008):

i. The calculation of arithmetic averages is nonsensical. Then neither will it be to model a change of support based on an arithmetic averaging. From the preceding, it becomes impossible to regularize the support of the data on the original variable (to create composite samples) and, ideally, one needs that sampling to be carried out in a constant support.

ii. It is not convenient to perform block kriging, as this implies a change of support. Only point-support kriging or point-support simulation is feasible to spatially interpolate the variable on the same support as the available samples (when they have the same support).

The lack of additivity of geotechnical variables is related to the extensively studied size or scale effect. Size effect means that the rigidity and strength of a region decrease as the size of this region increases. The size effect is highly affected by fracture characteristics, such as their density, strike, dip angle, and diameter. For an intact rock, heterogeneity is the most important factor for the size effect (Cunha, 1990). Elsewhere, the mechanical behavior of a rock mass depends on the strength of the blocks created by random patterns of discontinuities and their strength. Hoek and Brown (1980) show how the size effect influences the rock mass strength for a tunnel with a constant cross-section and joint directions, see Figure 1.. On a small scale, the rock was intact compared to a very jointed rock mass in their larger chosen scale. When the volume is greater or the dimensions of the tunnel cross-section are changed, it is evident that the scale of the construction versus the rock mass and its

block size has a great influence on the rock mass strength. Thereby, the failure mechanism varies with the scale, i.e., the rock mass is seen in a distinct manner depending on the rock volume involved.

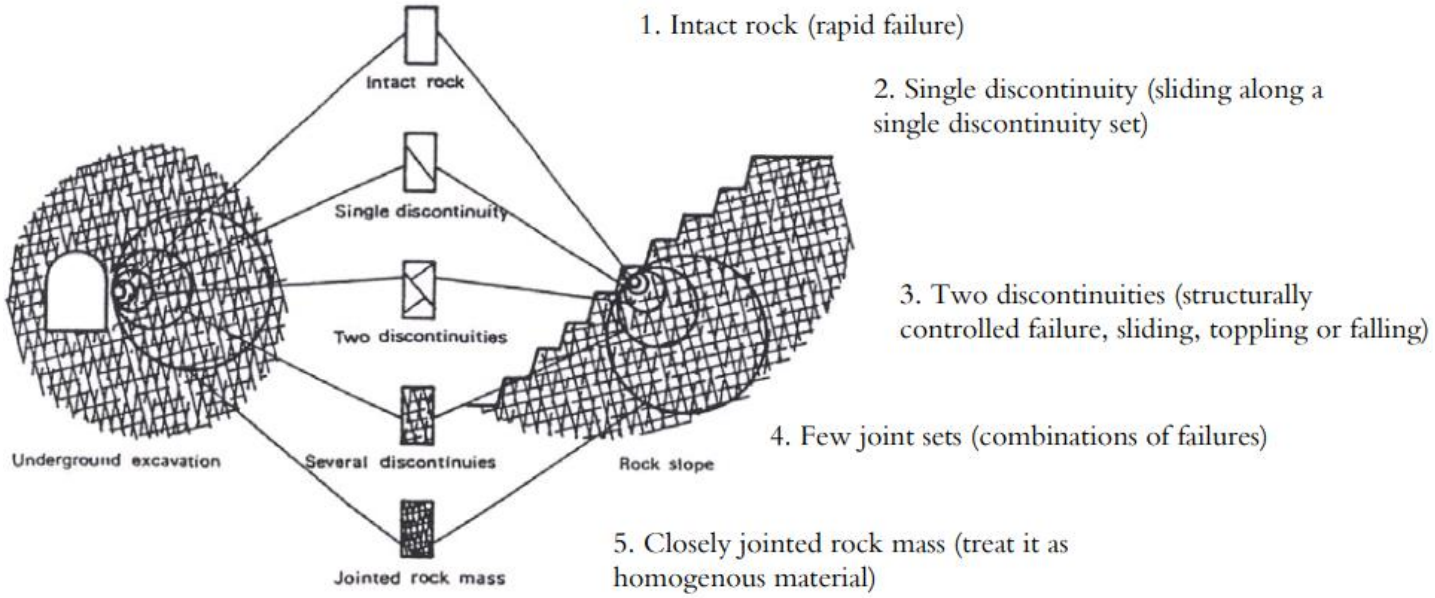

Figure 1.3. Size effect on rock strength and possible mechanisms of failure in a tunnel and a slope (Edelbroc, 2004 - modified from Hoek, 1983).

Discontinuities present less resistance and stiffness than blocks of intact material. These discontinuities produce the size/scale effect where the stiffness and strength of a region decrease as the size of the region increases. According to the concept of the size effect in rock masses, the characteristics of rock masses change gradually with increasing sample size. When the size is larger than a critical value, the characteristic values remain unchanged. The critical value is called the Representative Volume Element (REV) size. The concept of REV is introduced in the context of the abovementioned size effect (Esmaieli et al., 2010; Zhang et al., 2012). The REV is the basis to determine a rock mass mechanics model, and it is necessary to search the REV of fractured rock mass (Zhang et al., 2017). In Figure 1.4, one can see that, when the volume involved is higher than the REV, it is justifiable to use average properties for the rock mass as it can be considered as a homogeneous continuous equivalent whose discontinuities are implicit.

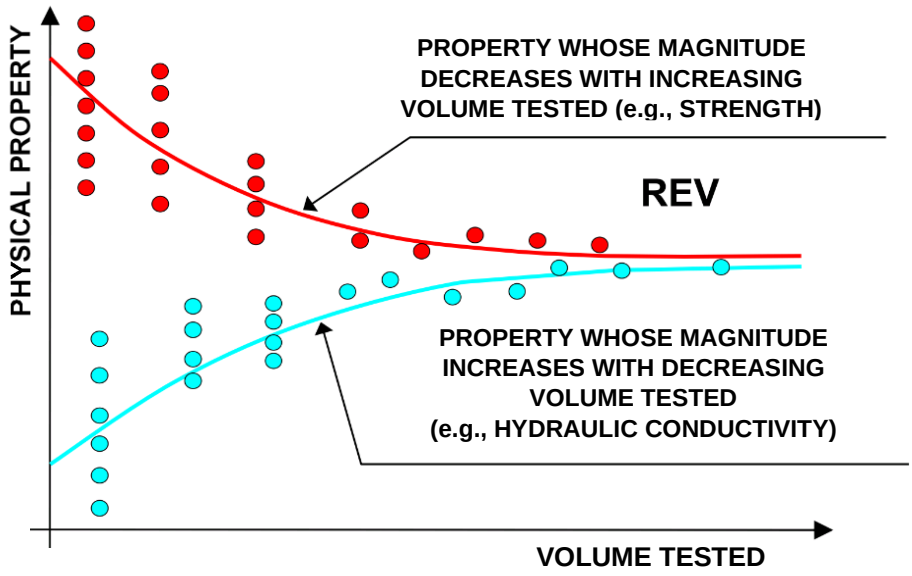

Figure 1.4. Influence of scale or size effects in the physical properties of a rock mass

Now, a block model is a discretization of the deposit into a three-dimensional array of cells or blocks, in each of which the geotechnical variables under study are predicted or simulated, but there is no agreement about the way to determine the REV. For example, Schultz (1996) says that the scale problem exceeds the block size by a factor of 5 to 10. Instead, Cundall et al. (2008) report that the REV is approximately 20 times the dimensions of the average block. Other authors, such as Rocha (1974), state that the REV is several times greater than the average spacing of discontinuities. Also, Esmaeili et al. (2010) suggested that the REV can be determined based on P_{30} (number of intersected fractures) and P_{32} (fracture area per unit rock volume). Although P_{32} does not depend on the fracture orientation and diameter distribution, it is influenced by the fracture spacing (Filion, 2018). As the fracture spacing is non-isotropic, since it depends on fracture orientation and the orientation of the mapped rock mass exposure, it follows that REV should be quantified on a directional basis. Thereby, it is complex to determine the REV by numerical methods and expensive through in situ testing. For the latter, generating an easy and economical way of calculating the REV is necessary.

Currently, empirical methods have been developed to skip the size effect and to determine the representative mechanical properties of a rock mass. These methods

combine intact rock measurements with discontinuity characteristics to classify/rate the rock mass. Subsequently, the classification correlates with the mechanical properties of the rock mass for the design of excavations. The rating attempts to "scale" features of the intact rock to the rock mass. In other words, the current solution is to consider that the rock mass at the engineering work scale is isotropic. Thus, the rock mass is isotropic when there is a sufficient number of discontinuities that are not widely spaced compared to the structure (slope, tunnel, etc.). The RMR and Q classification systems have an underlying assumption that the rock mass contains enough randomly oriented fractures and that it can be treated as a homogeneous isotropic mass (Hadjigeorgiou, 2012). Accordingly, rock mass classification systems may not be appropriate for rock masses with a dominant structural orientation (Milne et al., 1998). Therefore, the proposal of a classification system that allows for considering a wide range of mineral deposit types, including anisotropic and heterogeneous rock masses, is necessary.

1.3. Spatial correlation modeling on spheres

In application fields such as climatology, geophysics, oceanography and remote sensing, there has been a growing interest in modeling random fields defined on the sphere to deal data distributed globally over planet Earth (Emery et al., 2019.a). Other applications include astronomy and cosmology, where observations are associated with an azimuth and an altitude in the sky (Marinucci and Peccati, 2011). The spatial structure of such random fields is characterized by their covariance functions (or, following the common geostatistical practice, by their variograms), most often assumed to be isotropic, i.e., invariant under a rotation of the reference frame (Schoenberg, 1942; Gneiting, 1999, 2013; Lang and Schwab, 2015; Anh et al., 2018; Perón et al., 2018; Alegría et al., 2019).

The assumption of isotropy used in random fields on the sphere is similar to the assumption of stationarity (invariance of the finite-dimensional distribution under a translation) when dealing with random fields distributed in the Euclidean space. By restricting to the first- and second-order moments, the assumption of isotropy implies that the mean value exists and is constant on the sphere and that the covariance function only depends on the angular separation (geodesic distance) between the measurements. In the general case of vector random fields (multivariate models),

Schoenberg (1942) characterizes continuous isotropic covariances on the unit sphere $\mathbb{S}^d$ embedded in $\mathbb{R}^{d+1}$, expressed as matrix-valued functions of the form **C**(θ) whose elements are $\mathrm{C_{ij}}\big(\theta(\mathbf{x},\mathbf{x}')\big) = \mathrm{cov}\{\mathrm{Z_i}(\mathbf{x}), \mathrm{Z_j}(\mathbf{x}')\}$, where $\theta(\cdot,\cdot)$: $\mathbb{S}^d \times \mathbb{S}^d \rightarrow [0, \pi]$ is the geodesic distance defined as $\theta(\mathbf{x},\mathbf{x}') = \arccos(<\mathbf{x},\mathbf{x}'>)$. The matrix-valued covariance function **C** must be positive semi-definite, that is

$$\sum_{\ell=1}^{n}\sum_{r=1}^{n} \boldsymbol{a}_\ell \boldsymbol{C}\big(\theta(\boldsymbol{x}_\ell, \boldsymbol{x}_r)\big)\, \boldsymbol{a}_r \geq 0 \qquad (3)$$

for any positive integer n, $\{\boldsymbol{x}_1, \dots, \boldsymbol{x}_n\} \subset \mathbb{S}^d$ and $\{\boldsymbol{a}_1, \dots, \boldsymbol{a}_n\} \subset \mathbb{R}^p$, p being the number of variables under consideration. This condition is met if and only if (Yaglom, 1987)

$$\boldsymbol{C}(\boldsymbol{\theta}) = \sum_{\boldsymbol{k=0}}^{\infty} \boldsymbol{B}_{k,d} \mathcal{G}_k^{\lambda}(\cos\theta), \qquad \theta\epsilon[0,\pi] \qquad (4)$$

with $\lambda := \frac{d-1}{2}$, $\mathcal{G}_{\boldsymbol{k}}^{\boldsymbol{\lambda}}$ is the Gegenbauer polynomial of degree *k* and order λ (Abramowitz and Stegun, 1970) and $\{\boldsymbol{B}_{k,d}: k = 0, 1, \dots\}$ is a sequence of *p* × *p* positive semi-definite matrices, known as a multivariate d-Schoenberg sequence (Daley and Porcu 2014), such that $\sum_{k=0}^{+\infty} \boldsymbol{B}_{k,d}\, \mathcal{G}_{\boldsymbol{k}}^{\boldsymbol{\lambda}}(1)$ converges. Considering only the case d = 2, $\mathcal{G}_k^{1/2} = P_k$ is the Legendre polynomial of degree *k* (Abramowitz and Stegun, 1970), and the isotropic function **C**(θ) is a matrix-valued covariance on the 2D sphere if:

$$\boldsymbol{C}(\boldsymbol{\theta}) = \sum_{\boldsymbol{k=0}}^{\infty} \boldsymbol{B}_{k,2} P_k\ (\cos\theta) \qquad (5)$$

here $\{\boldsymbol{B}_{k,2}: k = 0, 1, \dots\}$ is a convergent sequence of positive semi-definite matrices.

For instance, the spherical and exponential models are valid covariances on the sphere when the Euclidean separation vector **h** is replaced by the geodesic distance θ (Huang et al., 2009), while this is not the case for the Gaussian model (Gneiting, 1999). Another subclass of valid isotropic models on the sphere is obtained by restricting isotropic covariances in the Euclidean 3D space (Yadrenko, 1983; Yaglom, 1987): in fact, because the Euclidean distance between two points separated by a central angle θ in the unit sphere is 2sin (θ/2), if $\mathrm{C_E}(\mathbf{h})$ is an isotropic covariance in $\mathbb{R}^3$, then the function

$$C(\theta) = C_E(2sen(\theta/2)) \quad (6)$$

it is a valid isotropic covariance model on the sphere. In that case, it is equivalent to work with covariance C and the central angular distance θ, or with covariance C_E and the separation distance **h** in the Euclidean space.

Geometric anisotropy, which is widely used in the geographical space, has no equivalent in the sphere. Anisotropic models exhibiting non-stationarity along latitude and/or longitude, such as axially symmetric models, have been proposed in the past decade (Jones, 1963; Stein, 2007; Jun and Stein, 2008; Porcu et al., 2019; Emery et al., 2019.b).

1.4. Spatial correlation modeling on spheres crossed with Euclidean spaces

As mentioned earlier, the direction dependence of geotechnical variables suggests that a regionalized variable can be defined not only in the Euclidean space but also on the sphere or, more generally, in a five-dimensional space (product of the 3D Euclidean space and the 2D sphere) with coordinates consisting of the easting, northing, elevation, azimuth and dip of the measurement. There have been few model developments in such spaces, except for some works on the sphere crossed with time aimed to represent global phenomena on the Earth's surface that evolve in time (Porcu et al., 2018).

Emery et al. (2021) gives spectral representations together with some parametric families of scalar-valued and matrix-valued covariance functions on product spaces consisting of a sphere crossed with a Euclidean space, that are isotropic (depending only on the geodesic distance) on the sphere and stationary (depending only on the Euclidean distance) in the Euclidean space. A simple approach, which will be used in the next chapter of this thesis, is given by the so-called separable model, where the covariance function is the product (elementwise product in the multivariate case) of a second-order stationary covariance function defined the Euclidean space and an isotropic covariance function defined on the sphere.

CHAPTER II.

MODELING OF DIRECTIONAL VARIABLES IN A 5D SPACE

Consider a direction-dependent geotechnical variable distributed in a region of the 3D Euclidean space and measured along borehole samples. The measured value varies with the geographic coordinates of the sample and with its direction, that is:

$$z = \{z(\mathbf{x},\mathbf{u}): \mathbf{x} \in \mathrm{R}^3 \text{ and } \mathbf{u} \in \mathrm{S}^2\}, \quad (7)$$

where x is a vector indicating the in-situ position in the geographic space (R^3), while **u** is a vector on the unit 2D sphere (S^2) representing the in-situ direction of the sample. The geostatistical model interprets the regionalized variable *z* as one among many possible realizations of a random field *Z*, defined in the same space:

$$Z = \{Z(\mathbf{x},\mathbf{u}): \mathbf{x} \in \mathrm{R}^3 \text{ and } \mathbf{u} \in \mathrm{S}^2\}. \quad (8)$$

The basis of the model, therefore, is to define the regionalized variable and the parent random field in a five-dimensional space ($\mathrm{R}^3 \times \mathrm{S}^2$) that accounts for the real spatial continuity. The modeling of random fields in more complex spaces than Euclidean spaces is not new in spatial statistics. In particular, there has been a growing interest in sphere-time models that attempt to represent global phenomena distributed over the surface of the planet Earth and evolving through time, which are regionalized in a space consisting of the Cartesian product of a Euclidean space with a sphere; the reader is referred to Porcu et al. (2018) for a thorough review. The proposed in this work is to replace the 1D time axis with the 3D geographic space, a generalization that seems to be novel.

2.1. Spatial correlation modeling

2.1.1. Modeling in the three-dimensional Euclidean space

In the Euclidean space, one traditionally uses the assumption of stationarity in the geostatistical modeling of random fields. The concept enables the inference of the random field parameters from a finite set of data, such as the expected value, the covariance or the variogram, by replacing the repetition over the realizations of the random field (which is theoretically needed to infer expected values) by a repetition in space over the same realization. In a nutshell, the underlying idea is that the values observed in different regions of space have the same statistical characteristics, so that they can be considered as different realizations of the same random process. From a mathematical viewpoint, the (strict) stationarity hypothesis occurs when every finite-dimensional distribution of the random field, based on k points $x_1 \ldots x_k$ in space, is invariant under an arbitrary translation of the points by a vector h:

$$P\{Z(x_1) < z_1, \ldots, Z(x_k) < z_k\} = P\{Z(x_1 + h) < z_1, \ldots, Z(x_k + h) < z_k\}, \qquad (9)$$

with P indicating a probability measure.

In other words, stationarity means that the regionalized phenomenon is homogeneous in space and repeats itself throughout space, so that the properties of a dataset do not depend on their absolute positions in space, but only on their relative positions. When the random field is stationary, its moments, if they exist, are invariant through translations.

In practice, the hypothesis can be weakened in several ways, by assuming that only the first- and second-order moments are invariant by translation (second-order stationarity) or that the increments of the random field are second-order stationary (intrinsic stationarity). In the former case, the mean value of the random field is constant and the covariance between the two random variables located at **x** and **x**′ depends only on the separation vector **h** = **x**′-**x**. One convenient approach to model the covariance function of a second-order stationary random field is the linear model of regionalization (Wackernagel, 2003), where the covariance is constructed as a positive linear combination of basic nested correlation functions:

$$C(\mathbf{h}) = \sum_{s=1}^{S_{\max}} b_s \, \rho_s(\mathbf{h}) \tag{30}$$

where, for $s = 1,\ldots S_{\max}$, $b_s \geq 0$ and ρ_s is a correlation function (positive semi-definite function taking the value 1 at $\mathbf{h} = \mathbf{0}$).

2.1.2. Modeling in the two-dimensional sphere

For random fields on the sphere, the above assumption of stationarity cannot be defined and is often traded off against an assumption of isotropy, that is, an invariance of the finite-dimensional distributions under a rotation. In the case of data on the unit sphere S^2, a simplification is to assume that the first- and second-order moments exist and are invariant under a rotation. In such a case, the mean value of the random field is constant and the covariance between the two random variables located at **u** and **u**′ depends only on the angular separation (geodesic distance)

$$\delta(\mathbf{u},\mathbf{u}') = \arccos(<\mathbf{u},\mathbf{u}'>), \tag{41}$$

where < , > denotes the inner product.

The covariance function of an isotropic random field on the sphere S^2, viewed as a function of the geodesic distance $\delta \in [0,\pi]$, has a representation similar to the linear model of regionalization. Indeed, Schoenberg (1942) showed that it can be expanded into a positive linear combination of the following form:

$$C(\delta) = \sum_{n=0}^{+\infty} b_n \, P_n(\cos\delta), \tag{52}$$

where P_n is the Legendre polynomial of degree n, $b_n \geq 0$ and $\sum_{n=0}^{+\infty} b_n < +\infty$.

Legendre polynomials form an orthogonal basis of polynomials for an internal product defined as the simple product of continuous functions in the closed interval $\mathbf{x} \in [-1, 1]$, defined as follows:

$$\int_{-1}^{1} P_m(\mathrm{x}) P_n(\mathrm{x}) dx = \frac{2}{2n+1} \delta_{mn} \tag{13}$$

where δ_{mn} denotes the Kronecker delta, equal to 1 if m = n and 0 otherwise. Therefore, any function in the interval [−1, 1] can be express in that basis:

$$f(x) = \sum_{k=0}^{\infty} \underbrace{\frac{2k+1}{2}\left[\int_{-1}^{1} f(t)P_k(t)dt\right]}_{a_k} P_k(x) \tag{6}$$

Legendre polynomials are symmetric or antisymmetric according to $P_n(-x) = (-1)^n P_n(x)$, that is, they have a definite parity relationship for all *n*. In geotechnical applications, since a borehole core sample taken along a direction **u** is the same as the one taken along the opposite direction -**u**, one needs to add a restriction on the isotropic models, so the symmetric property of Legendre polynomials will be used. In spherical coordinates, changing **u** into -**u** amounts to changing $\delta(\mathbf{u},\mathbf{u}')$ into $\pi-\delta(\mathbf{u},\mathbf{u}')$, and $P_n(\cos\delta)$ into $P_n(-\cos\delta)$. In this regard, the covariance model in Eq. (12) can be invariant when one only considers the Legendre polynomials of even degrees, which are even functions, and discards the Legendre polynomials of odd degrees that are odd functions, i.e.:

$$C(\delta) = \sum_{n=0}^{+\infty} b_{2n} P_{2n}(\cos\delta), \tag{75}$$

where $b_{2n} \geq 0$ and $\sum_{n=0}^{+\infty} b_{2n} < +\infty$.

2.1.3. Modeling in the product of the 3D Euclidean space and 2D sphere

To model the spatial correlation of regionalized data in a 5D space consisting of the product of the 3D geographic space R^3 and the 2D sphere S^2, the simplest approach is to consider (strict or second-order) stationarity in the geographic space and (strict or second-order) isotropy on the sphere. Accordingly, the covariance function between the two random variables located at (**x**,**u**) and (**x**′,**u**′) in $\mathrm{R}^3 \times \mathrm{S}^2$ only depends on the separation vector **h** = **x**′-**x** and on the geodesic distance or angular separation $\delta(\mathbf{u},\mathbf{u}')$ = arcos(<**u**,**u**′>). Based on the previous statements, the linear model of regionalization can be extended in the following form:

$$C(\mathbf{h},\delta) = \sum_{s=1}^{S_{\max}} b_s C_s(\mathbf{h},\delta) \tag{16}$$

where, $b_s \geq 0$ for $s = 1,\ldots S_{max}$, and C_s is a basic correlation (positive semi-definite) function defined on $\mathrm{R}^3 \times [0,\pi]$. A simple family of such basic correlation functions are separable models of the form

$$C_s(\mathbf{h},\delta) = \rho_s(\mathbf{h})\rho'_s(\delta), \tag{178}$$

with ρ_s a second-order stationary correlation function in R^3 and ρ_s' an isotropic correlation function on S^2 obtained by combining Legendre polynomials of even degrees. This model can be rewritten in terms of the variogram:

$$\gamma(\mathbf{h},\delta) = \sum_{s=1}^{S_{max}} b_s\,\gamma_s(\mathbf{h},\delta), \tag{18}$$

with $\gamma_s = 1 - \rho_s$.

In practice, a linear model of regionalization of the form (16) or (18) can be fitted to a given experimental covariance or variogram by choosing an appropriate set of the separable basic structures $\{C_s: s = 1\ldots S_{max}\}$ and nonnegative coefficients $\{b_s: s = 1\ldots S_{max}\}$. The model parameters can be determined with automatic algorithms that reduce the deviations between experimental and modeled covariances or variograms, in the same way as it is done in standard 3D geostatistics (Goulard and Voltz, 1992).

Note that the restricted class of covariance models on $\mathrm{R}^3 \times \mathrm{S}^2$ formed by models of the form (16) with separable basic covariances (Eq. 17) is not the only one that can be considered. More general models, not limited to sums of separable covariances, can be designed by extending to 5D the models presented by, for instance, Porcu et al. (2016) in the case of the sphere-time processes.

2.2. Multivariate modeling

It is common for several regionalized variables to refer to the same phenomenon, requiring joint analysis to consider the relationships between them and the information provided by auxiliary variables on the main variable of interest. To

analyze the spatial continuity of the variables, the assumption is maintained that the associated random fields are jointly stationary and isotropic, so their direct and cross covariances will be functions of the separation vector between data (**h**) and the geodesic distance (δ). Simple and cross covariances of a set of variables cannot be modeled independently due to mathematical constraints. In particular, the linear co-regionalization model satisfies the constraints on the matrix-valued covariance function $\mathbf{C}(\mathbf{h},\delta)$, which must be positive semi-definite. The direct and cross covariances are assumed to be combinations of the same set of basic models:

$$\forall i,j \in [1,N], C_{ij}(\boldsymbol{h},\delta) = \sum_{s=1}^{S_{max}} b_{ij}^{s} C_s(\boldsymbol{h},\delta) \quad (19)$$

To ease the notation, the upper indices represent the different basic nested models (not to be confused with a power). That is, matricially

$$\mathbf{C}(\boldsymbol{h},\delta) = \sum_{s=1}^{S_{max}} \boldsymbol{B}_s C_s(\boldsymbol{h},\delta) \quad (20)$$

where $\mathbf{C}(\boldsymbol{h},\delta) = \left[C_{ij}(\boldsymbol{h},\delta)\right]_{i,j=1\ldots N}$ is the matrix of direct and cross covariances, and $\boldsymbol{B}_s = \left[b_{ij}^{s}\right]_{i,j=1\ldots N}$ is called a coregionalization matrix, with all the eigenvalues of $\mathbf{B}_s$ being positive or zero.

2.3. Non-conditional simulation

A typical assumption requested in geostatistics to simulate quantitative variables is that the observed process is a realization of a Gaussian random field $Z = \{Z(\mathbf{x},\mathbf{u})$: $\mathbf{x} \in \mathrm{R}^3$ and $\mathbf{u} \in \mathrm{S}^2\}$. This assumption will be made throughout for the observed process itself or for a transform of it (through an anamorphosis procedure).

The problem therefore amounts to simulating a Gaussian random field in a five-dimensional space ($\mathrm{R}^3 \times \mathrm{S}^2$) that reproduces the desired mean (hereafter, set to zero, which does not lose generality) and the covariance represented by a linear model of regionalization (Eqs. 19-20). A few generic simulations algorithms, such as the covariance matrix decomposition and the sequential algorithm, can be used for this purpose, but when the number of locations targeted for simulation is too large (more than a few tens of thousands), these algorithms are no longer applicable or become approximate (Emery and Peláez, 2011; Chilès and Delfiner, 2012). Henceforward, we propose an algorithm that does not suffer from this limitation and

relies on simulating Z as a sum of products of a geographic component and a directional component, i.e.: $\forall\ \mathbf{x} \in \mathrm{R}^3$, $\forall\ \mathbf{u} \in \mathrm{S}^2$, $Z_s(\mathbf{x},\mathbf{u}) = T_s(\mathbf{x})\ W_s(\mathbf{u})$, where the subscript s stands for the index of the basic nested structure used in the linear model of regionalization.

The geographic component T_s is a stationary random field in the Euclidean space R^3 with zero mean and correlation function $\rho_s(\mathbf{h})$. It can be simulated, for instance, by the continuous spectral or the turning bands methods (Matheron, 1973; Lantuéjoul, 2002; Emery and Lantuéjoul, 2006).

Concerning the directional component, for $\mathbf{u} \in \mathrm{S}^2$, let us introduce its spherical coordinates $\theta(\mathbf{u}) \in [0,\pi]$ (colatitude) and $\varphi(\mathbf{u}) \in [0,2\pi[$ (longitude). In a first instance, consider the problem of simulating an isotropic random field W_n with zero mean and covariance function $P_n(\cos\delta)$, where n is a nonnegative integer and δ is the geodesic distance (angular separation). Following Lantuéjoul et al. (2019) and Emery and Porcu (2019), the simulation can be obtained by putting:

$$\forall \mathbf{u} \in \mathrm{S}^2, W_n(\mathbf{u}) = 2\sqrt{\pi}\, U\, Y_{n,L}(\theta(\mathbf{u}), \varphi(\mathbf{u})) \tag{21}$$

where L is a random integer uniformly distributed on $[-n,\ldots,n]$, U is a random variable with zero mean and unit variance (e.g., a standard Gaussian variable) independent of L, and $Y_{n,\ell}$ is the real (tesseral) spherical harmonic of degree n and order ℓ, which can be expressed as a function of an associated Legendre polynomial and sine or cosine functions (Arfken and Weber, 2005):

$$\boldsymbol{Y_{n,\ell}(\theta,\varphi)} = \begin{cases} (-\mathbf{1})^{\ell}\sqrt{\mathbf{2}}\sqrt{\frac{(\mathbf{2n+1})(\mathbf{n-|\ell|})!}{(\mathbf{4\pi})(\mathbf{n-|\ell|})!}}\ \boldsymbol{P_n^{|\ell|}}(\mathbf{cos}(\boldsymbol{\theta}))\,\mathbf{sin}(|\boldsymbol{\ell}|\boldsymbol{\varphi})\ \ \boldsymbol{if\ \ell < 0}, \\ \sqrt{\frac{\mathbf{2n+1}}{\mathbf{4\pi}}}\boldsymbol{P_n^0}(\mathbf{cos}(\boldsymbol{\theta}))\ \boldsymbol{if\ m = 0} \\ (-\mathbf{1})^{\ell}\sqrt{\mathbf{2}}\sqrt{\frac{(\mathbf{2n+1})(\mathbf{n-\ell})!}{(\mathbf{4\pi})(\mathbf{n-\ell})!}}\ \boldsymbol{P_n^{\ell}}(\mathbf{cos}(\boldsymbol{\theta}))\,\mathbf{sin}(\boldsymbol{\ell\varphi})\ \ \boldsymbol{if\ \ell > 0}, \end{cases} \tag{22}$$

where P_n^{ℓ} stands for the associated Legendre polynomial of degree n and order ℓ. The fact that $W_n(\mathbf{u})$ has a zero expected value comes from the fact that U has a zero

mean and is independent of L. For $\mathbf{u}$ and $\mathbf{u}'$ on S^2, the covariance between $W_n(\mathbf{u})$ and $W_n(\mathbf{u}')$ is

$$\begin{aligned}\operatorname{cov}\{W_n(\mathbf{u}), W_n(\mathbf{u}')\} &= 4\pi \mathrm{E}\{U^2\}\mathrm{E}\{Y_{n,L}(\theta(\mathbf{u}),\varphi(\mathbf{u}))Y_{n,L}(\theta(\mathbf{u}'),\varphi(\mathbf{u}'))\} \\ &= \frac{4\pi}{2n+1}\sum_{\ell=-n}^{n} Y_{n,\ell}(\theta(\mathbf{u}),\varphi(\mathbf{u}))Y_{n,\ell}(\theta(\mathbf{u}'),\varphi(\mathbf{u}')).\end{aligned} \tag{93}$$

Using the addition theorem for spherical harmonics (Arfken and Weber, 2005) it is seen that this covariance matches the desired one:

$$\operatorname{cov}\{W_n(\mathbf{u}), W_n(\mathbf{u}')\} = P_n(<\mathbf{u},\mathbf{u}'>) = P_n(\cos\delta(\mathbf{u},\mathbf{u}')) \tag{24}$$

Accordingly, the random field W_n defined at Eq. 20 is isotropic on S^2, with zero mean and covariance function $P_n(\cos\,\delta)$, where δ is the geodesic distance on the sphere.

Without losing the generality, the linear model of regionalization in Eqs. (16)-(18) can be rewritten as follows:

$$C(\mathbf{h},\delta) = \sum_{s=1}^{S_{\max}} b_s\, \rho_s(\mathbf{h})\, P_{2n(s)}(\cos\delta) \tag{28}$$

with $S_{\max} \in \mathrm{N} \cup \{+\infty\}$ a nonnegative integer, $n(s) \in \mathrm{N}$, $b_s \geq 0$ and $b = \sum_{s=0}^{S_{\max}} b_s < +\infty$.

Based on the previous statements, the simulation of a random field with such a covariance can be achieved as follows:

1) Simulate a nonnegative integer S such that $\mathrm{P}\{S = s\} = b_s/b$.

2) Simulate a second-order stationary random field T_S in R^3 with zero mean and correlation function $\rho_S(\mathbf{h})$.

3) Simulate an isotropic random field W_S on S^2 with zero mean and correlation function $P_{2n(S)}(\cos\,\delta)$, such that, conditionally on $S = s$, W_s and T_s are independent.

4) Generate the simulated random field as

$$\forall \mathbf{x} \in \mathrm{R}^3, \forall \mathbf{u} \in \mathrm{S}^2, Z(\mathbf{x},\mathbf{u}) = \sqrt{b}\, T_S(\mathbf{x}) W_S(\mathbf{u}) . \tag{25}$$

Conditional to $S = s$, Z is the product of two zero-mean independent random fields (T_s and W_s) and a positive scalar coefficient ($b^{1/2}$). Accordingly, its mean value is zero and its covariance function is b times the product of the covariances of T_s and W_s, i.e., $b\ \rho_s(\mathbf{h})\ P_{2n(s)}(\cos\delta)$. The prior mean and covariance function are obtained by randomizing s:

$$\forall\ \mathbf{x} \in \mathrm{R}^3,\ \forall\ \mathbf{u} \in \mathrm{S}^2,\ \mathrm{E}\{Z(\mathbf{x},\mathbf{u})\} = \sum_{s=1}^{S_{\max}} \frac{b_s}{b} \mathrm{E}\{Z(\mathbf{x},\mathbf{u}) \mid S = s\} = 0 \tag{26}$$

$$\forall \mathbf{x}, \mathbf{x}' \in \mathrm{R}^3, \forall \mathbf{u}, \mathbf{u}' \in \mathrm{S}^2, \mathrm{E}\{Z(\mathbf{x},\mathbf{u})\, Z(\mathbf{x}',\mathbf{u}')\} = \sum_{s=1}^{S_{\max}} \frac{b_s}{b} \mathrm{E}\{Z(\mathbf{x},\mathbf{u})\, Z(\mathbf{x}',\mathbf{u}') \mid S = s\}$$

$$= \sum_{s=1}^{S_{\max}} b_s\, \rho_s(\mathbf{h})\, P_{2n(s)}(\cos\delta). \tag{27}$$

Finally, to obtain a random field whose finite-dimensional distributions are approximately Gaussian, it suffices to add and to rescale a large number of independent copies of (29):

$$\forall \mathbf{x} \in \mathrm{R}^3, \forall \mathbf{u} \in \mathrm{S}^2, Z(\mathbf{x},\mathbf{u}) = \sqrt{\frac{b}{K}} \sum_{k=1}^{K} T_{S(k),k}(\mathbf{x}) W_{S(k),k}(\mathbf{u}) \tag{28}$$

where K is a large integer and $\{(S(k),\ T_{S(k),k},\ W_{S(k),k}):\ k = 1,\ldots K\}$ are independent copies of $(S,\ T_S,\ W_S)$.

2.4. Conditional simulation

Under the multivariate Gaussian assumption, conditioning the simulation to a set of sampling data can be achieved classically by means of a kriging step (Chilès

and Delfiner, 2012). Let $\{Z_{NCS}(\mathbf{x},\mathbf{u})$: $\mathbf{x} \in \mathrm{R}^3$, $\mathbf{u} \in \mathrm{S}^2\}$ be a non-conditional simulation of Z. Then, the random field defined by

$$\forall \mathbf{x} \in \mathbb{R}^{\mathbf{3}}, \forall \mathbf{u} \in \mathbb{S}^{\mathbf{2}}, Z_{CS}(\mathbf{x},\mathbf{u}) = Z_{NCS}(\mathbf{x},\mathbf{u}) + [Z(\mathbf{x},\mathbf{u}) - Z_{NCS}(\mathbf{x},\mathbf{u})]^{SK} \quad (29)$$

constitutes a conditional simulation, i.e. it reproduces the distribution of $\{Z(\mathbf{x},\mathbf{u})$: $\mathbf{x} \in \mathrm{R}^3$, $\mathbf{u} \in \mathrm{S}^2\}$ conditional to the Z-data. In Eq. (27), the superscript SK stands for a simple kriging (with mean zero and covariance $C(\boldsymbol{h},\delta)$) at location $(\mathbf{x},\mathbf{u})$ based on the values at the data locations.

To summarize, the conditional simulation is constructed as follows:

1. Generate a non-conditional realization at all the target locations $(\mathbf{x},\mathbf{u})$ and the data locations.
2. Compute the deviations (residuals) between the data values and simulated values at the data locations.
3. Perform simple kriging of the residual from its values at the data locations.
4. Add the result to the non-conditional realization, following Eq. (29).

2.5. Multivariate simulation

Let $\mathbf{Z}$ be a vector Gaussian random field with p scalar components defined in $\mathrm{R}^3 \times \mathrm{S}^2$. To jointly simulate the components of $\mathbf{Z}$, one can split this vector random field as follows:

$$\forall\, \mathbf{x} \in \mathrm{R}^3,\ \forall\, \mathbf{u} \in \mathrm{S}^2,\ \boldsymbol{Z}(\mathbf{x},\mathbf{u}) = \sum_{s=1}^{S_{max}} \boldsymbol{Z}_s(\mathbf{x},\mathbf{u}). \quad (30)$$

According to the linear coregionalization model, $\mathbf{Z}_1, \ldots, \mathbf{Z}_s$ are independent vector Gaussian random fields, with $\mathbf{B}_1\rho_1, \ldots, \mathbf{B}_{Smax}\rho_s$ as their respective matrices of direct and cross-covariance functions. Since each coregionalization matrix is positive semi-definite, it can be decomposed as follows:

$$\mathbf{B}_s = \mathbf{Q}_s \Delta_s \mathbf{Q}_s^T = \mathbf{A}_s \boldsymbol{A}_s^T \quad (31)$$

where T is the transposition operator, $\mathbf{Q}_s$ is an orthogonal matrix of eigenvectors, Δ_s a diagonal matrix of non-negative eigenvalues and $\mathbf{A}_s = \mathbf{Q}_s\sqrt{\Delta_s}$.

Let $\mathbf{W}_s$ be a vector random field with independent components, each with covariance function ρ_s. Then, it can be shown that the random field $\mathbf{A}_s\mathbf{W}_s$ has the same correlation structure as $\mathbf{Z}_s$. The simulation of the target vector random field **Z**, therefore, reduces to simulating independent scalar random fields (the components of $\mathbf{W}_s$ for $s = 1, \ldots, S_{max}$) with covariance functions equal to the basic nested structures used in the linear coregionalization model. The simulation of the components of $\mathbf{W}_s$ can be performed via any Gaussian simulation algorithm.

Note that other multivariate simulation algorithms that accurately reproduce the covariance structure of the vector random field have been proposed in the recent literature, based on spectral representations of **Z** through finite expansions into spherical harmonics (Emery and Porcu, 2019), or finite expansions into Legendre polynomial waves (Alegría et al., 2020).

To make the simulated vector random field conditional to a set of pre-existing data, one can post-process the obtained simulations with an additional step of cokriging of the difference between the simulation at the data locations and the actual conditioning data values.

CHAPTER III.

APPLICATION IN GEOTECHNICS TO THE SIMULATION OF THE LINEAR DISCONTINUITY FREQUENCY

This chapter addresses the problem of simulating the linear discontinuity frequency in a porphyry copper deposit (El Teniente, central Chile), based on a regionalization of the variable in a 5D space. The contents of this chapter have been published in Computers & Geosciences:

> Sánchez, L.K., Emery, X., Séguret, S.A., 2019. 5D geostatistics for directional variables: application in geotechnics to the simulation of the linear discontinuity frequency. Computers & Geosciences, 133: article 104325.

Abstract

In geotechnics and geomechanics, many rock mass properties are quantified by numerical variables defined by the observation or the testing of a borehole core sample. The value measured depends not only on the in-situ geographic coordinates of the sample, but also on the in-situ borehole direction. Interpolating such numerical variables in space without accounting for their directionality may produce misleading results, insofar as the interpolated values are representative of the rock mass properties in the sampling directions and not necessarily in other directions. A solution to this issue is to regionalize the geotechnical variables in a five-dimensional space, consisting of the Cartesian product of the three-dimensional Euclidean space and the unit 2-sphere, in order to account for both their geographic and directional variations. Spatial correlation analysis can be performed easily under an assumption of stationarity in the three-dimensional Euclidean space and isotropy on the sphere, so that the covariance or the variogram between two data only depends on their geographic and angular separations. The fitting of nested separable covariance functions eases the search for a valid spatial correlation model and for algorithms to simulate the geotechnical variables in the above-defined five-dimensional space. The concepts are applied to the modeling of the linear frequency of weak veins in a Chilean porphyry copper deposit, where the importance of accounting for directionality is demonstrated. Regionalized azimuthal projections are introduced as a visualization tool for structural geologists and geotechnicians to map the directional variations of the weak vein frequency at given locations in the geographic space.

Key words: 5D geostatistics; spatio-angular regionalization; nested separable covariances; Legendre polynomials; regionalized azimuthal projections; simulation

3.1. Introduction

The geotechnical characterization and classification of rock masses is critical in mining engineering in order to assess the nature and geological structure of the subsoil, to quantify the stability of slopes in open pit mining or the fortification of galleries in underground mining, and to ensure the security of the infrastructures and the personnel working in the mine. Similar issues are met in civil, petroleum and geothermal engineering, groundwater resources management and underground

nuclear wastes disposal, to design underground works. Rock masses exhibit spatial heterogeneities with transitions from zones with higher resistance and rigidity to others with lower resistance and rigidity, sometimes at short distances, making the mechanical behavior of the rock mass difficult to predict.

Two main avenues have been explored for such a characterization and classification. The first one focuses on the modeling of the geological discontinuities viewed as objects distributed in space, such as faults, fractures, veins or joints, which often control the rock mass properties. In such a case, the parameters of interest are the number, position, orientation, spacing, shape, dimension, aperture and thickness of the discontinuities within the study area. The main challenges are the inference without bias of the distributions of these parameters using different data sources, such as borehole, scanline or window surveys or remote sensing information, and the simulation of discontinuity networks (Chilès, 2005; Dowd et al., 2007; Xu and Dowd, 2010; Lato et al., 2013; Hyman et al., 2015).

The second avenue does not focus on the discontinuity network as a set of objects in space, but on numerical properties measured on continuous or discrete quantitative scales, for instance the rock quality designation (RQD), the uniaxial compressive strength (UCS), the rock mass rating (RMR), the geological strength index (GSI), the rock tunneling index (Q) or the discontinuity intensity (Pxy, where x is the dimension being measured and y is the dimension of the measurement). Being regionalized, these properties can be modeled and interpolated in space on the basis of sampling information. A common practice is to define “geotechnical domains” and to assign an average value to each domain, which provides a rather rough characterization. To get a more detailed spatial modeling, geostatistical tools and methods can be used. In the past two decades, kriging and conditional simulation have been applied to the prediction of RQD (Ozturk and Nasuf, 2002; Madani and Asghari, 2013; Ozturk and Simdi, 2014; Séguret and Guajardo, 2015), UCS (Abdideh et al., 2014; Doostmohammadi et al., 2015), RMR (Choi and Park, 2002; Oh et al., 2004; Stavropoulou et al., 2007; Choi et al., 2009; Jeon et al., 2009; Egaña and Ortiz, 2013; Ferrari et al., 2014; Pinheiro et al., 2016a, 2016b; Santos et al., 2018), GSI (Deisman et al., 2013; Ozturk and Simdi, 2014), Q (Exadaktylos and Stavropoulou,

2008), P10 (Ellefmo and Eidsvik, 2009; Séguret et al., 2014) and P32 (Hekmatnejad et al., 2017).

The geostatistical modeling of geotechnical variables faces specific difficulties that require attention. In particular, many variables are directional, i.e., their values depend not only on the in-situ position of the measurement, but also on its in-situ direction (Séguret and Emery, 2019). The definition of these variables is especially meaningful when the volumetric support of the measurement is a cylinder, e.g., a borehole core sample. Since the cylinder diameter is usually small in comparison with its length, the measurement can be approximated by a line segment and identified not only by the in-situ geographic coordinates (easting, northing, elevation) of its center of gravity, but also by its orientation (azimuth and dip in geological coordinates, or colatitude and longitude in spherical coordinates). Examples of directional variables include RQD, UCS, RMR, Q and P_{10}, the latter variable representing the number of discontinuities per meter and being also known as the linear discontinuity frequency or linear fracture frequency (FF). In most cases, directionality stems from the fact that discontinuities perpendicular to the direction of the measurement are more prone to be observed than discontinuities in other directions (Terzaghi, 1965), which implies that the (geo)statistical properties of the variables are direction-dependent. This feature makes difficult a change of support or upscaling when the shape of the target support is not a line segment. It is also likely to affect the manner in which geotechnical variables are interpolated for any support, even a point-support, as will be demonstrated in this work. However, these aspects have not been addressed in most of the previously cited publications, with the notable exception of Séguret et al. (2014) and Séguret and Guajardo (2015).

In this context, the goal of this work is to present a geostatistical methodology to model directional geotechnical variables together with an application to the simulation of the linear discontinuity frequency in a Chilean copper deposit. The background and technical details of the proposed methodology are explained in Section 3.2 and the case study is presented in Section 3.3. Conclusions follow in Section 3.4.

3.2. Methodology

3.2.1. Representation of directional variables in a five-dimensional space

Consider a directional geotechnical variable *z* distributed in a region of the 3D Euclidean space and measured by borehole sampling. The values of this variable vary with the geographic coordinate of the measurement (center of gravity of the borehole core sample) and with its direction, that is:

$$z = \{z(\mathbf{x},\mathbf{u}): \mathbf{x} \in \mathrm{R}^3 \text{ and } \mathbf{u} \in \mathrm{S}^2\}, \quad (1)$$

where **x** is a vector indicating the in-situ position in the geographic space (R^3), while **u** is a vector on the unit 2-sphere (S^2) representing the in-situ direction of the sample. In a geostatistical context, the regionalized variable *z* is viewed as a realization of a random field *Z*:

$$Z = \{Z(\mathbf{x},\mathbf{u}): \mathbf{x} \in \mathrm{R}^3 \text{ and } \mathbf{u} \in \mathrm{S}^2\}. \quad (2)$$

The basis of the model, therefore, is to define that the regionalized variable and the parent random field in a five-dimensional space ($\mathrm{R}^3 \times \mathrm{S}^2$). The use of the product of a Euclidean space with a sphere is not new, as there is a growing interest, especially in remote sensing, climatology and atmospheric sciences, in modeling variables distributed over the planet Earth and evolving through time. Here, the 1D time axis is replaced with the 3D geographic space, a generalization that seems to be novel.

3.2.2. Spatial correlation modeling

In practice, some simplifying assumptions are necessary to infer and model the spatial correlation of regionalized data. In the case of data in the Euclidean space R^3, most often the random field is assumed to be second-order stationary, i.e., its first- and second-order moments exist and are invariant through translation (Matheron, 1971). Under such an assumption, the mean value of the random field is constant and the covariance between two random variables located at **x** and **x′**

depends only on the separation vector **h** = **x**′-**x**. A widespread approach to model the covariance function of a second-order stationary random field is the linear model of regionalization (Wackernagel, 2003), based on a positive linear combination of basic nested correlation functions:

$$C(\mathbf{h}) = \sum_{s=1}^{S_{\max}} b_s \, \rho_s(\mathbf{h}) \,, \tag{3}$$

where, for s = 1,… $S_{\max}$, $b_s \geq 0$ and ρ_s is a correlation function (positive semi-definite function taking the value 1 at **h** = **0**).

In the case of data on the unit sphere S^2, the simplest assumption is that of isotropy, i.e., the first- and second-order moments exist and are invariant under a rotation. In such a case, the mean value of the random field is constant and the covariance between two random variables located at **u** and **u**′ depends only on the angular separation (geodesic distance) δ(**u**,**u**′) = arccos(<**u**,**u**′>), where < , > denotes the inner product. Schoenberg (1942) proved that the covariance function of an isotropic random field on S^2 can be expanded into a positive linear combination of the following form:

$$C(\delta) = \sum_{n=0}^{+\infty} b_n \, P_n(\cos\delta) \,, \tag{4}$$

where P_n is the Legendre polynomial of degree n, $b_n \geq 0$ and $\sum_{n=0}^{+\infty} b_n < +\infty$.

A restriction on the isotropic models is needed in geotechnical applications, insofar as the borehole core sample taken along a direction **u** is the same as the one taken along the opposite direction -**u**. Changing **u** into -**u** amounts to changing δ(**u**,**u**′) into π-δ(**u**,**u**′), and P_n(cos δ) into P_n(-cos δ). To be invariant, the covariance model in Eq. (4) must therefore only consider the Legendre polynomials of even degrees, which are even functions, and discard the Legendre polynomials of odd degrees that are odd functions, i.e.:

$$C(\delta) = \sum_{n=0}^{+\infty} b_{2n} \, P_{2n}(\cos\delta) \,, \tag{5}$$

where $b_{2n} \geq 0$ and $\sum_{n=0}^{+\infty} b_{2n} < +\infty$.

The previous hypotheses can be combined for a random field defined in $\mathrm{R}^3 \times \mathrm{S}^2$, by considering second-order stationarity in the geographic space and isotropy on the sphere. Accordingly, the covariance function between two random variables located at (**x**,**u**) and (**x**′,**u**′) only depends on the separation vector **h** = **x**′-**x** and on the angular separation $\delta(\mathbf{u},\mathbf{u}') = \arccos(<\mathbf{u},\mathbf{u}'>)$. The linear model of regionalization can be extended in the following form:

$$C(\mathbf{h},\delta) = \sum_{s=1}^{S_{\max}} b_s\, C_s(\mathbf{h},\delta)\,, \tag{6}$$

where, for $s = 1,\ldots S_{\max}$, $b_s \geq 0$ and C_s is a correlation (positive semi-definite) function defined in $\mathrm{R}^3 \times [0,\pi]$. A simple family of such correlation functions are separable models of the form

$$C_s(\mathbf{h},\delta) = \rho_s(\mathbf{h})\,\rho'_s(\delta)\,, \tag{7}$$

with ρ_s a second-order stationary correlation function in R^3 and ρ_s' an isotropic correlation function on S^2 obtained by combining Legendre polynomials of even degrees. This model can be rewritten in terms of the variogram:

$$\gamma(\mathbf{h},\delta) = \sum_{s=1}^{S_{\max}} b_s\,\gamma_s(\mathbf{h},\delta)\,, \tag{8}$$

with $\gamma_s = 1 - \rho_s$. Given an experimental covariance or variogram, the fitting of a linear regionalization model can be done by choosing a suitable set of separable basic structures $\{C_s: s = 1\ldots S_{\max}\}$ and nonnegative coefficients $\{b_s: s = 1\ldots S_{\max}\}$. Automatic algorithms can be used to determine the model parameters that minimize the deviations between experimental and modeled covariances or variograms as is done in standard 3D geostatistics.

Models of the form (6) with separable basic covariances (Eq. 7) constitute a restricted – yet flexible – class of covariance models on $\mathrm{R}^3 \times \mathrm{S}^2$. More general models, not limited to sums of separable covariances, can be designed by extending to 5D the models presented by Porcu et al. (2016) in the case of sphere-time processes.

3.2.3. Conditional simulation

We now deal with the problem of simulating a random field with zero mean and covariance represented by a linear model of regionalization (Eqs. 6-7) and with multivariate normal finite-dimensional distributions (Gaussian random field model). The covariance matrix decomposition and the sequential algorithms can be used to this end, but these algorithms are not applicable, or become approximate, when the number of locations targeted for simulation is large (Chilès and Delfiner, 2012). Hereafter, we propose an algorithm that does not suffer from this limitation.

Without loss of generality, the model in Eqs. (6) and (7) can be rewritten as

$$C(\mathbf{h},\delta) = \sum_{s=1}^{S_{\max}} b_s \, \rho_s(\mathbf{h}) \, P_{2n(s)}(\cos\delta), \tag{9}$$

with $S_{\max} \in \mathrm{N} \cup \{+\infty\}$, $n(s) \in \mathrm{N}$, $b_s \geq 0$ and $b = \sum_{s=0}^{S_{\max}} b_s < +\infty$.

A random field with zero mean and such a covariance function can be simulated as follows (Appendix A):

1) Simulate a nonnegative integer S such that Prob$\{S = s\} = b_s/b$.
2) Simulate a second-order stationary random field T_S in R^3 with zero mean and correlation function $\rho_S(\mathbf{h})$.
3) Simulate an isotropic random field W_S on S^2 with zero mean and correlation function $P_{2n(S)}(\cos\ \delta)$, such that, conditional to $S = s$, W_s and T_s are independent.
4) Generate the simulated random field as

$$\forall \mathbf{x} \in \mathrm{R}^3, \forall \mathbf{u} \in \mathrm{S}^2, Z(\mathbf{x},\mathbf{u}) = \sqrt{b}\, T_S(\mathbf{x}) W_S(\mathbf{u}). \tag{10}$$

To obtain a random field whose finite-dimensional distributions are approximately Gaussian, it suffices to add and rescale a large number of independent copies of (10):

$$\forall \mathbf{x} \in \mathrm{R}^3, \forall \mathbf{u} \in \mathrm{S}^2, Z(\mathbf{x},\mathbf{u}) = \sqrt{\frac{b}{K}} \sum_{k=1}^{K} T_{S(k),k}(\mathbf{x}) W_{S(k),k}(\mathbf{u}), \quad (11)$$

where K is a large integer and $\{(S(k), T_{S(k),k}, W_{S(k),k}): k = 1,\ldots K\}$ are independent copies of (S, T_S, W_S). Many algorithms are available to simulate the random fields needed at steps 2) and 3), such as turning bands, discrete or continuous spectral algorithms (Emery and Lantuéjoul, 2006; Chilès and Delfiner, 2012) for T_S, and algorithms based on expansions into spherical harmonics (Lang and Schwab, 2015; Le Gia et al., 2019; Lantuéjoul et al., 2019; Emery and Porcu, 2019) or cosine waves (Emery et al., 2019.c) for W_S.

Under the multivariate Gaussian assumption, conditioning the simulation to a set of sampling data can be achieved classically by means of kriging (Chilès and Delfiner, 2012).

3.3. Case study

3.3.1. Data presentation

The previous concepts are now applied to the modeling of the discontinuity frequency (P_{10}) in the El Teniente porphyry copper deposit, located in the Chilean central Andes, approximately 70 km southeast to Santiago. The rock mass comprises several rock types, in particular a poorly mineralized breccia diatreme lying at the center of the deposit (Braden pipe), anhydrite breccias, felsic intrusive rocks (dioritic to tonalitic dacites and porphyries) and mafic intrusive rocks (gabbros, diabases and a mafic complex referred to as CMET, acronym for “Complejo Máfico El Teniente”) (Skewes et al., 2002, 2006).

Two types of discontinuities are observed in the mined primary ore: a system of wide-spaced faults (Skewes et al., 2006) and a stockwork of closely-spaced veins cemented with quartz, sulfides and anhydrite (Cannell et al., 2005) (Figure 3.1). El Teniente geologists and geotechnicians have observed that the latter, particularly the "weak veins" corresponding to veins and veinlets filled with a weak mineral assemblage (hardness less than 3 in the Mohs scale) and with a thickness greater than 1 mm, are the most important factors in explaining rock fragmentation, rock bursts and geomechanical instabilities in the mine (Brzovic and Villaescusa, 2007; Brzovic, 2009).

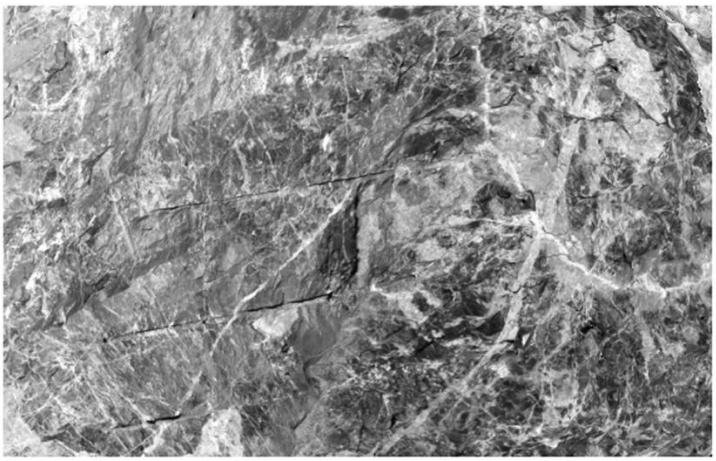

Figure 3.1. Stockwork of veins (white and light gray rectilinear or curvilinear structures) in the primary ore, which are less resistant than the intact rock and affect the rock mass strength

Geotechnical borehole data collected in the CMET rock between 2010 and 2016 are available for this study. The boreholes were drilled from the surface or from underground galleries and, for each of them, several intervals (with a length generally comprised between 20 and 30 m) were logged. The logging information consists of a record of the positions of the weak veins intersecting the borehole and the angles between their poles and the borehole axis. Based on this information, the linear frequency of weak veins P_{10} was calculated for 10-meter long composites along the boreholes, yielding a set of more than 3500 data within in a volume of 1800 × 2100 × 950 m^3 (Figure 3.2). For confidentiality reasons, the values were modified by a multiplicative factor and rounded to one decimal place, therefore they do not represent the true values used for geotechnical modeling in El Teniente deposit. The purpose of this case study is to illustrate the methodology proposed in Section 3.2 on modeling and simulating geotechnical variables by accounting for their directionality.

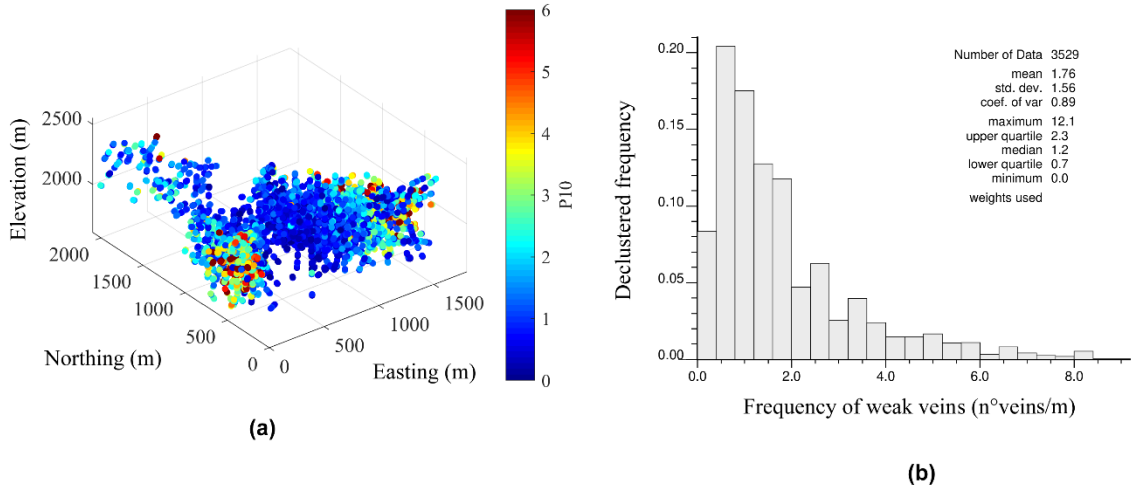

Figure 3.2. (a) 3D location map and **(b)** histogram of weak vein frequency of borehole data composited at a length of 10 m

3.3.2. Data modeling

The P_{10} composite data are declustered with the cell method (Journel, 1983) and then normal-score transformed. The mapping that back-transforms the normal scores into original P_{10} values (anamorphosis) is modeled by a piecewise linear function within the data range and an exponential function beyond the extremal experimental values (Figure 3.3) (Emery and Lantuéjoul, 2006).

The sample variogram of the normal scores data is calculated in the horizontal and vertical directions, which are the directions with the highest and lowest variability, respectively, for different separation angles (δ) between paired data (Table 3.1). Each data pair is weighted by the geometric mean of the declustering weights assigned to both data.

The behavior of the experimental variogram depends on the angular separation (δ) between the paired data used for variogram calculation. In particular, for geographic separation distances less than 100 m, the variogram increases with the distance if the paired data have an angular separation of 30° or less (Figure 3.4a, b), but decreases if the angular separation is greater than 60° (Figure 3.4c, d). This behavior at short distances is deemed representative, as the calculations involve a large number of data pairs (up to several hundreds).

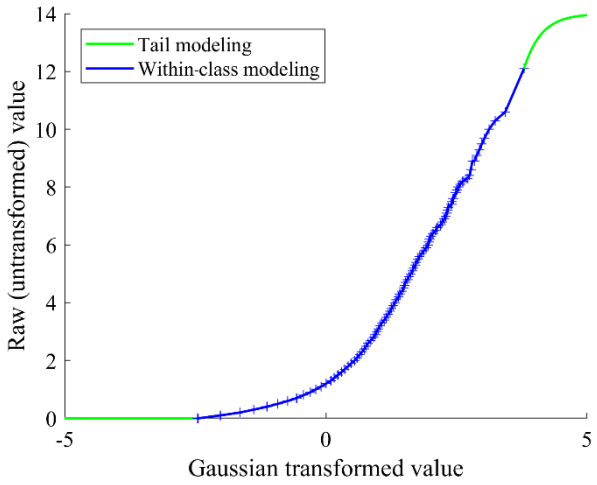

Figure 3.3. Gaussian anamorphosis giving the original P10 values as a function of their normal scores

Table 3.1. Parameters for experimental variogram calculations

	Horizontal direction	Vertical direction
Azimuth (°)	0	0
Dip (°)	0	90
Lag (m)	20	30
Number of lags	25	17
δ-angle between data (°)	0, 30, 60, 90	0, 30, 60, 90
Azimuth tolerance (°)	90	90
Dip tolerance (°)	20	20
Lag tolerance (m)	10	15
δ-angle tolerance (°)	15	15

A linear model of regionalization (Eq. 9) consisting of S_{max} = 4 nested structures is fitted to the experimental variogram. The first structure is defined by the product of a short-range (40 m in the horizontal plane and 60 m in the vertical direction) spherical covariance and a Legendre polynomial of degree 2. The latter switches from positive to negative values when the angular separation increases, which allows modeling the change in the behavior (from increasing to decreasing) of the variogram at short distances. The second nested structure is also defined by the product of a spherical covariance, this time with a range of 500 m, and a Legendre polynomial of degree 2. The last two structures consider the product of large-range spherical models with a Legendre polynomial of degree 0, which equals 1 irrespective of the angular separation, so that these two structures depend only on the geographic separation. The variogram model is superimposed on the experimental variogram in Figure 3.4 and its parameters are given in Table 3.2.

The negative values taken by the first two nested structures when the angular separation is large suggest that the weak vein stockwork is locally anisotropic, with (part of) the veins having approximately the same orientation, which may explain a negative correlation between measurements taken at the same geographic location along perpendicular directions (Appendix B). This behavior is not incompatible with a *global* isotropy assumption, insofar as the *local* orientation of the veins can vary in the geographic space so as to be, all in all, uniformly distributed on the unit sphere.

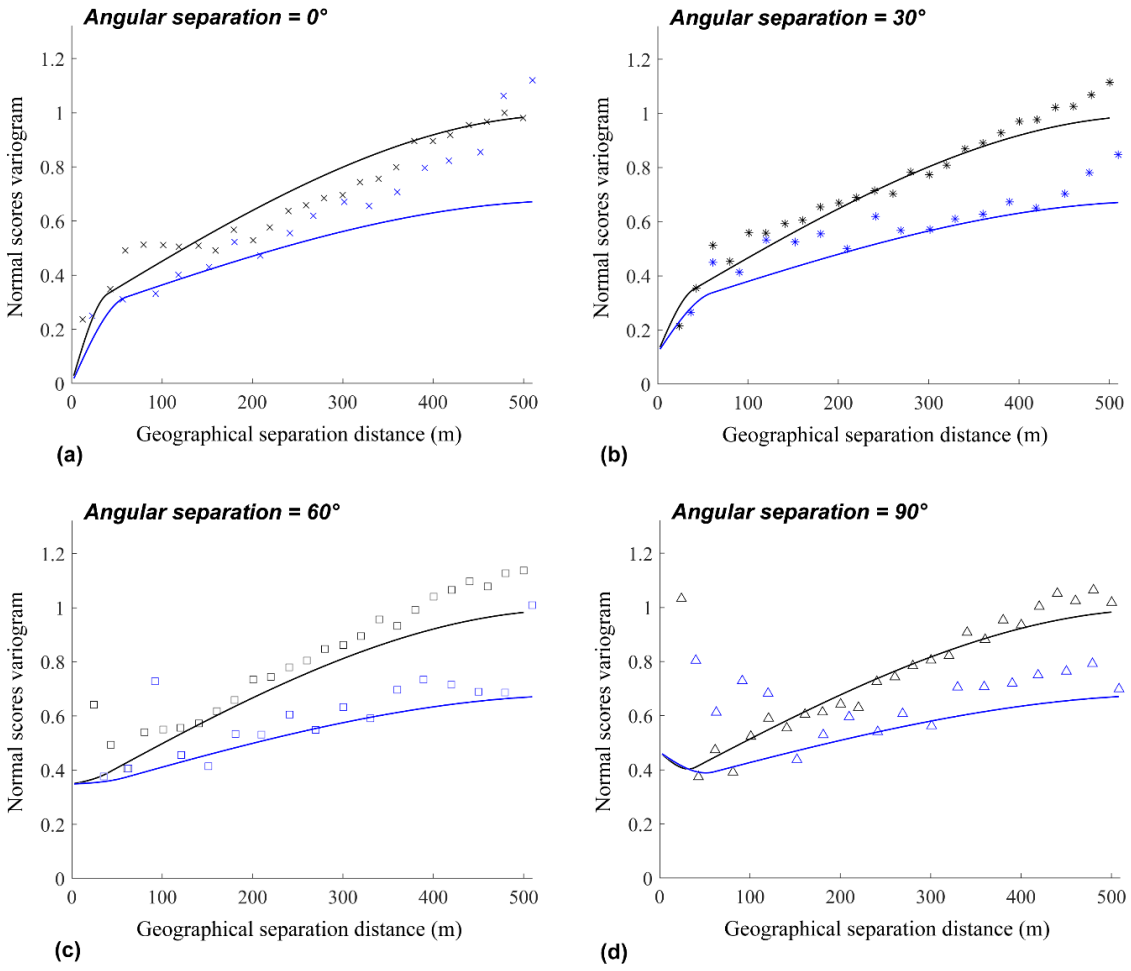

Figure 3.4. Experimental (crosses, stars, squares or triangles) and modeled (solid lines) variograms of the normal scores data in the horizontal (black) and vertical (blue) directions, for geographic separation distances ranging from 0 to 500 m and angular separations between paired data ranging from 0° (a) to 90° (d)

Table 3.2. Parameters of the fitted variogram model

Nested structure	Sill	Geographic component	Directional component			
		Type	Horizontal range (m)	Vertical range (m)	Type	Degree
1	0.25	spherical	40	60	Legendre	2
2	0.06	spherical	500	500	Legendre	2
3	0.25	spherical	500	500	Legendre	0
4	0.44	spherical	600	3000	Legendre	0

3.3.3. Conditional simulation

The weak vein frequency is simulated with the algorithm presented in Section 3.2.3, with K = 10,000 basic random fields as defined in Eq. (10), at the nodes of a regular grid covering part of the sampled region for three target directions: north, east and vertical. For k = 1,…, 10,000, the geographic component $T_{S(k)}$ is simulated by using a piecewise linear function (Emery and Lantuéjoul, 2006), whereas the directional component $W_{S(k)}$ is simulated by using a spherical harmonic (Appendix C). The computational complexity of this algorithm (number of required floating point operations) is directly proportional to the number of target grid nodes, which makes it extremely fast. Conditioning is done by using the dual form of kriging, allowing a unique neighborhood implementation. Maps of the first realization and of the average of one hundred realizations are depicted in Figure 3.5.

The average of the realizations is smoother in the southern sector of the grid, where the conditioning data are absent. Conversely, the northern part exhibits clear contrasts in the realization average, depending not only on the geographic position, but also on the direction in which the weak vein frequency is simulated. These contrasts are explained by the presence of nearby conditioning data.

3.3.4. Regionalized azimuthal projections

The proposed approach allows for interesting representations of geotechnical variables. Instead of mapping the geographic variations of the weak vein frequency for a few target directions, such as in Figure 3.5, one can map the directional variations for a few locations in the geographic space, e.g., via azimuthal projections in which the upper hemisphere of S^2 is represented on a disc, the parallels appearing as concentric circles and the meridians as line segments radiating from the center. These projections are helpful for the structural geologist or the geotechnician to assess both the geographic and directional regionalization of the weak vein frequency.

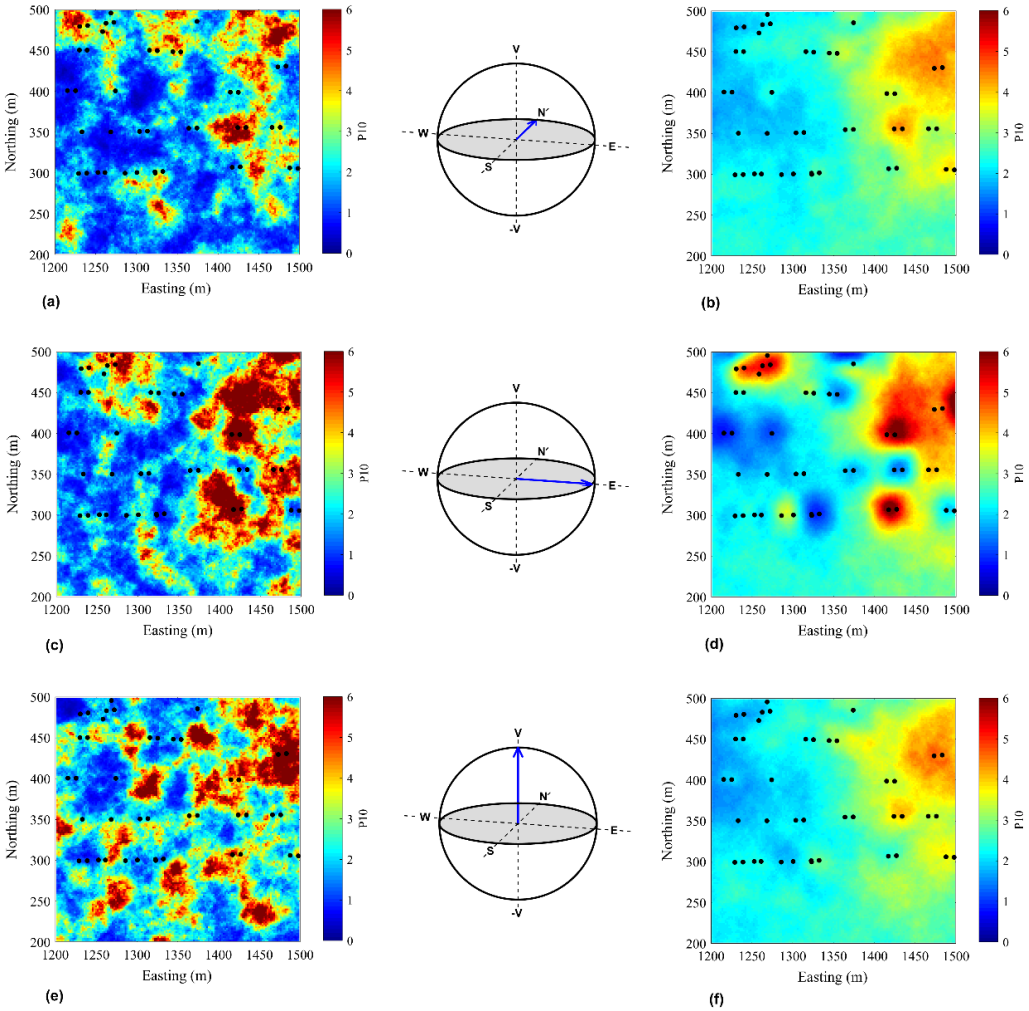

Figure 3.5. Map of (a, c, e) the first realization and (b, d, f) the average of 100 realizations of the weak vein frequency in the north (a, b), east (c, d) and vertical (e, f) directions. The target directions (N, E and V, respectively) are represented by a vector on the unit sphere in the central part of the figure. The target locations are on a grid located at 2000 m above mean sea level and the positions of the conditioning data distant less than 20 m from this grid are superimposed.

As an illustration, Figure 3.6 shows orthographic azimuthal projections at six regularly-spaced locations in the area under study. They suggest that the vein stockwork is locally anisotropic, with an orientation changing in the geographic space. Specifically, veins oriented in a vertical north-south plane are abundant near the locations with coordinates (1425 m, 400 m, 2000 m) and (1425 m, 300 m, 2000 m), for which the predicted weak vein frequency in the east direction is the highest, whereas they are scarce near the locations with coordinates (1425 m, 350 m, 2000 m) and (1325 m, 300 m, 2000 m).

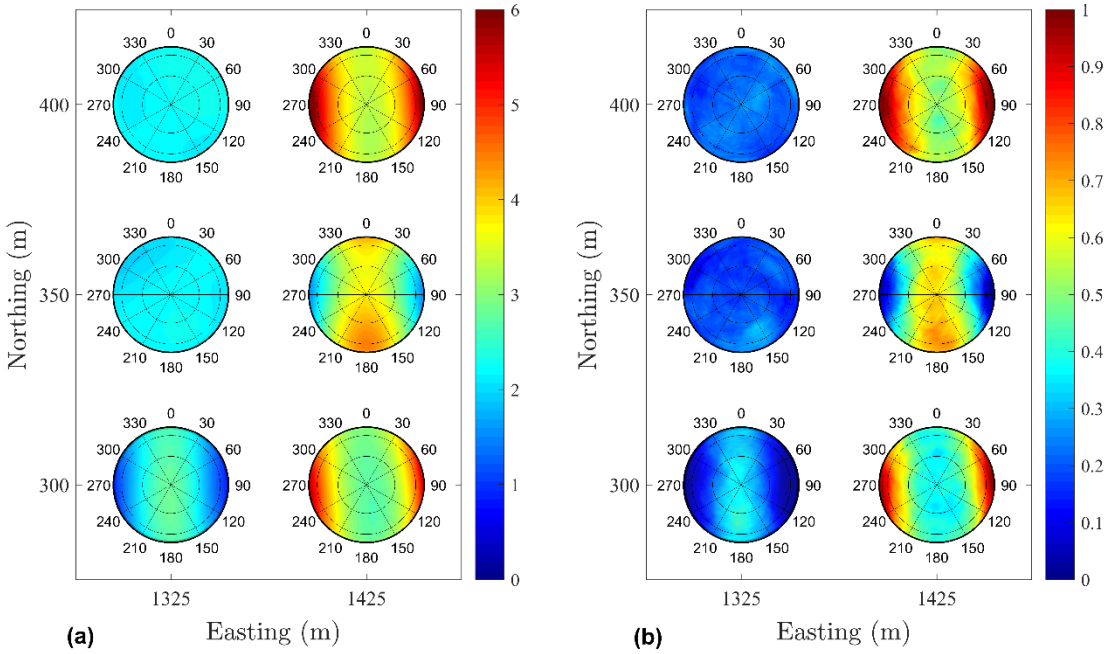

Figure 3.6. Regionalized azimuthal projections of (a) the average weak vein frequency over 100 realizations and (b) the probability that the true frequency is greater than 3 veins per meter. Each projection corresponds to a location in the geographic space, at an elevation at 2000 m above mean sea level, and uses a discretization of the northern hemisphere of S2 into 1800 pixels. Parallels and meridians every 30° are superimposed, and azimuths (measured clockwise in degrees from the north) are indicated outside the projection.

3.3.5. Checking the model hypotheses

The assumption that the random field associated with the weak vein frequency is second-order stationary in the geographic space is corroborated by the fact that

the experimental variogram of the normal scores data (Figure 3.4) reaches the expected unit sill.

The assumption of isotropy on the sphere is consistent with that of El Teniente geologists, who are not aware of any preferential direction of the vein stockwork, and with the illustration in Figure 3.1, which shows veins and veinlets distributed in various directions. It is possible to go further by using the original borehole logging information: for each observed vein, the angle α between the borehole axis and the pole of the vein has been recorded. Should the vein stockwork be isotropic, the pole of each vein would be uniformly distributed on the upper hemisphere of S^2, so that its scalar product with the unit vector oriented upward along a borehole would be uniform between 0 and 1, i.e., the cosine of the recorded angle α should be uniform in [0,1]. Because the records of α are semi-quantitative (most often, a multiple of 10°), the distribution of $\cos(\alpha)$ is calculated for five discrete classes (0 to 0.2, 0.2 to 0.4, until 0.8 to 1) and declustering weights are used to account for the irregular sampling design. The resulting histogram shows a reasonable agreement with a uniform distribution (Figure 3.7a).

Finally, the assumption of multivariate Gaussian distributions can be assessed by comparing the variogram $\gamma(\mathbf{h},\delta)$ and the variograms of order 1 and 0.5 ($\gamma_1(\mathbf{h},\delta)$ and $\gamma_{1/2}(\mathbf{h},\delta)$, respectively) of the normal scores data. For $\omega > 0$, the following relation should hold (Emery, 2005):

$$\gamma_\omega(\mathbf{h},\delta) = \frac{2^{\omega-1}}{\sqrt{\pi}}\Gamma\left(\frac{\omega+1}{2}\right)[\gamma(\mathbf{h},\delta)]^{\omega/2}. \qquad (12)$$

This relation, linear in a log-log scale, is reasonably verified by the experimental variograms (Figure 3.7b).

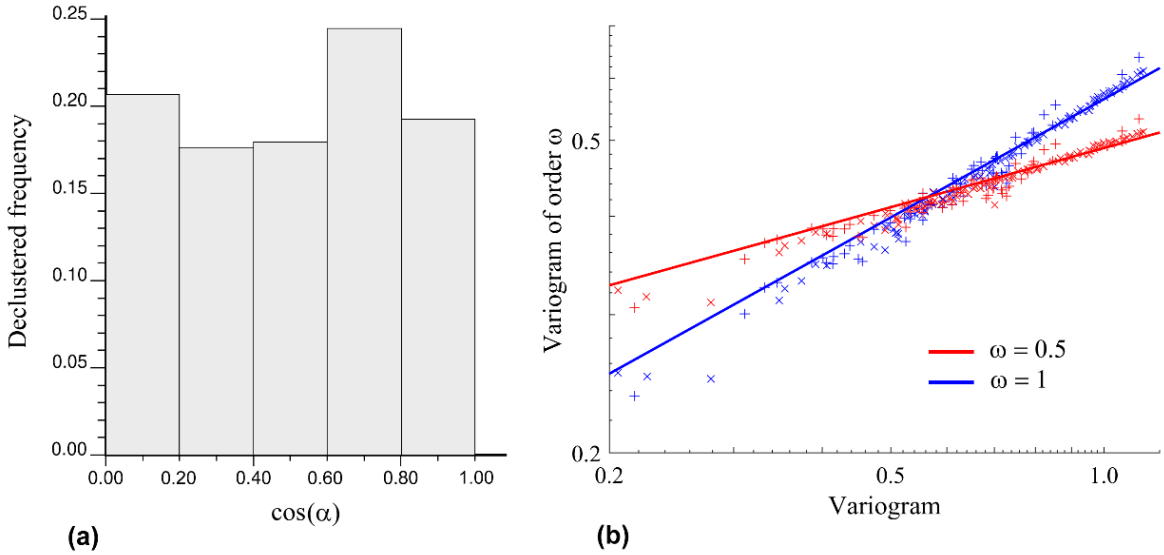

Figure 3.7. (a) Declustered histogram of cos(a), with a the angle between the vein pole and the borehole axis. **(b)** Variograms of order 1 (blue) and of order 0.5 (red) as a function of the experimental variogram of the normal scores data; the crosses indicate the experimental values, while the solid lines represent the theoretical relationship under a multivariate Gaussian assumption

3.3.6. Validation of the results

The quality of the realizations is assessed by leave-one-out cross-validation, consisting of simulating 500 times the weak vein frequency at each data location by using only the data situated at a distance of at least 20 m from the target location. The weak vein frequency at any data location is predicted by averaging the 500 realizations. The predictor so obtained is conditionally unbiased, and therefore also globally unbiased, as the regression of the scatter diagram between the predicted and true vein frequencies coincides with the 45° line (Figure 3.8a). On the other hand, for $p \in [0,1]$, a p-probability interval bounded by the 1-p/2 and 1+p/2 quantiles of the 500 simulated values is constructed at each data location. It would be expected that a proportion p of the sampling data should belong to such an interval (Deutsch, 1997), which is the case here, regardless the value of p between 0 and 1 (Figure 3.8b). This indicates that the fluctuations across the realizations correctly quantify the uncertainty attached to the true weak vein frequency.

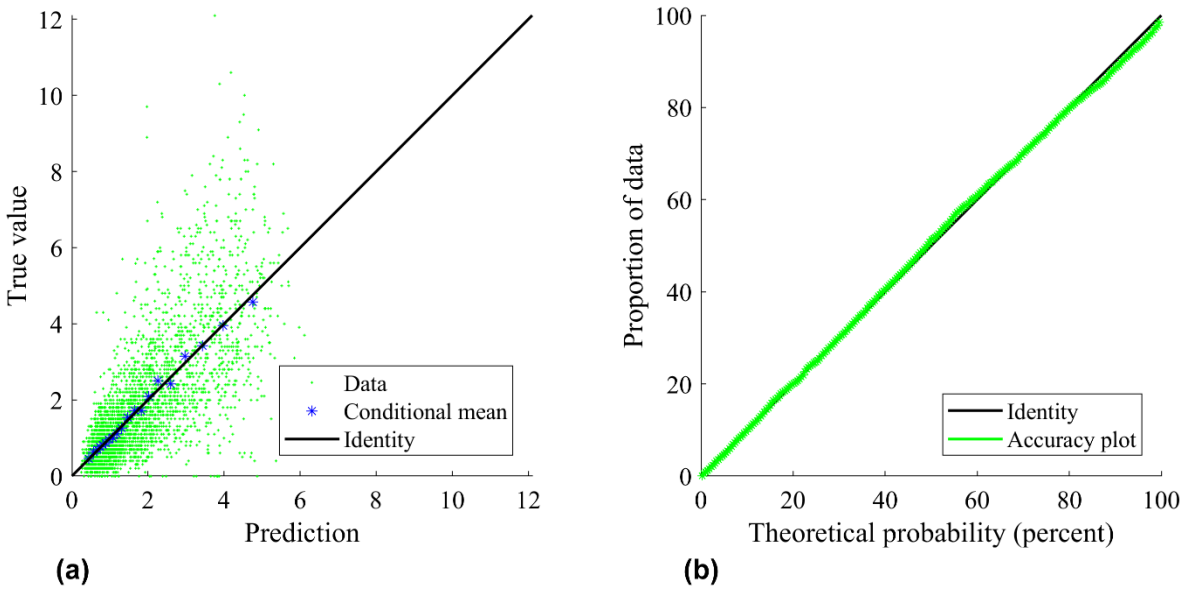

Figure 3.8. (a) Scatter diagram between the actual weak vein frequency (ordinate) at the sampling locations and the average of 500 realizations (abscissa) conditioned to the data distant at least 20 m from the target location. **(b)** Accuracy plot showing the proportion of data belonging to a probability interval as a function of the interval probability

3.3.7. Importance of a spatial correlation model that accounts for directionality

The impact of the directionality of P_{10} is assessed by mapping the simulated values that are obtained by using the "traditional" approach, in which the weak vein frequency is regionalized only in the three-dimensional geographic space, but not on the sphere (Figure 3.9a). In such a case, the results no longer depend on the target direction for measuring P_{10}. Furthermore, the average of 100 realizations (Figure 3.9b) is close to the map displayed in Figure 3.5d and is sensibly different from the values mapped in Figures 5b and 5f. This coincidence is an artefact, insofar as most of the boreholes in the area under study are close to horizontal and oriented in the east-west direction, as indicated by the positions of the composited data superimposed on the maps. The map in Figure 3.9b is therefore conditioned to the weak vein frequency observed in this particular borehole direction but is likely to be globally or conditionally biased for the vein frequency in another direction.

Even if the vein stockwork is isotropic, taking into account the directionality of the vein frequency has a strong impact on the simulation results because the

correlations between measurements depend on their directions. In particular, a measurement is highly informative of the values at surrounding locations in the same or quasi-parallel directions, as indicated by the low variogram values at short separation distances and small separation angles (Figure 3.4a,b), but brings much less information on the vein frequency in a perpendicular direction (Figure 3.4d).

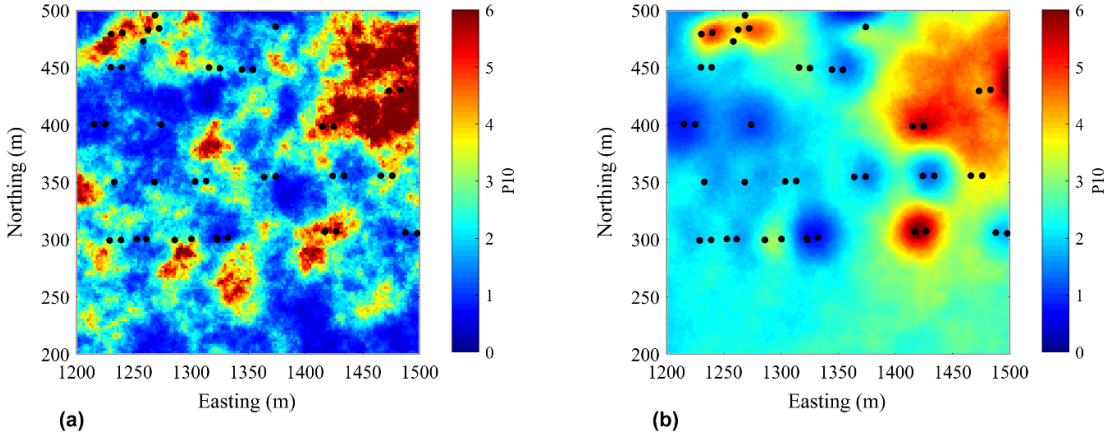

Figure 3.9. Map of (a) the first realization and (b) the average of 100 realizations of the weak vein frequency (simulation ignoring the directionality of P10). The target grid is located at 2000 m above mean sea level and the conditioning data distant less than 20 m from this grid are superimposed

3.4. Conclusions

The values of geotechnical variables such as *RQD*, *UCS*, *RMR*, *Q* and P_{10} measured on a borehole core sample depend not only on the in-situ geographic position of the sample, but also on its in-situ direction. Regionalizing such geotechnical variables in a 5D space ($\mathrm{R}^3 \times \mathrm{S}^2$) accounts for directionality. Under an assumption of stationarity in R^3 and isotropy on S^2, their spatial correlation structure depends only on the geographic separation vector **h** and on the angular separation δ between measurements, which facilitates the calculation of experimental covariances or variograms, the fitting of a model by means of separable nested structures, as stated in Eq. (9), as well as the simulation by means of products of basic random fields defined in R^3 and S^2, as stated in Eq. (11). The applicability of the tools and algorithms has been demonstrated with a case study on the modeling of the discontinuity frequency in El Teniente deposit, Chile, where attention has been paid

to the checking of the model assumptions and to the cross-validation of the simulation results.

As a complement to the standard tools used for the three-dimensional representation of regionalized variables, the proposed methodology provides new visualization tools for structural geologists and geotechnicians, such as regionalized azimuthal projections to map the directional variations of rock mass properties at given locations in the geographic space.

Future work includes the generalization of the proposed methodology to multivariate models aimed at jointly simulating cross-correlated geotechnical variables such as *RQD*, *UCS* and P_{10}. Also, the design of models and simulation algorithms using non-separable covariances in $\mathrm{R}^3 \times \mathrm{S}^2$ or anisotropic covariances in S^2, together with exploratory tools to identify preferred directions of anisotropy on the sphere on the basis of sampling information, is of utmost interest to broaden the scope of application of the presented proposal.

Appendix A

Consider the random field Z defined in Eq. (10). Conditional to $S = s$, Z is the product of two zero-mean independent random fields (T_s and W_s) and a positive scalar coefficient ($b^{1/2}$). Accordingly, its mean value is zero and its covariance function is b times the product of the covariances of T_s and W_s, i.e., $b\ \rho_s(\mathbf{h})\ P_{2n(s)}(\cos\delta)$. The prior mean and covariance function are obtained by randomizing s:

$$\forall \mathbf{x} \in \mathrm{R}^3, \forall \mathbf{u} \in \mathrm{S}^2, \mathrm{E}\{Z(\mathbf{x},\mathbf{u})\} = \sum_{s=1}^{S_{\max}} \frac{b_s}{b} \mathrm{E}\{Z(\mathbf{x},\mathbf{u}) \mid S = s\} = 0 \qquad (13)$$

$$\forall \mathbf{x}, \mathbf{x}' \in \mathrm{R}^3, \forall \mathbf{u}, \mathbf{u}' \in \mathrm{S}^2, \mathrm{E}\{Z(\mathbf{x},\mathbf{u})\, Z(\mathbf{x}',\mathbf{u}')\} = \sum_{s=1}^{S_{\max}} \frac{b_s}{b} \mathrm{E}\{Z(\mathbf{x},\mathbf{u})\, Z(\mathbf{x}',\mathbf{u}') \mid S = s\}$$
$$= \sum_{s=1}^{S_{\max}} b_s\, \rho_s(\mathbf{h})\, P_{2n(s)}(\cos\delta). \tag{14}$$

Appendix B

In the two-dimensional plane, consider a network of parallel discontinuities (Figure 3.10). Denote by $Z(\mathbf{x},\mathbf{u})$ and $Z(\mathbf{x},\mathbf{u}')$ the discontinuity frequencies for two composite samples taken at the same geographic position $\mathbf{x}$ along two perpendicular directions $\mathbf{u}$ and $\mathbf{u}'$. One has (Terzaghi, 1965):

$$\begin{cases} Z(\mathbf{x},\mathbf{u}) = Z(\mathbf{x},\mathbf{u}_0)\, |<\mathbf{u},\mathbf{u}_0>| = Z(\mathbf{x},\mathbf{u}_0)\, |\cos\alpha| \\ Z(\mathbf{x},\mathbf{u}') = Z(\mathbf{x},\mathbf{u}_0)\, |<\mathbf{u}',\mathbf{u}_0>| = Z(\mathbf{x},\mathbf{u}_0)\, |\sin\alpha| \end{cases} \tag{15}$$

where $\mathbf{u}_0$ is a unit vector in the direction of the discontinuity poles and α is the angle between $\mathbf{u}$ and $\mathbf{u}_0$.

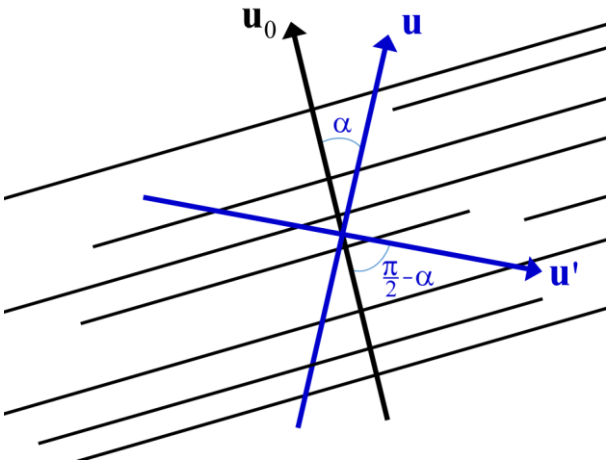

Figure 3.10. Network of parallel discontinuities in the plane (black) and two perpendicular sampling directions (blue)

In this case, the covariance between $Z(\mathbf{x},\mathbf{u})$ and $Z(\mathbf{x},\mathbf{u}')$ when $\mathbf{u}$ is uniformly distributed on the unit circle (α uniformly distributed between 0 and $\pi/2$) is found to be negative:

$$\operatorname{cov}\{Z(\mathbf{x},\mathbf{u})\,Z(\mathbf{x},\mathbf{u}')\} = \frac{1}{\pi}(1-\frac{4}{\pi})E\{Z^2(\mathbf{x},\mathbf{u}_0)\} < 0\,. \tag{16}$$

A high value for one of the measurements occurs when this measurement is taken along a direction close to $\mathbf{u}_0$, implying a low value for the measurement taken along the perpendicular direction.

Appendix C

For $\mathbf{u} \in S^2$, let $\theta(\mathbf{u}) \in [0,\pi]$ be its colatitude and $\varphi(\mathbf{u}) \in [0,2\pi[$ its longitude. For $n \in \mathbb{N}$, define the random field W_n as

$$\forall \mathbf{u} \in S^2, W_n(\mathbf{u}) = 2\sqrt{\pi}\,U\,Y_{n,L}(\theta(\mathbf{u}),\varphi(\mathbf{u}))\,, \tag{17}$$

where L is an integer uniformly distributed in [-n,n], U is an independent random variable with zero mean and unit variance (e.g., Gaussian), and $Y_{n,\ell}$ is the real (tesseral) spherical harmonic of degree n and order ℓ, which can be expressed as a function of an associated Legendre polynomial and sine or cosine functions (Arfken and Weber, 2005).

Because U has a zero mean and is independent of L, the expected value of $W_n(\mathbf{u})$ is zero. For $\mathbf{u}$ and $\mathbf{u}'$ on S^2, the covariance between $W_n(\mathbf{u})$ and $W_n(\mathbf{u}')$ is

$$\begin{aligned}\operatorname{cov}\{W_n(\mathbf{u}),W_n(\mathbf{u}')\} &= 4\pi\,\mathrm{E}\{U^2\}\,\mathrm{E}\{Y_{n,L}(\theta(\mathbf{u}),\varphi(\mathbf{u}))Y_{n,L}(\theta(\mathbf{u}'),\varphi(\mathbf{u}'))\} \\ &= \frac{4\pi}{2n+1}\sum_{\ell=-n}^{n} Y_{n,\ell}(\theta(\mathbf{u}),\varphi(\mathbf{u}))Y_{n,\ell}(\theta(\mathbf{u}'),\varphi(\mathbf{u}'))\,.\end{aligned} \tag{18}$$

The addition theorem (Arfken and Weber, 2005) therefore gives:

$$\operatorname{cov}\{W_n(\mathbf{u}),W_n(\mathbf{u}')\} = P_n(<\mathbf{u},\mathbf{u}'>) = P_n(\cos\delta(\mathbf{u},\mathbf{u}'))\,. \tag{19}$$

Accordingly, the random field W_n is isotropic on S^2, with zero mean and covariance function $P_n(\cos\delta)$, where δ is the geodesic distance on the sphere.

CHAPTER IV.

GEOSTATISTICAL MODELING OF ROCK QUALITY DESIGNATION (RQD) AND GEOTECHNICAL ZONING ACCOUNTING FOR DIRECTIONAL DEPENDENCE AND SCALE EFFECT

This chapter addresses the problem of simulating the rock quality designation (RQD) in a polymetallic deposit, coupled with a change of support that accounts for the direction dependence of RQD. The contents of this chapter have been published in Engineering Geology:

> Sánchez, L.K., Emery, X., Séguret, S.A., 2021. Geostatistical modeling of Rock Quality Designation (RQD) and geotechnical zoning accounting for directional dependence and scale effect. Engineering Geology, 293: article 106338.

Abstract

The characterization of rock masses is an essential component for the planning and development of engineering designs in rock mechanics and rock engineering. The Rock Quality Designation (RQD) is a widely used rock mass characterization system that is direction-dependent, i.e., the measurement of a core sample depends not only on the sample position but also on its orientation. This paper outlines the critical aspects of the determination of RQD and proposes a physically-based upscaling strategy from borehole samples to large blocks, based on block-averaging the RQD values corresponding to the same direction, then calculating the minimum value over all the directions. An anisotropy index indicating how much RQD varies between one direction, and another is also derived. Using geostatistical simulation, our proposal allows interpolating and upscaling direction-dependent geotechnical variables like RQD at any place in the geographical space for any direction, avoiding directional biases. We illustrate this proposal by predicting RQD in a polymetallic deposit, achieving geotechnical zoning and comparing the results with those of the traditional approach where the directional dependence of RQD is ignored.

Keywords: RQD; geostatistical simulation; geotechnical zoning; directional dependence; upscaling.

4.1. Introduction

Proper zoning or domaining of areas presenting similarities in the lithological, structural, hydrogeological and rock quality components is of utmost importance for successful geotechnical designs in mining, geological and geotechnical engineering. The strength and deformability parameters of rock masses and the nature of the discontinuity network constitute complex information whose incorporation into the definition of different geotechnical domains is challenging and still a subject of significant uncertainties (Barton, 1990; Hudson, 2012; Chowdhury et al., 2012) that

do not evade to the well-known RQD (Rock Quality Designation; Deere et al., 1967) classification system.

The RQD values are sensitive to the direction in which the core sample is collected (Palmström, 1982; Elsayed and Sen, 1991; Choi and Park, 2004; Emery and Séguret, 2020) and cannot be extrapolated straightforwardly to a more voluminous support, e.g., a three-dimensional block or the entire rock mass (Hoek and Brown,1980; Sen and Kazi, 1984; Cunha, 1990) without a proper management of the directional nature of the measurements. The directional dependence and the change of volumetric support (upscaling) are two critical aspects overlooked today by many practitioners, preventing a correct understanding of the spatial behavior of the rock mass and leading to inaccurate predictions.

The widely accepted practice of scaling the mechanical properties from a small piece of rock (e.g., a cylindrical borehole core, idealized as a 'line' support) to a three-dimensional 'block' support implies an assumption of isotropy (i.e., no directional dependence) of these properties at the working scale. Nevertheless, the geological materials often present spatial heterogeneities exhibiting a high contrast of the mechanical properties measured at two different locations, even at small distances (e.g., Cai, 2011; Song et al., 2011; Matonti et al., 2015; Pinheiro et al., 2016; Vatcher et al., 2016; Gao et al., 2018). Such a contrast may also vary with the relative angle between the measurements, being less when comparing two parallel borehole cores than when comparing two perpendicular cores. The integration of these subsurface variabilities into models to simulate the behavior of the rock masses would be theoretically the right way to go. Therefore, the predictive reliability of any model applied to rock engineering is strongly dependent on an accurate representation of the spatial and directional variability of the modeled variable(s). In this context, we propose to use a geostatistical model taking account of the directional sensitiveness of RQD to facilitate the upscaling from line-supports to block-supports and to obtain a better representation of the degree of jointing or fracturing of rock masses.

Geostatistical tools allow integrating spatial variability into the modeling of the rock mass. The application of geostatistics in geotechnics is not a new topic (e.g., Oh et al., 2004; Stavropoulou et al., 2007; Exadaktylos and Stavropoulou, 2008; Choi et al., 2009; Ferrari et al., 2014; Pinheiro et al., 2016; Chen et al., 2017; Hekmatnejad et al., 2017; Boyd et al., 2019). However, the traditional geostatistical modeling applied to RQD for characterizing rock masses (Ozturk and Nasuf, 2002; Ozturk and Simdi, 2014; Madani and Asghari, 2013) only considers its variability in the three-dimensional geographical space, disregarding its directional dependence, e.g., when there is a predominant joint set, such as foliation and schistosity joints in metamorphic rocks. This work aims to compare the traditional approach (ignoring directional dependence) with a new proposed approach considering the directional dependence of RQD, illustrated with a case study of a polymetallic deposit. The results will highlight the advantages of the latter approach in the geotechnical zoning, knowledge of the spatial behavior of rock masses, and management of uncertainties in underground projects. The background and details of the proposed methodology are explained in Sections 4.2 and 4.3 and Appendix A, whereas the case study is presented in Section 4.4. A discussion, conclusions, and perspectives for future work follow in Sections 4.5 and 4.6.

4.2. Background: directional dependence and upscaling of RQD

The RQD rating (Deere et al., 1967) provides a quantitative measure of the degree of jointing or fracturing of rock mass from boreholes, consisting of 100 times the ratio between the total length of core pieces larger than 100 millimeters and the total core run length. The RQD classification system uses a continuous scale ranging from 0 to 100 to assign the rock mass quality and position it within one of five classes (excellent, good, fair, poor, very poor). In addition to the direct RQD calculation method, indirect methods have also been developed to estimate RQD considering different input data (Priest and Hudson, 1976; Palmström, 1982, 2005; Zheng et al., 2018) and to incorporate it into rock classification schemes (Bieniawski, 1973; Barton et al., 1974; Hoek et al., 2013). However, already since its conception, there is an

awareness of one of its most obvious shortcomings: its directional dependence (e.g., Deere, 1989; Choi and Park, 2004). In the following, the directional dependence and upscaling will be described, providing details on how previous researchers have tackled them and how we will deal with them in our geostatistical model.

4.2.1. Directional dependence

The RQD values vary in space and according to the angle between the direction of the sample (borehole or scanline) and the discontinuities present in a rock mass. Since this directional dependence cannot be fixed, it is impossible to directly assess joint spacing conditions unless they do not depend on the direction (isotropic discontinuity network, whose properties are invariant under a rotation). Some attempts to minimize the biases caused by the directional dependence focused on drilling as many boreholes with different directions as possible (Deere, 1989), modifying the original RQD concept, such as estimating RQD from the volumetric joint count J_v (Palmström, 2005), considering Terzaghi's correction and a fractured zone effect (Haftani et al., 2016), or performing the calculation based on weak zones (core washed, crushed zones, karst cavities) and joint orientation (Azimian, 2016). However, an alternative definition of RQD is unknown to most engineers, practitioners, and researchers. Moreover, these new RQD conceptualizations lose their most potent and engaging property: simplicity. On the other hand, cost-efficiency and other practical considerations limit the number of boreholes drilled for an underground exploratory campaign.

An alternative solution to deal with RQD directional dependence has been proposed by Séguret and Guajardo (2015), who classified the borehole samples according to their sampling directions. However, this proposal does not circumvent all the limitations since RQD values can be predicted only in the directions that have been drilled, lacking any proper interpolation between them. Recently, Zheng et al. (2018) provide a new perspective about the directional dependence of RQD, considering this property as an advantage and proposing to estimate an anisotropy index of the jointing degree. The latter authors suggest selecting the minimum RQD value and its corresponding direction as the most representative of a specific rock

mass, which potentially reflects its real jointing degree and directly compares with other rock masses. However, this approach only applies to scanlines (in outcrops or excavation faces) with different orientations for the same location, in relatively intact rock masses (from medium weathered to fresh hard), and statistically homogeneous regions. Except for the case of an isotropic discontinuity network, the selection of a representative direction (here, the one corresponding to the minimum RQD) implies a loss of information on the directional behavior of RQD.

We build on the best of each previous attempt to propose an alternative solution that considers the real regionalization space of RQD as the usual geographical 3D space crossed by the 2D space of dip and azimuth. Specifically, the RQD for one composite sample depends on the geographical position $\boldsymbol{x}$ (x_1, y_1, z_1) of its gravity center and the direction $\boldsymbol{u}$ (α, ϕ) of the sample, with **u** a point of the unit sphere S^2 of R^3 characterized by its azimuth α and dip ϕ, see Figure 4.1 and Appendix A. This approach leads to the RQD measurements being assigned to five coordinates, which will allow evaluating the correlation between RQD values observed at different locations of this five-dimensional space (thus, depending not only on the geographical coordinates of the measurements but also on their angular coordinates).

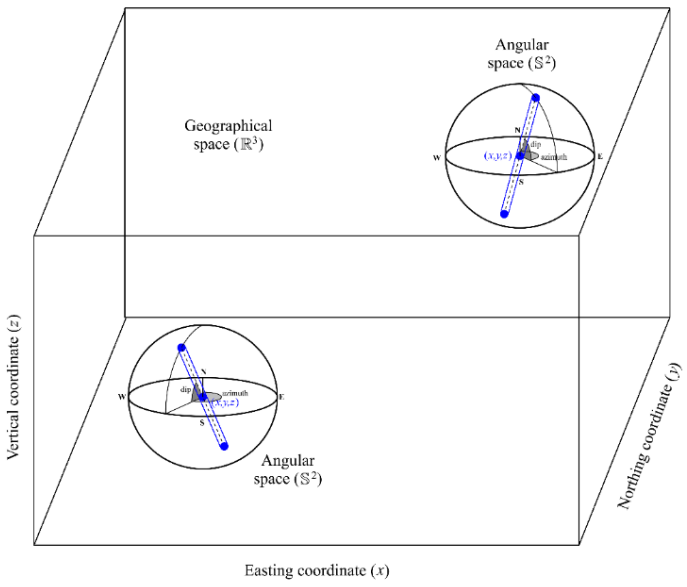

Figure 4.1. Geographical and angular spaces. Each core sample (blue cylinder) is indexed by the easting, northing and vertical coordinates of its gravity center in the geographical space, as well as its azimuth and dip in the angular space, totaling 5 coordinates. The measured RQD values depend on both the geographical and angular coordinates.

4.2.2. Upscaling

The dependence of the mechanical properties of a rock mass with the geometric dimensions of the sample is known as the scale or support effect (Bieniawski, 1968; Pratt et al., 1972; Bandis et al., 1981; Barton, 1990; Cunha, 1990; Cuisiat and Haimson, 1992). This effect is a potential drawback for the spatial interpolation of mechanical properties observed at a limited (in size) sample to the overall rock mass. Considering that RQD in line supports (at borehole core or scanline scale) has a directional dependence, this dependence should remain in any subsequent change of support. In particular, such a change of support should not mix RQD values measured along different directions unless the discontinuity network in the rock mass is isotropic, in which case directional dependence does not arise.

In practice, the support effect can be overlooked when a particular rock mass consists of purely intact rock or individual jointed block pieces are too small compared to the overall size of the engineering structure being considered. Hoek and Brown's criterion can thus be applied at the excavation/pit scale (Edelbro, 2004, Marinos and Carter, 2018). In such a situation, rock masses can be assumed as a continuum and isotropic medium, and the calculation of arithmetic averages from boreholes or scanlines (line-supports) to rock mass (block-supports) is justifiable (Marinos et al., 2005; Hoek, 2006). Then, when comparing the construction scale of rock excavations with the block size of intact rock, one can assume the rock mass is closely jointed and be treated as a homogeneous continuous equivalent whose discontinuities are implicit. However, such an assumption is not always possible and rarely occurs due to the nature of geological materials affected by tectonism, weathering, and alteration processes.

Our approach to addressing the support effect is twofold. On the one hand, it is proposed to define a direction-dependent upscaled RQD value in a given block by averaging the RQD values measured along the same direction at different points discretizing the block, without mixing values measured in different directions. In this way, it is possible to know the directional variability of RQD in each block, accounting for the anisotropy of the rock mass and giving insights into the geometry of the fragments formed by the intersection of joints in a rock mass. On the other hand, in

addition to this 'directional' block-support RQD, we will also propose a 'non-directional' block-support RQD by selecting the minimum RQD value (not the average) across all the directions of the two-dimensional angular space represented by a unit sphere, which is deemed the most representative value of the real jointing degree of the block. Accordingly, the 'directional' block-support RQD will be regionalized in the five-dimensional (geographical × angular) space, as is the RQD measured on core samples, while the 'non-directional' one will be regionalized only in the 3D geographical space.

4.3. Methodology: geostatistical modeling and simulation

Since it is defined on a continuous quantitative scale, RQD can be transformed into a variable (hereafter, denoted as Z) with a standard Gaussian distribution, a process known as Gaussian anamorphosis or normal-scores transformation (Chilès and Delfiner, 2012). Such a transformation is the first stage for geostatistical modeling, where the transformed variable (Z) is viewed as a Gaussian random field. In practice, the characterization of such a random field reduces to that of its mean value (here, the mean is set to zero) and its autocovariance function or, equivalently, its variogram.

To simulate RQD, the following steps should be accomplished (details in Appendix A):

I. The original RQD data are transformed into Gaussian data (normal scores), and an anamorphosis function that maps the RQD data into normal scores is defined.

II. A variogram analysis of the normal scores data is performed, consisting in computing an experimental variogram that measures half the variance of the increment between two measurements based on their geographical and angular separations when RQD is regionalized in a 5D space or just on their geographical separation when RQD is

regionalized in the 3D space. Subsequently, the experimental variogram is fitted with a theoretical model.

III. A Gaussian random field is simulated at all the target locations and conditioned to the available data. The latter implies that the simulated values at locations with data must coincide with the data values. Here, we use the turning bands algorithm (Matheron, 1973) for the random field simulation and a post-processing kriging (Chilès and Delfiner, 2012) for conditioning the simulated outcomes to the sampling data.

IV. The Gaussian simulation is back-transformed to the RQD original scale by using the anamorphosis function defined at step I.

4.4. Case study: jointed rock mass in a polymetallic deposit

To illustrate the proposed methodology and compare it with the traditional approach, we present a case study corresponding to an underground mining operation. The aims are to simulate RQD within the deposit, considering its directional dependence and a change of support that can adequately characterize a volumetric support and be used for geotechnical zoning.

4.4.1. Geological setting and data preparation

The case study corresponds to a polymetallic deposit, the name and location of which will not be disclosed for confidentiality reasons. In an irregular tubular body, the mineralization is of the distal skarn type, related to intrusives of intermediate composition, where the most frequent alterations are chloritization and skarn type. The ore zone mainly comprises skarn and limestones.

The deposit is located along a deformed belt composed of back-arc siliciclastic and carbonates rocks, unconformably covered with volcanic rocks, intruded by intermediate granodiorite and quartz-monzonite stocks and sills, the emplacement of which is structurally controlled by north-to-south-oriented faults. The structural evolution involves compressional reactivation of pre-existing extensional faults and

strike-slip episodes of deformation. Two main structural domains have been identified: an ENE-vergent fold-and-thrust system with steep dip angles (75° SE), while the second one is linked to dextral strike-slip movements with variable strikes and steep dips angles (60-80° SE). The discontinuities identified from geotechnical boreholes can be grouped into three main families, two sub-vertical and one sub-horizontal, the orientations of which corroborate the influence of the regional structural background at the ore deposit scale rock mass (Figure 4.2). Locally, sub-vertical and mid-dip secondary discontinuity systems also arise.

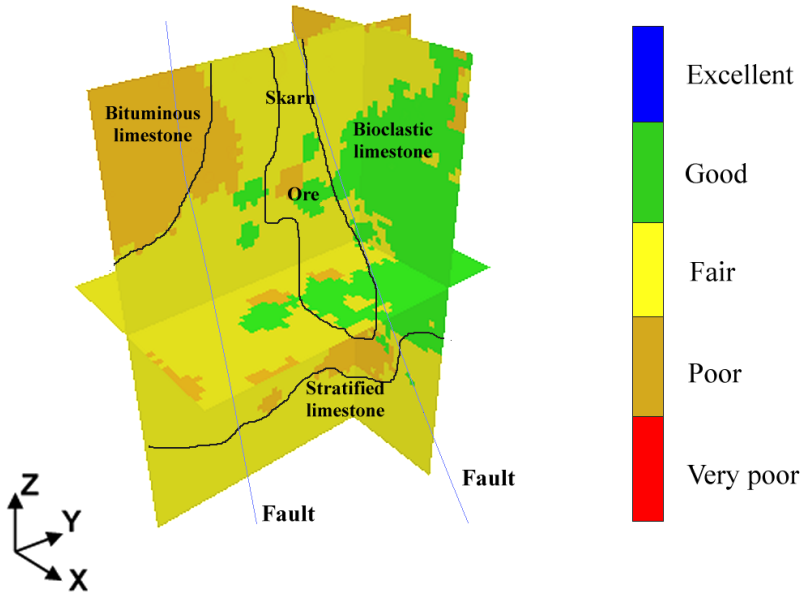

Figure 4.2. Block modeling of rock mass class (based on rock quality designation observed at 3800 core samples) in a volume of 350 m along the east direction, 500 m along the north direction, and 700 m along the vertical direction (polymetallic deposit). The classes can be associated with lithological and structural characteristics of the deposit.

The rock mass is stratified with a moderate weathering, the spacing of the strata being between 6 and 20 cm, with a persistence greater than 20 m, opening less than 1 mm without filling, except for a slime patina. The metamorphosed limestone rock mass is more competent than rocks of similar composition, but is more brittle, with a higher Hoek-Brown modulus value (mi = 14) compared with their unmetamorphosed parent carbonate rocks (mi = 12). The ore zone and its environment have rock mass qualities that generally range from fair to good (RMR between 50 and 75), except for localized fault zones where the rock mass quality is poor (RMR between 25 and 35). The water condition is humid and adversely

influences the stability of the underground excavations and can vary to wet due to water seepage in fault areas.

Boreholes have been drilled from the surface and from underground galleries, along which geologists have measured RQD and other geotechnical variables on intervals of lengths varying between 1 and 4 m. To model RQD, we calculated average values for 3 m long composites along the boreholes. The resulting database contains 3800 composited data with their locations (easting, northing, elevation, azimuth, dip) and rock quality designations. The sampled volume is about 350 × 500 × 700 m^3.

4.4.2. RQD modeling

As the distribution of RQD differs significantly from a Gaussian distribution (Figure 4.3), a normal score transformation (anamorphosis) is performed before variogram analysis and simulation. The transformation accounts for declustering weights calculated with the cell method (Journel, 1983), giving more importance to isolated data and downweighting clustered data to correct the effects caused by the irregularities of the sampling mesh.

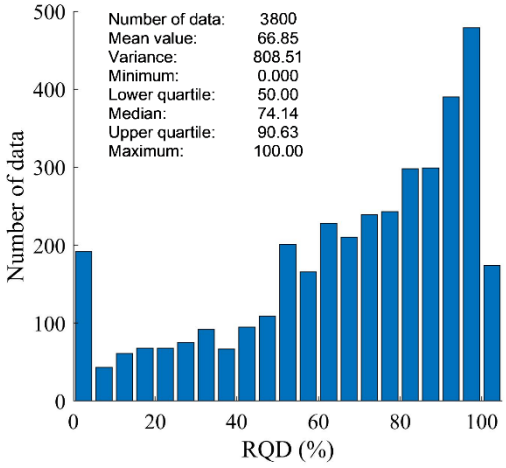

Figure 4.3. Experimental histogram of Rock Quality Designation (RQD) of borehole data composited at a length of 3 m.

We performed variogram calculations according to the parameters listed in Table 4.1 to identify preferential directions of continuity in the geographical space. The calculated variograms (Figure 4.4) show that no significant anisotropy in the geographical space exists for the normal scores data, be they regionalized in the 3D or the 5D space. The latter owes to experimental variograms calculated along different directions of the 3D space (with a fixed angular separation between paired data in the 5D approach) overlap to a great extent. Thus, henceforth, only omnidirectional variograms are calculated in the geographical space (Figure 4.5). The discontinuity observed at the origin ('nugget effect') is interpreted as a consequence of the small-scale variability of RQD, where continuity is not perceptible. On the other hand, it is also seen that the experimental variogram increases with the geographical separation distance and with the angular separation of the paired data until it reaches a sill at geographical separations of about 60 to 100 m. The better continuity of RQD (slower increase and lower sill) occurs when the angular separation between the measurements is low.

Table 4.1. Parameters for experimental variogram calculations

	Horizontal variograms	Vertical variograms
Azimuth (°)	0, 90, 0	0, 0, 0
Dip (°)	0, 0, 45	90, 0, 135
Lag separation (m)	10	10
Number of lags	45	45
Angular separation between data (°)	0, 30, 60, 90	0, 30, 60, 90
Azimuth tolerance (°)	90, 20, 90	90, 20, 90
Dip tolerance (°)	20	20, 90, 20
Lag tolerance (m)	5.0	5.0
Angular separation tolerance (°)	15	15

These experimental variograms of the 5D regionalized data are fitted by basic nesting models, each being the product of two components: a stationary geographical correlation and an isotropic angular correlation. The fitted variogram model is the following:

$$\gamma_{RQD}(\boldsymbol{h},\delta) = (0.19)nugget(\boldsymbol{h}) + (0.20)sph_{20,0}(\boldsymbol{h},\delta) + (0.35)sph_{40,0}(\boldsymbol{h},\delta) + (0.14)sph_{130,0}(\boldsymbol{h},\delta) + (0.10)sph_{130,2}(\boldsymbol{h},\delta) + (0.14)sph_{\infty,2}(\boldsymbol{h},\delta)$$

with $\boldsymbol{h}$ and δ being the geographical and angular separations between two measurements (Figure 4.4e), and $sphL_{a,n}(\boldsymbol{h},\delta)$ being one minus the product of an

isotropic spherical correlation with a range *a* evaluated at ***h,*** and a Legendre polynomial of degree *n* evaluated at cos(δ), see Eq. (A.4) in Appendix A.

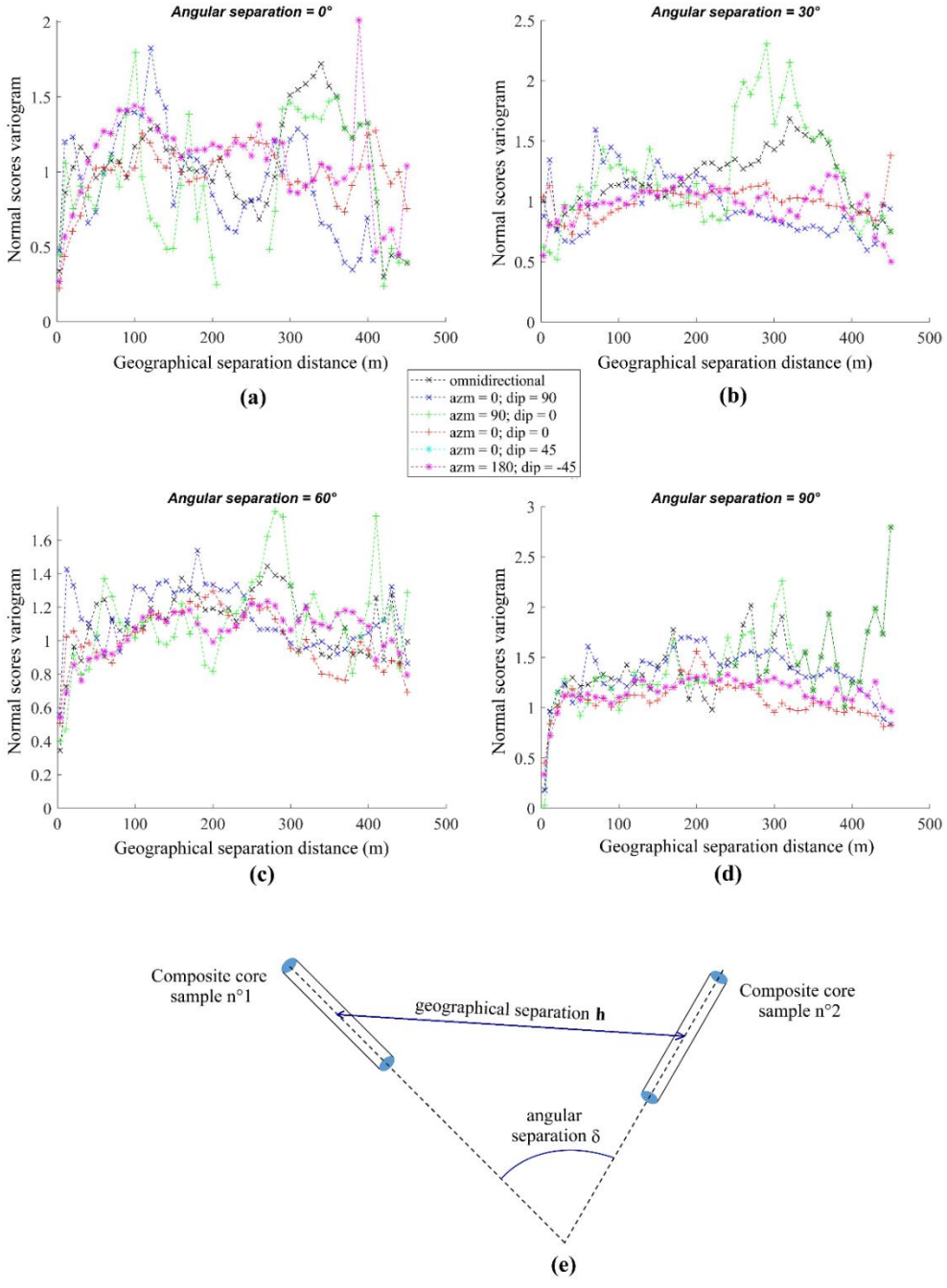

Figure 4.4. Experimental variograms of normal scores data in horizontal, vertical, and oblique directions, for geographical separations ranging from 0 to 500 m and angular separations equal to (a) 0°, (b) 30°, (c) 60°, and (d) 90°. The geographical separation measures the distance between the gravity centers of the paired samples, while the angular separation measures the difference between their orientations (e).

The variogram model for the 5D regionalized data fits quite well the calculated experimental points for all the different geographical and angular separations between paired data (Figure 4.5). The first milestone on the ordinate axis corresponds to the nugget effect, with a partial sill of 0.19. After that, one uses three nested structures corresponding to the product of a spherical covariance with a range of 20, 40, or 130 m and a zero-degree Legendre polynomial. The latter is identically equal to 1, so that the three nested structures exclusively depend on the geographical separation. Finally, two nested structures consider the product of long-range spherical covariances with a second-degree Legendre polynomial, varying with the angular separation. The use of a zonal anisotropy (spherical structure with an infinite range) and the fact that the second-degree Legendre polynomial changes from positive to negative values as the angular separation increases allow modeling the increase in the variogram sill with the angular separation.

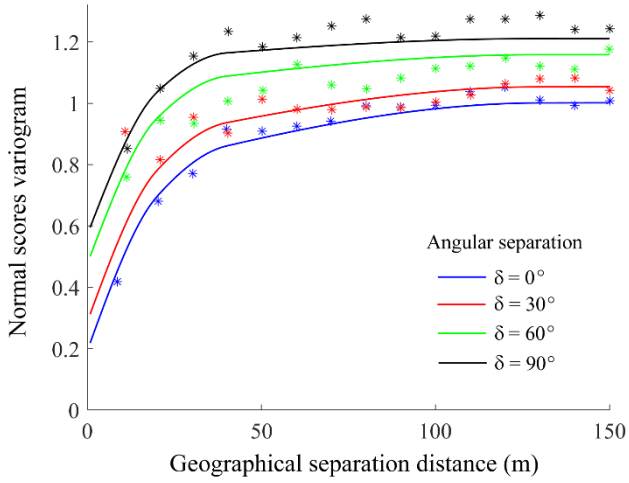

Figure 4.5. Experimental (asterisks) and modeled (solid lines) variograms of the normal scores data for geographical separation distances ranging from 0 to 150 m and angular separations between paired data ranging from 0° to 90°.

For the traditional approach (3D regionalized data), we consider only the basic nested structures that depend on the geographical coordinates, and the variogram model remains as follows:

$$\gamma_{RQD}(\boldsymbol{h}) = (0.19)nugget(\boldsymbol{h}) + (0.20)sph_{20,0}(\boldsymbol{h}) + (0.35)sph_{40,0}(\boldsymbol{h}) + (0.24)sph_{130,0}(\boldsymbol{h})$$

The proposed variogram models (for both the traditional and directional approaches) are validated using leave-one-out cross-validation techniques (Figure 4.6). The RQD at each data location is simulated 500 times conditionally to the neighboring data in a radius of 200 m, excluding the five adjacent composites from either side of the same borehole to avoid considering data too close to the target location. The outcomes of the 500 simulations are then averaged to obtain a prediction at the data location, which is compared against the true RQD value. The dispersion diagram between predicted and true RQD values for both approaches has a regression line that matches the first bisector (Figs. 6a, c), proving that the simulations are conditionally unbiased (Chilès and Delfiner, 2012). Furthermore, accuracy plots (Goovaerts, 2001) allow evaluating the capability of the 500 simulations to measure the uncertainty associated with the true values: the fraction of true values belonging to the *p*-probability interval is practically equal to *p*, whatever this probability is in [0,1] (Figs. 6b, d).

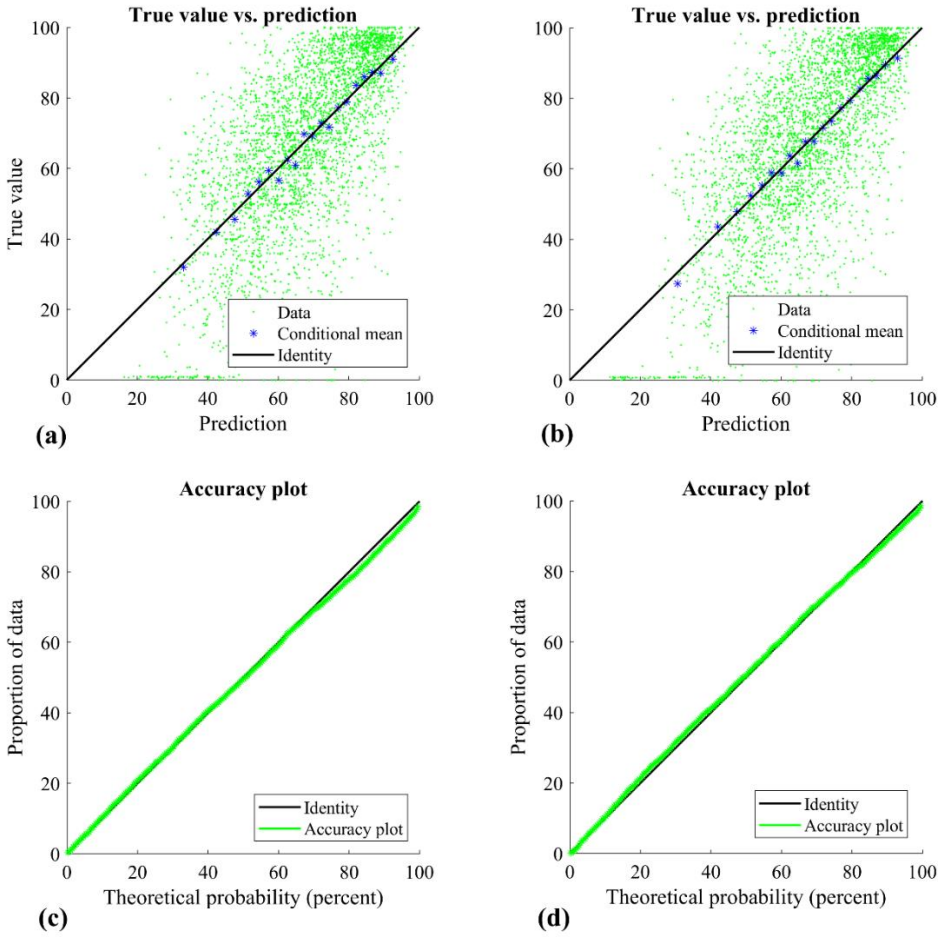

Figure 4.6. Leave-one-out cross-validation results: (a, c) scatter plots between true RQD (vertical axis) at the sampling locations and the average of 500 simulations (horizontal axis) conditioned to the data in a neighborhood of the target location (excluding the five nearest composites on either side of the same borehole), and (b, d) accuracy plots showing the proportion of data belonging to a probability interval as a function of the interval probability, (a, b) for traditional and (c, d) directional approaches.

4.4.3. Conditional simulation

Simulation is performed in the geographical space on a regular grid with a mesh of 2 m x 2 m x 20 m covering part of the sampled region, for three directions in the angular space: north, east and vertical. Five hundred simulations of RQD are constructed at each target grid node and direction. The maps plotted in Figs. 7 and 8 show a horizontal slice (43,750 nodes) at elevation 350 m above the mean sea level of the geographical space. The borehole data distant less than 10 m from the target grid (Figure 4.7) or less than 10 m from the target grid and 45° from the target direction (Figure 4.8) are superimposed, together with envelopes delimitating 'confidence regions' inside which the kriging error variance is less than 90% of the data variance (i.e., the borehole data are informative and significantly reduce the uncertainty inside the envelope). In the maps of the average of the 500 simulations, the most remarkable contrast in RQD is observed in areas where the borehole data are present for both the traditional (Figure 4.7b) and directional (Figs. 8b, d, f) approaches. This contrast is consistent with field information, according to which the rock mass quality is good (RQD > 75) in the eastern side of the sampled area, corresponding to the ore zone, and becomes regular (RQD < 50) in the western side.

For both approaches, the simulated RQD values vary from a poor (RQD ~40%) to an excellent (RQD >90%) rock quality in just a few tens of meters apart (Figs. 7a, 8a, 8c, 8e). The map for the average of the 500 simulations using the traditional approach (Figure 4.7b) shows a more significant similarity with the average map of the directional approach when RQD is simulated along the north direction (Figure 4.8b). This coincidence is an artifact since most of the boreholes in the study area are oriented sub-horizontally and mainly in a north-southeast direction, as corroborated by the superimposed borehole data on the maps.

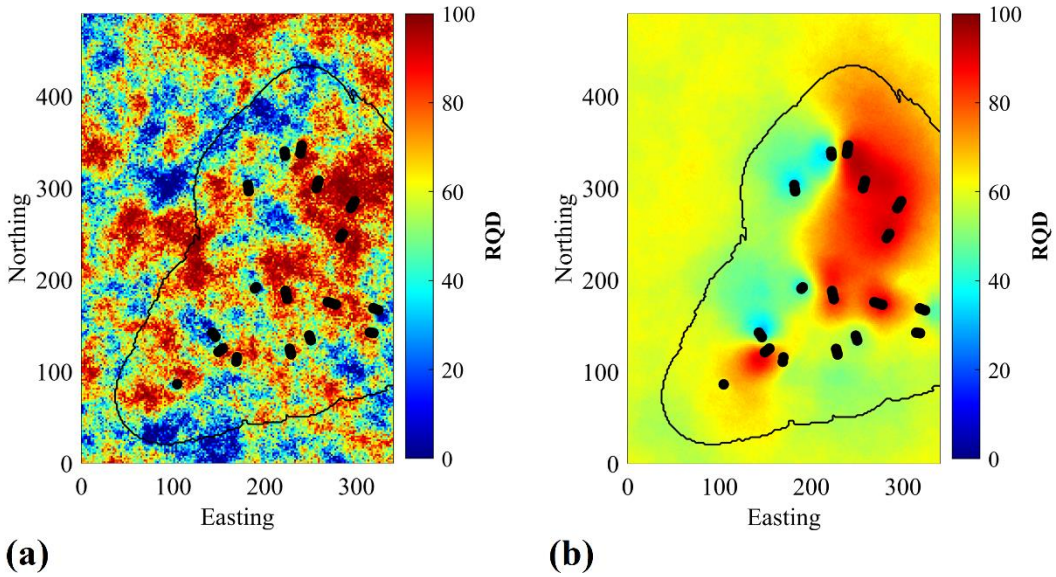

Figure 4.7. Simulation of RQD using the traditional approach (ignoring directional dependence and regionalizing RQD in the 3D geographical space only). (a) Map of the first simulation. (b) Map of the average of 500 simulations. Black dots correspond to the borehole data distant less than 10 m from the grid, and the contour represents the envelope of the kriging variance equal to 0.9 times the data variance.

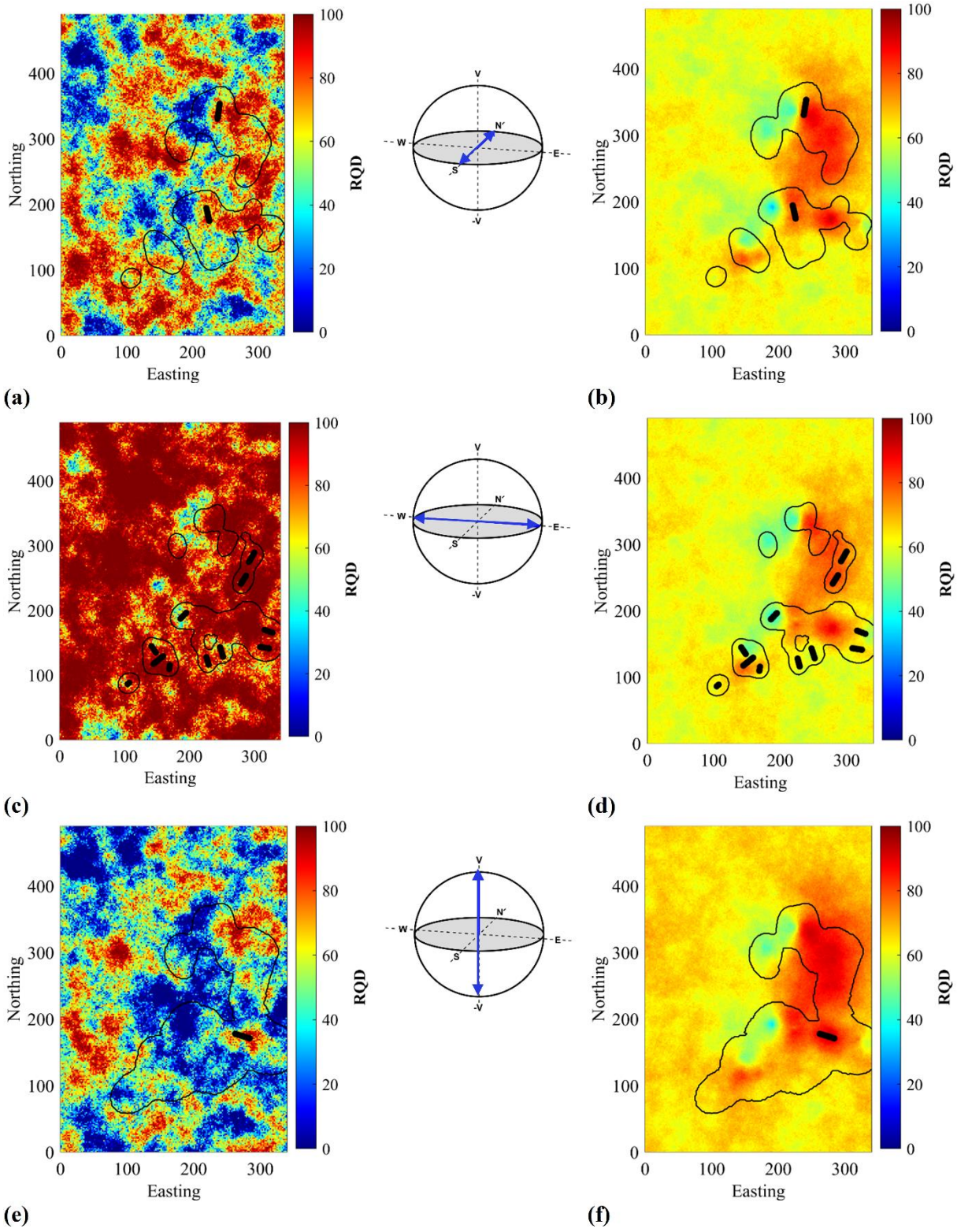

Figure 4.8. Simulation of RQD using the directional approach (regionalizing RQD in the 3D geographical space crossed with the 2D angular space). (a, c, e) Maps of the first simulation for (a) north, (c) east, and (e) vertical target directions. (b, d, f) Maps of the average by direction of 500 simulations for (b) north, (d) east, and (f) vertical target directions. Black dots correspond to the borehole data distant less than 10 m from the grid and 45° from the target direction. The contour represents the envelope of the kriging variance equal to 0.9 times the data variance.

Geologists and mining engineers could interpret very favorable conditions towards the east of the study area only based on Figure 4.7b (traditional approach), corroborating the influence of the major structural domains (ENE-vergent fold-and-thrust system with dip angle 75° SE, and dextral strike-slip movements with dips angles 60-80° SE). Even though it is true that a better rock quality is present in that sub-area, this interpretation is conditioned by the RQD values measured along a specific sampling direction, which is likely to be biased with respect to the RQD measured in other directions for the same area. The risk of bias is minimized when RQD is simulated along different directions using the directional approach, and one can be aware of the variations of RQD in the geographical space and the angular space. The good rock quality towards the east, evidenced in all the maps, above all along the vertical and north directions (Figs. 8b, d, f), can be confidently interpreted as the real behavior of the rock mass. The comparison between the simulation results in the absence or presence of a directional component allows visualizing the spatial variability to be expected in the field for a given direction. The latter is helpful in quantitatively define favorable conditions for the advance of the excavation from a quantitatively and non-qualitatively point of view, as is currently done in Bieniaswski's RMR classification.

4.4.4. Change of support (upscaling)

The change from the sample support (cylindrical borehole composite) to block support implies averaging simulated RQD values in the geographical space. However, it does not make sense to average RQD values associated with different directions. For the change of support to be meaningful, a single direction has to be chosen, and all the RQD values being averaged should correspond to this direction. In the traditional approach, the selection of an appropriate direction to conduct a change of support is a challenge, insofar as it is necessary to find a 'representative' direction for (a) measuring RQD and (b) averaging the RQD values on the block: otherwise, one calculates a non-directional block-support RQD value that mixes different directions (Figure 4.9, right panel). In the proposed (directional) approach, the problem is solved straightforwardly by defining as many block-support RQD as directions of interest, with no need for the data to be measured along the same

direction because RQD can be simulated for each geographical coordinate and each direction (Figure 4.9, top left). The regionalization in a 5D space (left panel) therefore allows calculating a directional RQD. All the calculations can be made on each simulation separately or averaged over the 500 simulations to obtain a prediction.

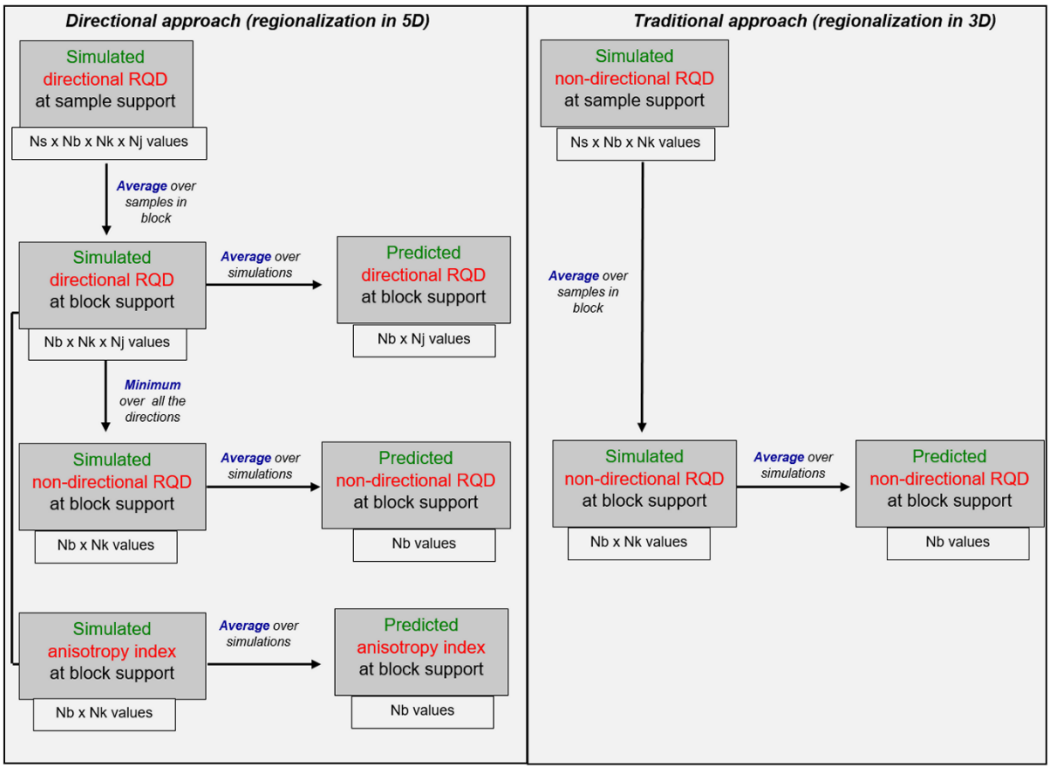

Figure 4.9. A synthesis of the different upscaling proposals. Ns stands for the number of samples per block, Nb for the number of blocks in the geographical space, Nk for the number of simulations, and Nj for the number of directions in the angular space.

If a block has to be characterized by a single RQD value, the minimum RQD over all the directions should be considered, which leads to a 'non-directional' block-support RQD (Figure 4.9, middle left). In such a case, the change of support is essentially non-additive as it relies on a minimum and not an average over the directions. Since the use of a single RQD value to represent the degree of jointing or fracturing in a block is less informative than a direction-dependent RQD (given the high variability in the angular space), we propose to complement the non-directional (minimum) RQD with an anisotropy index (AI) of jointing degree for rock masses, following Zhen et al. (2018). The AI measures the spread or dispersion of the RQD for each block within the angular space. In this work, the AI of the jointing degree is defined for each block and each simulation as one hundred times the difference between the maximum and minimum RQD values across all the directions, divided by the maximum RQD value (Figure 4.9, bottom left):

$$AI = 100\left(\frac{RQD_{max} - RQD_{min}}{RQD_{max}}\right).$$

Figure 4.10 shows that the anisotropy index is between 30% to 80%, with a marked contrast in the eastern part of the map close to the sampled area. This anisotropy of the jointing degree for the rock mass (directional variability of RQD) is not negligible and cannot be detected when RQD is regionalized in the three-dimensional geographical space and the directional component is discarded (i.e., using the traditional approach).

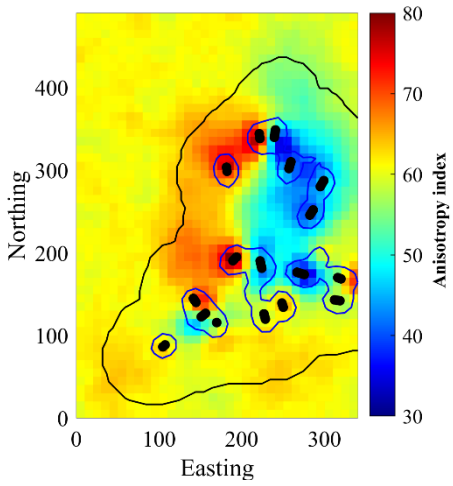

Figure 4.10. Map of anisotropy index (AI) of jointing degree using the directional approach (average index over 500 simulations). The blue contour represents the envelope inside which the kriging variance in all the directions is less than 0.9 times the data variance (intersection of the directional envelopes as defined in Figure 4.8). The black contour represents the envelope inside which the kriging variance in at least one direction is less than 0.9 times the data variance (union of the directional envelopes as defined in Fig. 8). Both envelopes enclose 'confidence regions' in which the borehole data are informative.

In addition to the minimal RQD over all the directions (as the representative value of a block) and the anisotropy index (indicating how much RQD varies from one direction to another), one can identify the direction for which the minimal RQD is reached. This direction sheds light on the anisotropy of the discontinuity network in the rock mass and on the existence of preferential fracturing directions, as in the Terzaghi concept (Zhen et al., 2018) (the minimum RQD is expected to occur along the direction perpendicular to the fracture planes). Such an analysis can be made locally (for a single block) or for a group of blocks. As an illustration, Figure 4.11 is an azimuthal projection of the upper hemisphere of an equal-angle polar net (Priest, 1985) showing the directional concentration for the minimum simulated RQD at a

regular grid of the geographical space (1,750 blocks) and 100 directions spanning the space at intervals of 36° and 18° in azimuth and dip, respectively, where the gray dots represent the sampling directions. On average, the RQD rating decreases by 20.66% when considering the direction of the minimum value per block due to its directional dependence. The minimum RQD is more frequently reached along directions of azimuth between 330° to 350° and dip between 30° and 45°, or directions with azimuth between 285° and 315° and dip between 30° and 45°. The latter suggests that the fracture planes tend to be sub-horizontal to oblique with a northwest-north direction, similar to the orientation of the parallel structural domain (NW-SE).

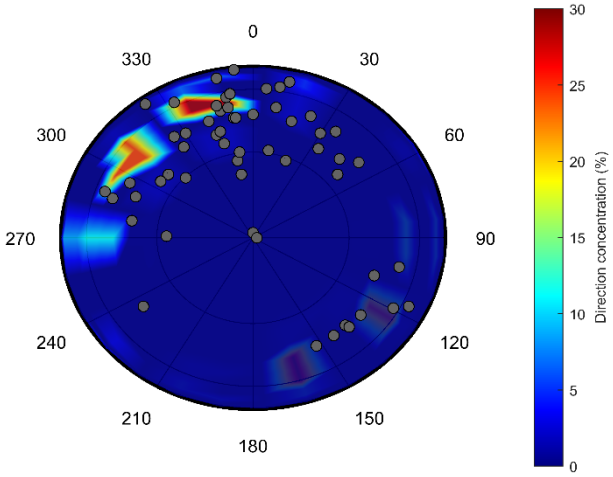

Figure 4.11. Upper hemispherical equal angle polar projection net or regionalized azimuthal projection showing the concentration of the directions for which the minimum block-support RQD is reached. Calculations consider 500 simulations and 1,750 blocks of 10 × 10 × 20 m in a horizontal section of the geographical space. The sphere is discretized into 100 directions. Concentric circles represent the dip/plunge each 30°, increasing from outside and azimuths measured clockwise in degrees from north indicated in the out end the projection. The grey dots correspond to the sampling directions of the borehole data.

RQD can be predicted at the block support by averaging the simulated RQD over many scenarios, as shown in Figs. 7 and 8 for the composite support. When the results of the 3D traditional approach (Figure 4.12a) are compared with those using the directional approach (Figure 4.12b-f), several differences arise, highlighting the influence of the directional dependence of RQD in the geomechanical zoning of the rock mass. In essence, Figure 4.12a bears more resemblance to Figure 4.12e, where RQD is simulated along the north direction, than to Figure 4.12e and 12f corresponding to RQD simulated along the east and vertical directions. This reveals a bias of the RQD predicted with the traditional approach, conditioned to particular

sampling directions, and cannot be extrapolated to other directions. In contrast, the directional block-support RQD (Figure 4.12d-f) is more informative and helpful for geotechnical designs and rock mass rating or geotechnical zoning. Since it is an unbiased representation for a specific direction, it can evaluate the impact of the advance of the rock excavation in this direction in rock mass mechanical behavior.

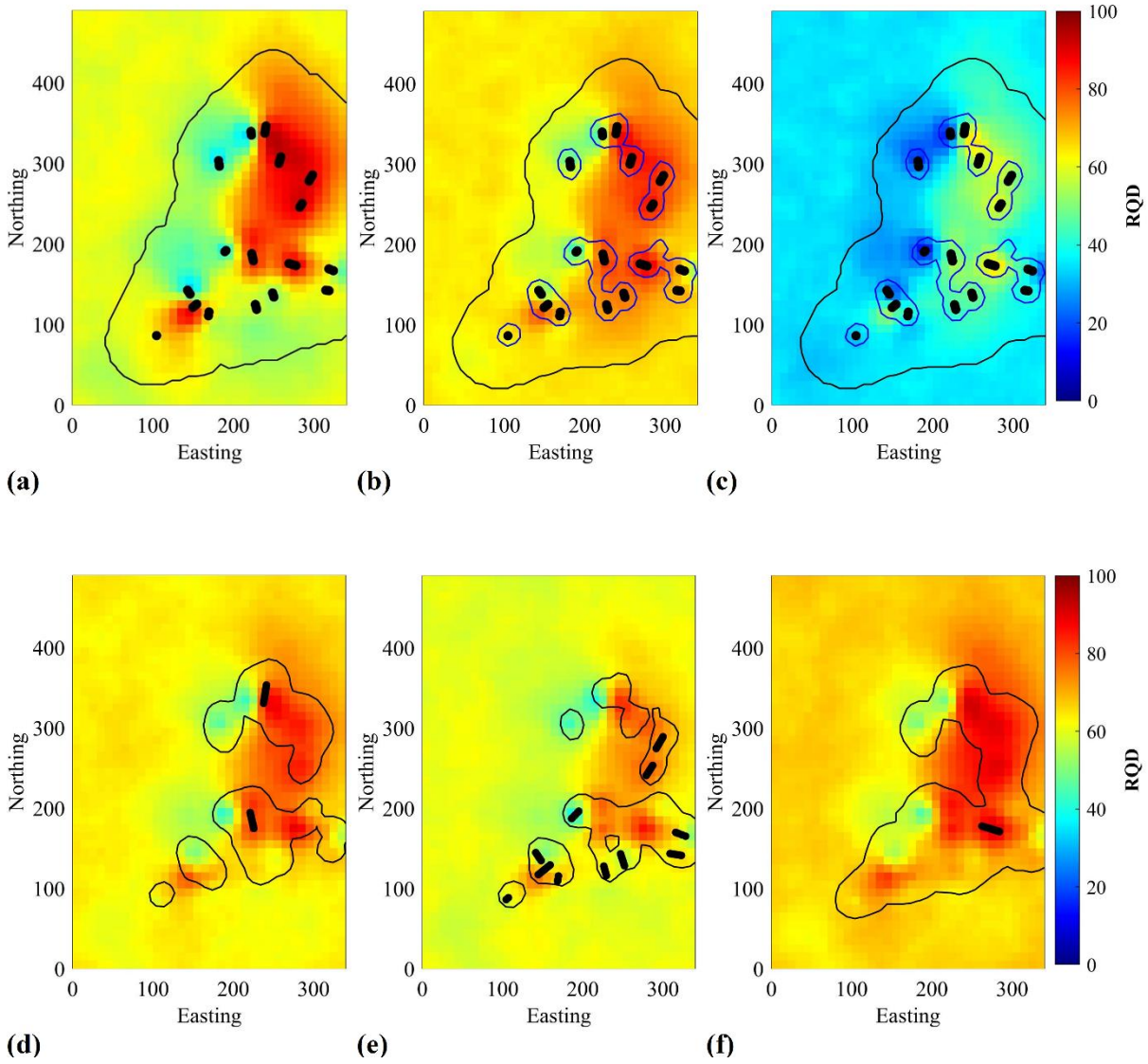

Figure 4.12. Map of the average of 500 simulations of block-support RQD obtained with the (a) 3D traditional approach and with the directional approach; (b) average block-support RQD over all the directions; (c) minimum block-support RQD over all the directions; directional block-support RQD along the (d) north, (e) east and (f) vertical directions. The maps in (a) and (b) mix different directions and do not have a clear physical meaning, while the maps in (c-f) only refer to a single direction per block (most conservative direction in (c), which may vary from block to block, and fixed direction in the other maps).

To exemplify the impact of directional RQD modeling in engineering decision-making, consider a tunnel bored along the north-south direction with a width of 30 ft (9.4 m) in an igneous/metamorphic rock, typical in the study area, where real rock pressures or swelling/squeezing ground do not exist. According to the rock support classification system based on RQD for tunnels of varying widths (Deere, 1989), either steel sets or reinforced shotcrete or RIB is compulsory almost everywhere if one relies on the RQD corresponding to the worst-case scenario for each block (Fig 12c), which may be too pessimistic. In contrast, based on the directional block-support RQD associated with the tunnel direction (north-south) (Fig 12d), only a pattern bolting (4-6 ft centers) or a 4-6 cm shotcrete is required in the eastern side of the area under study. On the other hand, considering the RQD models obtained with the traditional approach (Figure 4.12a) or with the average scenario (Fig 12b) (average RQD over all the directions and all the simulations) gives a misleading representation of the actual rock quality in the eastern part, with a minimal requirement (no support or local bolts, which is too optimistic).

4.4.5. Geotechnical zoning

The lithological characteristics and the degree of alteration are homogeneous in the studied area; therefore, the rock mass quality is the most relevant criterion for its geotechnical zoning. Our results on the upscaled RQD may conveniently be integrated into widely used rock mass classification systems, such as the RMR and its modifications (Bieniawski, 1973, 1989; Hoek et al., 2013; Bertuzzi et al. 2016), the Tunneling Quality Index (Q; Barton et al., 1974) and the Geological Strenght Index (GSI; Marinos and Carter, 2018). Following Deere et al. (1967), we relate our simulated block-averaged RQD value with the engineering rock mass quality and implement a geotechnical zoning map (Figure 4.13). For each block and each simulation, the simulated block-support RQD is assigned one of five classes (excellent, good, fair, poor, very poor), then the class that most frequently appears across the 500 simulations is retained as the final classification of the block.

The zoning maps so obtained strongly differ, depending on whether one considers the non-directional RQD calculated with the traditional approach (Figure 4.13a), or the average (Figure 4.13b) or the minimum (Figure 4.13c) RQD over all the directions calculated with the proposed approach. The former approach ignores the directional dependence of RQD and mixes measurements made in different drilling directions. Therefore, the map in Figure 4.13a lacks physical sense, where the primary class is a fair quality rock, with 85% of the blocks, followed by a good quality rock with 8%. The remaining are between poor (3.7%) and excellent (3.3%). A similar mixing arises with the map in Figure 4.13b: although RQD is regionalized in a 5D space, the simulated values are then averaged over all the directions, yielding zoning similar to the traditional approach (poor 0.3%, fair 88.1%, good 11.5%, and excellent 0.1%). In contrast, the map in Figure 4.13c only considers the 'worst' direction for each block (the one associated with the lowest RQD) and yields a more conservative definition of the geotechnical domains, where almost three-quarters of the blocks are classified as poor to fair rock (73.4%) and the rest as very poor. This is the price to pay to get geotechnical zoning that is non-directional and, at the same time, physically meaningful.

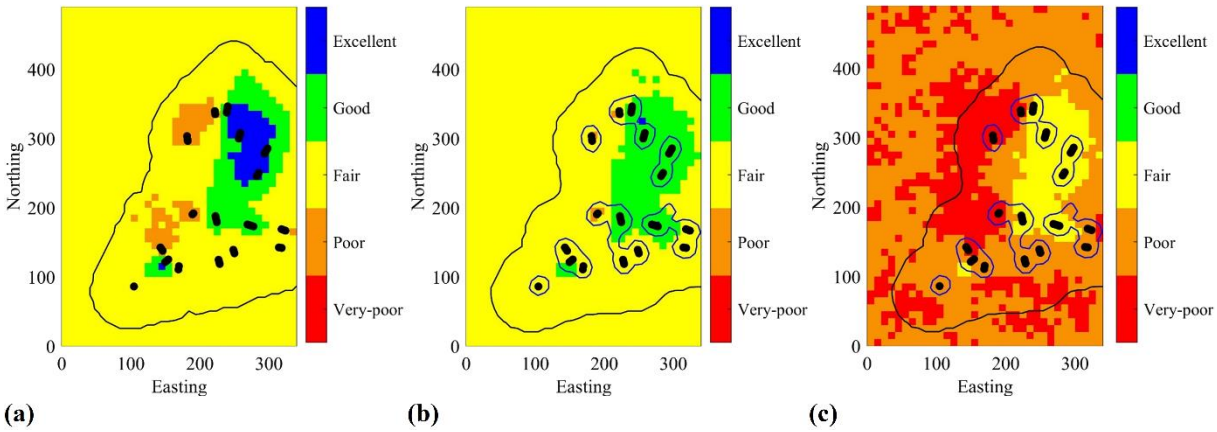

Figure 4.13. Geotechnical zoning map using block-support (upscaled) RQD. (a) The most probable class is based on 500 simulations obtained with the traditional 3D approach. (b) and (c) Most probable class based on 500 simulations obtained with the 5D directional approach: average over all the directions (b) and minimum RQD over all the directions (c).

4.5. Discussion

Contribution of our work. Like all types of one-dimensional measurements (borehole cores and scanlines), RQD depends not only on the geographical position of the sample but also on its direction, precluding a direct averaging that mixes different directions as a proper upscaling strategy. Upscaling must appropriately address the directional dependence to reduce uncertainties in geotechnical projects. Our proposal considers regionalizing the RQD data in a five-dimensional space corresponding to the three-dimensional geographical space crossed with the two-dimensional sphere, allowing RQD to be interpolated at any place in the geographical space and for any direction. Knowing the rock mass quality in specific directions is beneficial to evaluate the impact of the discontinuity orientations for tunnels, slopes, or foundation designs. The latter becomes critical, bearing in mind that the rock mass behavior is influenced by the regional geological structures rather than by the strength of intact rock, as shown, for instance, by the coincidence of the orientation of minimum RQD values (Figure 4.11) with regional structural faults.

Applicability. The 5D geostatistical approach requires sampling data with information on RQD and on the borehole positions and orientations, information that should always be logged and readily available in any good geotechnical database. The spatial and directional behaviors of RQD can be modeled in a flexible manner, using basic nested structures to fit the experimental variogram of the RQD data. This makes the proposal applicable to an extensive range of rock masses and conditions, including both weak and complex situations, such as tectonized (disturbed and broken by structural dislocation, shearing, folding, or compression) or heterogeneous (flysch formations or molassic formations) rock masses.

Practical limitations. If all the boreholes have the same or almost the same orientation (e.g., vertical), then it can be challenging to infer the directional behavior of RQD and to apply the 5D geostatistics approach. Other practical limitations of this approach are the assumptions of stationarity in the geographical space and isotropy on the sphere (see Appendix). The former assumption is often sensible after

partitioning the deposit into areas (‘geotechnical domains’) with similar structural and mechanical characteristics and performing the geostatistical analysis within each domain separately. As for the latter assumption of isotropy, it may be questionable when there is only one network of parallel fractures, in which case it would make sense to work with anisotropic variogram models on the sphere.

3D vs. 5D modeling. The traditional (three-dimensional, non-directional) and proposed (five-dimensional, directional) approaches to modeling RQD in rock engineering applications have been cross-validated, providing a good fit in terms of prediction and uncertainty assessment. Each approach has its pros and cons. For lower computational requirements and pre-processing time, the traditional approach achieves a globally good prediction of RQD but is locally biased as per the drilling direction. The directional approach is more demanding in terms of modeling and computational capacity but provides information on the directional RQD behavior, which is valuable for geotechnical zoning and decision-making as it reflects the inherent nature of the geotechnical parameters (their directional dependence) and can give an insight into the geometry of the rock fragments when combined with other direction-dependent parameters such as the fracture frequency. This approach accounts for the fact that, in the presented case study, one measurement of RQD provides much information about values at surrounding locations along the same or nearly parallel directions, as indicated by low variogram values at short separation distances and small separation angles (Figure 4.5). However, an RQD measurement provides less information in a perpendicular direction. Therefore, it constitutes good practice to account for the directional dependence of RQD in any geostatistical modeling and upscaling analysis.

4.6. Conclusions and perspectives

The common practice in geotechnical modeling overlooks the directional dependence of geotechnical variables and characterizes volumetric support assuming rock masses as a continuum and isotropic medium and extrapolating or averaging sample-support information (from boreholes or scanlines) to a three-

dimensional block support or to the rock mass. However, rock masses are seldom isotropic and are generally heterogeneous, hence our proposal to tackle the change of support problem by accounting for the inherent directional dependence of RQD (5D regionalization) and for its uncertainty at unsampled locations (use of geostatistical simulations). This change of support is performed by averaging the RQD simulated along a specific direction on a grid, discretizing each block in the geographical space. The upscaled directional RQD is practical, simple, and does not modify the original concept of RQD, making it suitable and serviceable in engineering applications, e.g., to determine required tunnel support. The directional approach better reproduces the geographical and directional heterogeneity and real nature of the rock mass. A non-directional upscaled RQD can also be derived from this approach by considering the minimum value obtained over all the directions (corresponding to the most unfavorable direction of fracturing, i.e., the worst-case scenario) and complemented with an anisotropy index of jointing degree (sensu Zheng et al., 2018). Both the directional and non-directional RQD so obtained directly impact the prediction of safety factors and control measures in rock engineering projects.

Our directional approach can be used for geotechnical zoning (Figure 4.13), i.e., classifying the rock mass into similar design areas. Besides helping determine fault zones, and by applying empirical formulas, it is also possible to calculate other mechanical parameters such as the modulus of elasticity or the unconfined compressive strength (Zhang and Einstein, 2004, Zhang, 2016). This approach is helpful in any stage of a geotechnical project. At the exploratory or early stages, it is suggested to use adaptive geometries in the block model: the size of the block will depend on the variability of the geotechnical parameter in the sector and the available information, i.e., the less amount of available information (and the more variability of RQD), the larger the block size. At the development and production stages, it is possible to model the geotechnical parameters, whether in a parallel or perpendicular direction, to advance the construction of the excavation in rock.

One way to optimize the analysis is to use adaptive geometries in the block model in further developments, giving a higher resolution (smaller block size) in

areas with a higher anisotropy index or vice versa. Moreover, for upscaling directional variables such as RQD, it is interesting to analyze the relationship between strength and stiffness versus block size to determine the Representative Volume Element size, REV (Zhang et al., 2017).

To broaden the scope of application of the presented proposal, future works in the 5D geostatistical modeling should include the design of variogram models and simulation algorithms using non-separable covariance functions or anisotropic covariances on the sphere, together with exploratory tools to identify preferred directions of anisotropy on the sphere based on sampling information.

Appendix A

A.1. Traditional approach: modeling RQD in the 3D Euclidean space

This approach considers that RQD varies only with the geographical coordinates (easting, northing, and elevation), i.e., regionalized in the Euclidean space R^3. A common practice for geostatistical modeling is to assume second-order stationarity, i.e., the mean value and the covariance function or the variogram are invariant under a translation in space, which allows their inference from a set of sampling data (Chilès and Delfiner, 2012). A convenient way to model the experimental covariance (or experimental variogram) is through a positive linear combination of basic nested structures:

$$C(\boldsymbol{h}) = cov\{Z(\boldsymbol{x}+\boldsymbol{h}), Z(\boldsymbol{x})\} = \sum_{s=1}^{Smax} b_s\, \rho_s(\boldsymbol{h}) \qquad (A.1)$$

where Z is the Gaussian random field associated with RQD, $\boldsymbol{x}$ and $\boldsymbol{x}$+$\boldsymbol{h}$ are two points in the geographical space separated by vector $\boldsymbol{h}$ and, for s = 1,… S_{max}, b_s is a nonnegative real value, and ρ_s is an autocorrelation function (positive semi-definite function taking the value 1 at $\boldsymbol{h}$ = **0**).

The Gaussian random field can then be simulated as a sum of S_{max} components, each associated with a particular nested structure:

$$Z^{(S)}(\boldsymbol{x}) = \sum_{s=1}^{Smax} \sqrt{b_s}\, Z_s^{(S)}(\boldsymbol{x}) \qquad (A.2)$$

where the superscript (S) stands for 'simulated'. The reader is referred to Emery and Lantuéjoul (2006) for algorithmic details on the simulation process for the nested structures commonly used in geostatistical applications.

A.2. Directional approach: modeling in a 5D product space

To account for the fact that RQD is direction-dependent, the associated random field Z is now defined in a five-dimensional space ($\mathrm{R}^3 \times \mathrm{S}^2$, with S^2 the unit sphere), i.e., Z = {Z(***x***,***u***): ***x*** $\in \mathrm{R}^3$ and ***u*** $\in \mathrm{S}^2$}, where ***x*** represents the geographical coordinates of the measurement, and ***u*** the direction (azimuth and dip) of this measurement.

The simplest way to model the spatial correlation of regionalized data in such a 5D space is to consider second-order stationarity in the geographical space and second-order isotropy on the sphere. These assumptions imply that the mean value is constant and that the covariance function or the variogram between the two random variables located at (***x***,***u***) and (***x***′,***u***′) in $\mathrm{R}^3 \times \mathrm{S}^2$ only depends on the separation vector ***h*** = ***x***′-***x*** and on the geodesic distance or angular separation δ(***u***,***u***′) = arcos(<***u***,***u***′>), with < , > the inner product. The modeling can be extended as follows:

$$C(\boldsymbol{h}, \delta) = \sum_{s=1}^{S_{max}} b_s C_s(\boldsymbol{h}, \delta) \qquad (A.3)$$

where, $b_s \geq 0$ for s = 1,… $S_{\max}$ and C_s is a basic autocorrelation (positive semi-definite) function defined on $\mathrm{R}^3 \times [0, \pi]$. In this work, separable basic autocorrelation functions are used:

$$C_s(\boldsymbol{h}, \delta) = \rho_s(\boldsymbol{h}) P_{n(s)}(\cos\delta) \qquad (A.4)$$

where ρ_s is an autocorrelation function in R^3 and P_n the Legendre polynomial of degree n. Schoenberg (1942) showed that the mapping $\delta \mapsto P_n(\cos\delta)$ is an isotropic correlation function on the sphere. Because the Legendre polynomial P_n has the

same parity as n, and because the RQD measurement along a direction $\boldsymbol{u}$ is the same as along the opposite direction -$\boldsymbol{u}$, the covariance should remain the same when changing $\delta(\boldsymbol{u},\boldsymbol{u}')$ into π-$\delta(\boldsymbol{u},\boldsymbol{u}')$, i.e., when changing $P_n(\cos\delta)$ into $P_n(-\cos\delta)$. Accordingly, only even degrees $n(s)$ should be considered in Eq. (A.4).

As for the previous approach, the Gaussian random field can be simulated as a sum of S_{max} components. Each component is associated with a particular nested structure and separates into the product of a geographical component and a directional component (Sanchez et al., 2019):

$$Z^{(S)}(\boldsymbol{x},\boldsymbol{u}) = \sum_{s=1}^{Smax} \sqrt{b_s}\, Z_s^{(S)}(\boldsymbol{x}) W_s^{(S)}(\boldsymbol{u}) \qquad (A.5)$$

with $Z_s^{(S)}(\boldsymbol{x})$ a zero-mean random field in the Euclidean space with autocorrelation $\rho_s(\boldsymbol{h})$, and $W_s^{(S)}(\boldsymbol{u})$ a zero-mean random field on the sphere with autocorrelation $P_{n(s)}(\cos\delta)$, see Emery and Porcu (2019) or Lantuéjoul et al. (2019) for examples on how to simulate random fields on the sphere.

CHAPTER V.

SLOPE CONSTRUCTABILITY ACCEPTANCE CRITERIA FOR OPEN PIT MINE DESIGN: A CASE STUDY ON A CHILEAN COPPER MINE

This chapter addresses the problem of simulating the slope mass rating (SMR) in a porphyry copper deposit (Radomiro Tomic, northern Chile), through a multivariate simulation of the underlying factors defining SMR. The realizations are post-processed to provide analyses on the slope performance and stability of open pit excavations. The contents of this chapter have been submitted to Rock Mechanics and Rock Engineering:

> Sánchez, L.K., Emery, X., Delonca, A., 2022. Slope constructability acceptance criteria for open pit mine design: A case study on a Chilean copper mine. Rock Mechanics and Rock Engineering, submitted.

Abstract

Geotechnical modeling plays a crucial role in the optimization of open pit mine planning and design, given that the final pit slope configurations are constrained by stability considerations. One of the most useful methods for rock slope stability analysis is the Slope Mass Rating (SMR) classification. SMR is obtained from the basic Rock Mass Rating (RMR) by means of corrective factors that depend on the pit slope and discontinuity orientations and on the excavation method. In this work, a methodology is proposed to map the geomechanical quality of the pit slope, which allows to predict structurally controlled failures and to determine stability classes at a local scale across a mineral deposit, to delineate likely instability zones. The key to our proposal is to regionalize the variables that define RMR in the geographical space crossed with an angular space, in order to account not only for their spatial variations but also for their directional dependence, and to construct outcomes of these variables through geostatistical simulation, in order to account for their uncertainty at unsampled locations. The methodology is applied to a data set from a Chilean copper mine and leads to the selection of acceptable slope design criteria for the pit, based on a chart considering SMR and height design to predict a safe slope angle.

Key words: geostatistical modeling, rock mass rating, slope mass rating, local prediction

5.1. Introduction

Geotechnical engineering in open pit mining deals with a rock mass whose behavior must be inferred from limited and expensive observations using geological knowledge and statistical reasoning. As the engineering properties of the rock are not well known, the probability of slope failure is uncertain. Discontinuities govern one typical breakage of the rock mass. It occurs according to formed surfaces by one or more joints., i.e., the mode of failure involves a block of material sliding on two or

three planes of discontinuity and may occur on either a bench scale or as a failure of the overall pit slope, and it is not unusual to encounter several of these failure types or combinations of failure types in an open pit slope. The consequences of a mine slope failure are varied, and slope risk profiles are commonly driven by short design-life scenarios and the ability to control access to the slope. The safety, environmental, and business risks associated with slope failures must be weighed against mining costs for a particular slope design. Still, it is formally considered in the decision-making process as a part of the cost structure for the mine. An excellent geotechnical mine slope design integrates all these factors to produce a balanced compromise between safety on the one hand, and operational and economic efficiency on the other. It means that the design must be adjusted until an acceptable trade-off is reached, which requires reliable approaches to cover both the structurally controlled failures (e.g., planar, wedge, and toppling) and circular type failures associated with strongly fractured rock masses.

The assessment of the stability of these slopes depends on good geological, geotechnical, and groundwater models and an understanding of the risks and economic consequences of slope instability. Geotechnical modeling is one of the essential components of the planning and development of open pit mining projects. The basis for a geotechnical model is often a resource geology model and an exploration drilling data set. Although engineering properties of soils and rocks in the slopes will vary from place to place around the mine site, current geotechnical approaches applied in most of the mining operations assume average values and uniformity of the geotechnical parameters such as the fracture frequency, strength, or rock mass quality (RQD, GSI, or RMR) over large distances. These assumptions have negative impacts on the design of the rock excavations because geological phenomena have spatial heterogeneities that result in high contrasts of strength and rigidity properties at a small scale. Spatial heterogeneity implies that a rock mass with good strength and rigidity can exhibit rapidly contrasting properties just a few meters apart. Consequently, predicting the mechanical behavior of the rock mass and reducing uncertainty is further complicated. Such complexities regarding the spatial variability and uncertainty measurement inherent to current rock mass modeling approaches can be addressed by using geostatistics.

Geostatistical techniques have been applied in geotechnics for over two decades, mainly in view of predicting or simulating geotechnical parameters for the classification of rock mass using empirical methods (e.g., Ozturk and Nasuf, 2002; Madani and Asghari, 2013; Ozturk and Simdi, 2014; Pinheiro et al., 2016; Santos et al., 2018). These works confirm the advantages of using geostatistics to model geotechnical parameters, but they lack a systematic analysis of the direction-dependence of most geotechnical variables. Direction-dependence means that the measured value depends not only on the geographical position of the sample, but also on the sampling direction. This is an intrinsic characteristic that must be incorporated into prediction or simulation methods to avoid biases when looking for a representative value of the classification of the rock mass (Séguret et al. 2015; Sánchez et al., 2019; Emery and Séguret, 2020).

Our proposal, detailed hereinafter, uses empirical rock and slope quality classification systems because it appears to be the most practical solution for the preliminary analysis of structurally controlled failures. Slope mass rating (SMR), suggested by Romana (1985), is a popular geotechnical slope classification system to predict potential failures controlled by discontinuities establishing a correlation between slope and discontinuity orientations. The effect of joints and other structural defects should be accounted for in the assessment of the rock mass strength (e.g., when using the Hoek-Brown strength criterion) and/or the stability analyses. We recognize and address these challenges of including all important defects in the rock mass classification. It means considering the directional dependence of the measurements (directional bias), heterogeneities (loss of spatial continuity introduced by the orebody genesis), large scale geometry, and orientation.

The outline is as follows. Section 5.2 presents empirical rock and slope quality classification systems that will be used. Section 5.3 includes a synthesis of how to tackle the directional-dependence and provides some technical details of the proposed methodology to model geotechnical variables in a five-dimensional space corresponding to the three-dimensional geographical space crossed with a two-dimensional angular space. Section 5.4 presents the results of a real study case in

the Radomiro Tomic copper mine in northern Chile. Finally, conclusions and future challenges are presented in Section 5.5.

5.2. Empirical classification systems

The backbone of all current limiting equilibrium and numerical methods of slope stability analyses is the Mohr-Coulomb failure criterion, which requires knowing friction and cohesion values for the rock mass. Since triaxial testing of representative rock mass samples is difficult by sample disturbance and equipment size limitations, the preferred method has been to derive empirical values of friction and cohesion from rock mass rating schemes. Rock mass rating schemes are based on subjective ratings of specific attributes of the rock mass to partition the rock mass into geotechnical domains or units. Further, most of the methods for estimating the shear strength of component materials for incorporation into continuum models are based on some form of rock mass rating scheme and, for the preliminary analysis of structurally controlled failures, the empirical rock and slope quality classification systems appear to be the most practical solution.

5.2.1. Rock mass rating (RMR)

In open pit slope engineering, one of the most used schemes nowadays is the Rock Mass Rating (RMR), originally introduced for tunneling and civil engineering applications (Bieniawski, 1973, 1976, 1979, 1989). The value of RMR determines the geotechnical quality of the rock mass on a scale that ranges from 0 to 100 and considers five classes: very good (RMR 100–81), good (80–61), fair (60–41), poor (40–21), and very poor (<20). The rock mass rating scheme is helpful exclusively for predesign stage. It is based on six parameters to which statistical rating significances are assigned:

- the uniaxial compressive strength of the intact rock (**UCS**), preferably based on UCS tests, or on point load strength index tests on rock lumps at the natural moisture content;

- the rock quality designation (**RQD**), a modified core recovery percentage and an index of rock quality;
- the joint or discontinuity spacing (**JS**), the linear distance between two adjacent discontinuities whose rating is for the most critically oriented discontinuities, or the lowest rating (Edelbro, 2004) given that the presence of joints reduces the strength of a rock mass and their spacing governs the degree of such a reduction (Bieniawski, 1973);
- the joint condition (**JC**), including roughness of discontinuity surfaces, their separation, length of continuity, weathering of the wall rock or the planes of weakness, and infilling (gouge) material;
- the groundwater condition (**GW**), for which the rock mass should be assumed to be completely dry, and any pore pressures in the rock mass should be accounted for in the stability analysis;
- the joint orientation, for which the influence of the strike and dip of joints is considered with respect to the direction of tunnel drivage, slope face orientation, or foundation alignment.

The sum of the ratings for the first five parameters provides the basic RMR score (Table 5.1), which does not discount the effect of the orientation of joints given that this study uses a factorial approach to rating adjustment for the discontinuity orientation parameter in the RMR scheme developed by Romana (1985):

$$RMR_{basic} = UCS + RQD + JS + JC + GW. \quad (1)$$

The modifications and extensions of RMR should not be interpreted as new schemes, e.g., the extensions slope stability (SMR, Romana, 1985) is a valuable new application but still a part of the same overall RMR scheme.

Table 5.1. RMR parameter ratings (Bieniawski, 1979)

Parameters			Range of values						
1	Strength of intact rock material	Point-load strength index	>8 MPa	4–8 MPa	2–4 MPa	1–2 MPa	For this low range uniaxial compressive test is preferred.		
		Uniaxial compressive strength	>200	100–200 MPa	50–100 MPa	25–50 MPa	10–25 MPa	3–10 MPa	1-3 MPa
	Rating		15	12	7	4	2	1	0
2	Drill core quality RQD		90–100%	75–90%	50–75%	25–50%	<25%		
	Rating		20	17	13	8	3		
3	Spacing of joints		>2 m	0.6–2 m	0.2–0.6 m	60–200 mm	<60 mm		
	Rating		20	15	10	8	5		
4	Condition of joints		Non-continuous structures. Very rough structures. Structures with unweathered and non-altered rock walls. Closed or sealed structures.	Slightly rough structures. Structures with slightly weathered and/or slightly altered rock walls. Open structures (aperture <1 mm) or filled structures (thickness <1 mm).	Slightly rough structures. Structures with weathered and/or altered rock walls. Open structures (aperture <1 mm) or filled structures (thickness <1 mm).	Continuous structures. Slickensided structures or open structures (aperture 1–5 mm), or structures with soft rouge fillings (thickness 1–5 mm).	Continuous structures Open structures (aperture >5 mm), or structures with soft gouge fillings (thickness >5 mm).		
	Rating		30	25	20	10	0		
5	Groundwater in joints		Completely dry	Damp	Wet	Dripping	Flowing		
			15	10	7	4	0		

5.2.2. Slope mass rating (SMR)

Slope Mass Rating (SMR) is an essential contribution in applying rock mass classification to assess the stability of a rock slope (Romana 1985), recognizing that rock slope stability is governed by the behavior of the discontinuities and that, in the original RMR system, specific guidelines for favorability of joint orientations are lacking. SMR is obtained from the basic RMR by adding a factorial adjustment depending on the relative orientation of joints and slope (through the product of three factors), and another adjustment factor depending on the excavation method. The basic RMR has a scalar character, but SMR endows the rock mass with a vector character by considering the direction and dip of the discontinuities that affect the rock mass. The adjustment rating for discontinuities is the product of three factors as follows (Figure 5.1):

F_1 reflects the parallelism between the discontinuity and slope face dip directions.

F_2 is a measure of the probability of joint shear strength, referring to the discontinuity dip angle in the plane mode.

F_3 denotes the relationship between the slope face and the discontinuity, referring to the probability that the discontinuities outcrop on the slope.

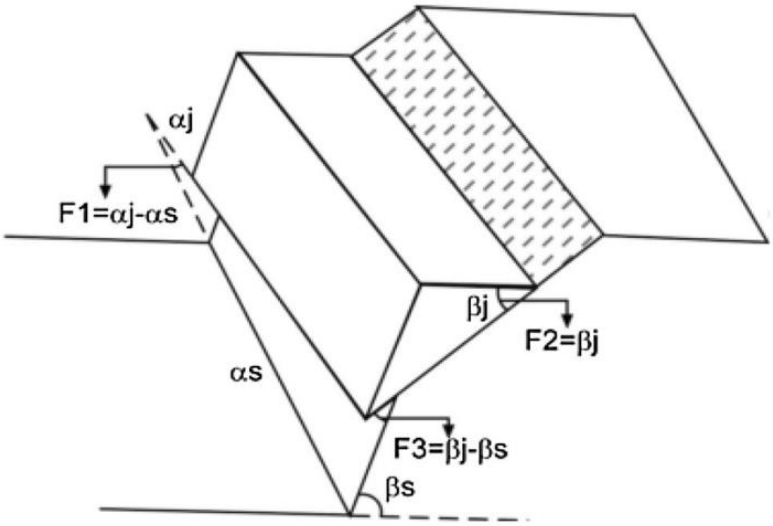

Figure 5.1. Adjusting factors for discontinuities (F1, F2, F3) (Singh and Goel, 1999)

The fourth factor **F_4** depends on the excavation method and on whether one deals with a natural slope, or one excavated by pre-splitting, smooth blasting, mechanical excavation, or poor blasting. Thus, SMR is given as:

$$SMR = RMR_{basic} - (F_1 \cdot F_2 \cdot F_3) + F_4 \quad (2)$$

where $F_1 = (1 - \sin A)^2$, with *A* being the angle between the strikes of slope angle and the discontinuity, $F_2 = \tan^2 B$, with *B* being the discontinuity dip angle, while F_3 is the rating adjustment for discontinuity orientation from the modification of Bieniawski's RMR (Bieniawski, 1979). In particular, if the difference between the slope face and the discontinuity dip is equal to 0° with F_3=-25, there is a normal condition, i.e., a few discontinuities will outcrop; otherwise, if the slopes dip more than the discontinuities, almost all of them outcrop, and the conditions will be very unfavorable (for differences higher than 10°) with F_3=-60 or unfavorable with F_3=-50 (for differences lower than 10°).

SMR is a tool for potential failure mode detection considering the slope and discontinuity orientations and has found good agreement with stability assessment (rock mass quality) predicted by the RMR system; therefore, it can be regarded as a reliable preliminary slope design tool (Yardimci and Karpuz, 2018) and provides a division into stability classes and recommendations for support and/or correction methods. Based on the failure modes, the suggested score intervals for factors F_1, F_2, and F_3 can be seen in Table 5.2. So, SMR is suitable for preliminary slope stability assessment in rock, including very soft or heavily jointed rock masses. The SMR concepts have been used in three different ways as a geomechanics classification, taking F_1, F_2 and F_3 as risk parameters (generally in natural slopes), and as a complementary method of work. The interpretation of SMR scores in terms of slope mass description, stability state, failure type, and support recommendation are summarized in Table 5.2.

Table 5.2. SMR adjustment factors for different failure types and discontinuity orientations (Romana 1985)

αj = dip direction of joint, αs = dip direction of slope, βj = dip of joint, βs = dip of slope

Adjusting factors for joints (F_1, F_2, F_3)		Very favorable	Favorable	Fair	Unfavorable	Very unfavorable
Plane failure $\lvert\alpha_j - \alpha_s\rvert$ Toppling $\lvert\alpha_j - \alpha_s - 180\rvert$		>30	30–20	20–10	10–5	<5
F_1 value		**0.15**	**0.40**	**0.70**	**0.85**	**1.00**
Equation		$F_1 = \left(1 - \sin\lvert\alpha_j - \alpha_s\rvert\right)^2$				
$\lvert\beta_j\rvert$		< 20 °	20° - 30°	30° - 35°	35° - 45°	> 45°
F_2 value	Plane failure	**0.15**	**0.40**	**0.70**	**0.85**	**1.00**
	Toppling	**1.00**				
Equation		$F_2 = tan^2 \beta_j$				
Plane failure $\beta_j - \beta_s$		>10º	10º - 0º	0º	0º-(-10º)	<(-10º)
Toppling $\beta_j + \beta_s$		< 110º	110º - 120º	> 120º	-	-
F_3 value		**0**	**- 6**	**- 25**	**- 50**	**- 60**
Excavation method		Natural slope	Presplitting	Smooth blasting	Blasting or Mechanical	Deficient blasting
F_4 value		**+ 15**	**+ 10**	**+ 8**	**0**	**- 8**
SMR Value						
		0-20	21-40	41-60	61-80	81-100
Class no.		Vb / Va	IVb / IVa	IIIb / IIIa	IIb / IIa	Ib / Ia
Description		Very bad	Bad	Fair	Good	Very good
Stability		Completely unstable	Unstable	Partially stable	Stable	Completely stable
Failures		Big planar or soil-like	Planar or big wedges	Some joints or many wedges	Some blocks	None
Support		Reexcavation	Important / corrective	Systematic	Occasional	None

5.3. Geostatistical modeling applied to geotechnics

5.3.1. Regionalizing geotechnical variables in a five-dimensional space

To predict the behavior of geotechnical variables, we will use a 5D geostatistical approach to solve directional dependence issues (Sánchez et al., 2019, 2021). The rationale is that the classical geostatistics we know in three dimensions (e.g., Chilès and Delfiner, 2012) is extended to five dimensions for the variogram analysis and simulation of geotechnical variables. The five-dimensional space consists of the 3D geographical space (with east, north, and elevation coordinates) crossed with a 2D sphere (with azimuth and dip angular coordinates) (Figure 5.2).

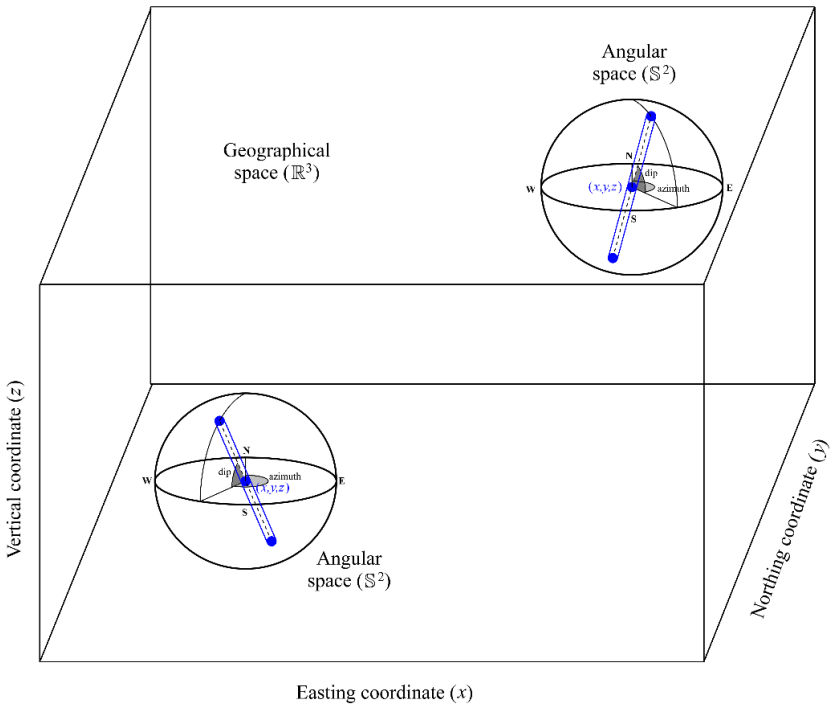

Figure 5.2. Each core sample (blue cylinder) is located by the easting, northing, and vertical coordinates of its gravity center in the geographical space (3D parallelepiped box), and by its azimuth and dip in the angular space (2D sphere), totaling five coordinates (Sánchez et al., 2021)

5.3.2. Spatial structure identification

Fitting a covariance or a variogram model, which is required to carry out geostatistical prediction or simulation, is a complex task when working in such a five-dimensional space, so simplifying assumptions are considered, namely the geotechnical variable of interest can be represented by a random field that is stationary (i.e., with translation-invariant finite-dimensional distributions) in the 3D geographical space and isotropic (i.e., with rotation-invariant finite-dimensional distributions) on the 2D sphere. These assumptions imply that the covariance function and the variogram between a pair of data only depend on their geographical separation vector (denoted by **h**) and on their angular separation (denoted by δ), i.e., the calculation of experimental covariances or variograms must be done for a fixed angular separation and a fixed geographical separation between paired data.

In the multivariate setting, covariances and variograms are matrix-valued functions, with the diagonal elements representing the autocorrelation of each variable and the off-diagonal elements representing the cross-correlation between each pair of variables (Chilès and Delfiner, 2012). Fitting the experimental covariances or variograms with a matrix-valued model is simplified by decomposing the covariance function as the product, or a sum of products, of a positive semidefinite matrix (called coregionalization or sill matrix), a purely spatial correlation function depending on the geographical separation vector **h** and a purely directional correlation function depending on the angular separation δ. The reader is referred to Sánchez et al. (2019, 2021) for details on spatio-angular covariance models and to Wackernagel (2003) for details on matrix-valued covariances and variograms.

5.3.3. Conditional simulation

Under an additional assumption of multivariate normality, the random field representing the geotechnical variable of interest can be simulated by a spectral method, consisting of adding and rescaling many independent repetitions of basic random fields with the prescribed correlation structure in the 5D space. This basic

random field can be obtained as the product of a geographical component (a cosine wave defined in the geographical space) and a directional component (a Legendre polynomial wave defined in the angular space), see Sánchez et al. (2019) for details. The computational complexity of such a method is proportional to the number of target locations, which makes it extremely fast for simulating geotechnical variables in a large region of the geographical space and for different target directions in the angular space. Conditioning the simulation to sampling data, so that the simulated random field reproduces the values observed at sampling locations, is done by a post-processing step based on kriging (univariate case) or cokriging (multivariate case) (Chilès and Delfiner, 2012).

5.4. Case Study

5.4.1. Research area and structural domain

The Radomiro Tomic mineral deposit in northern Chile is associated on a regional scale with the Domeyko strike-slip system (to the east of the West Fault and the west of the Mesabi Deformation Zone) (Tomlinson et al., 2018). It corresponds to a system of N-S oriented dextral transpression faults parallel to the Chilean oceanic trench, linked to a period of oblique convergence of plates (Maksaev et al., 1994; Tomlinson and Blanco, 1997).

The deposit is an Eocene-Oligocene copper-bearing porphyry located in the Chuquicamata mining district, immediately north of the homonymous deposit. It presents sericitic, argillic, intense potassic, background alterations, and the economic mineralization corresponds to copper oxides and sulfides. The orebody is limited in its EW extension by two main inverse faults with the movement of dextral trend and NS orientation: West Fault and Ckaari Fault. Namely, the deposit does not extend further to the East or the West because these faults prevent it or lock the deposit. Mineralizations along these N-S faults are called the Kala domain (for the western part of the deposit) and the Ckaari domain (for the eastern part of the deposit) (Figure 5.3). However, there are other NE and NW-oriented faults. Both systems

appear vertical or sub-vertical and are the ones that control the exotic mineralization and oxides. The NE-oriented fault system controls the hypogene mineralization (the deepest one, called the Kalatche domain). The NW-oriented faults control the supergene or exotic mineralization (the most superficial, called the Corina domain). Then one could say that blocks of rhomboid geometry are formed (seen in a plane), but the area is structurally complex at a general level. There are possibly clockwise block rotations. In summary, the main structural systems that control the mineralization and are considered in the calculation of SMR are (Rojas, 2021):

A) Kalatche system, NE/sub-vertical orientation

B) Corina system, orientation NW/70-80SW

C) Kala system, NS/sub-vertical orientation

D) Ckaari system, NS/80W to sub-vertical orientation.

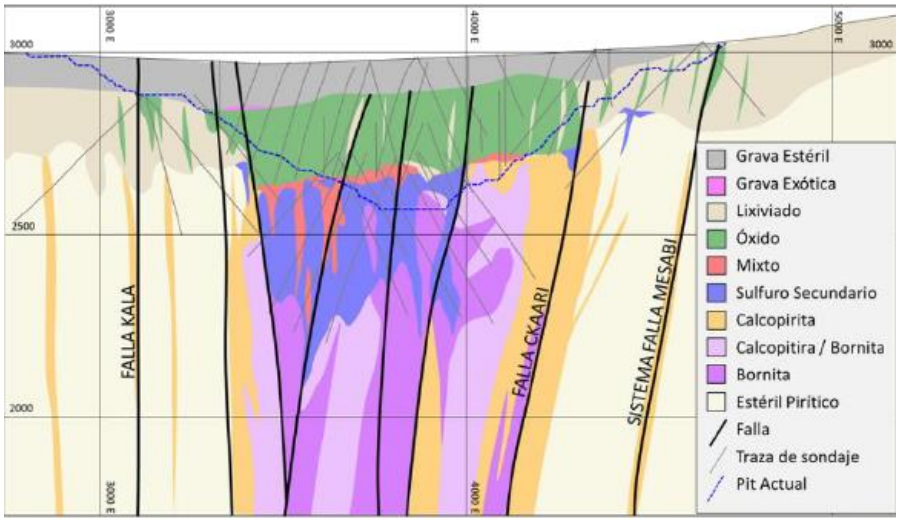

Figure 5.3. Mineralized zones in the Radomiro Tomic deposit (Rojas, 2021)

5.4.2. Presentation of data

A multivariable geotechnical dataset is available for this study. It comprises about 67,800 data from geotechnical drill core samples, each with a length of 1.5 meter, located at elevations between 935 m and 1145 m above mean sea level (Figure 5.4). Hereinafter, we consider the five parameters of the basic RMR, namely, the uniaxial compressive strength (UCS) of intact rock material, the rock quality

designation (RQD), the discontinuity spacing (JS), the condition of discontinuities (JC), and the groundwater conditions (GW).

The presence of groundwater in joints in the study area is considered constant due to its aridity (the rock mass is completely dry) and we will assign a rating of 15 at GW for all the data and target locations. Regarding UCS, the intact rock sample is homogeneous, not containing zones of weaker rock due to internal defects such as microfractures, foliation, or weaker mineral clasts. It is therefore considered that the intact rock strength (IRS) value is equal to the UCS value.

The sampling is further affected by a so-called crushing phenomenon, which corresponds to the solid section of the core over its nominal length (1.5m) (Emery and Séguret, 2020). In other words, the drill core loses its integrity in sections whose length changes from place to place, making it difficult to have an accurate measurement of JS: there is a bias given that the observed core length is variable and cannot consider the crushed fraction (Séguret, 2016). To address this issue, we propose to replace JS with its calculation from its empirical relation with RQD, given that RQD does not change with crushing, because the intact length greater than 10 cm leaves out the crushed drilling sections. Specifically, we assume that JS has a negative exponential distribution and that, for values between 6/m to 16/m, the following relation linear holds (Priest and Hudson, 1976):

$$RQD = 110 - 3.68\,JS. \tag{3}$$

Based on the previous assumptions, we can derive the basic RMR using only RQD, JC and IRS.

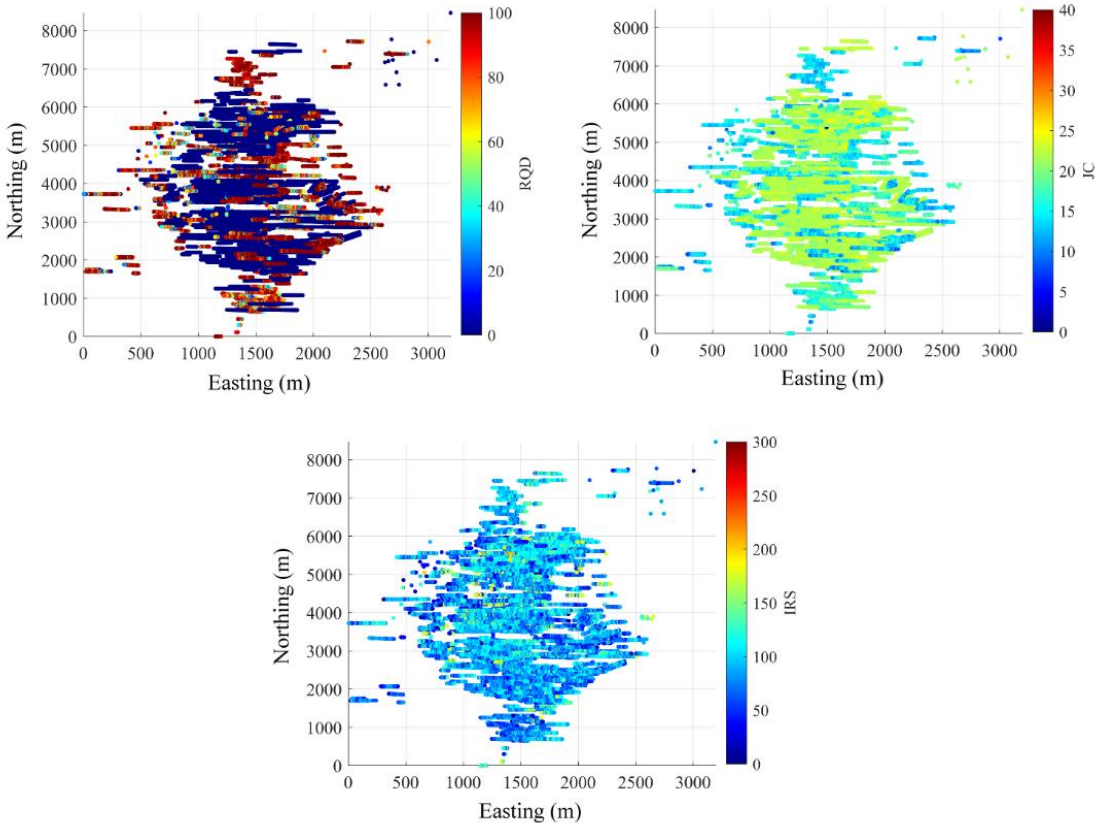

Figure 5.4. Horizontal projection of the available core samples, colored according to the measured RQD, JC and IRS values

5.4.3. Spatial structure analysis

Since the spectral simulation technique produces a Gaussian random field (Chilès and Delfiner, 2012), the geotechnical data of each target variable (RQD, JC and IRS) are first transformed into normal scores (i.e., data with a standard Gaussian distribution), prior to perform variogram analysis and simulation. The experimental variograms of the normal scores data are calculated omnidirectionally in the geographical space (i.e., each variogram is considered a function of the geographical distance, but not of the direction, between paired data) for distances ranging from 0 to 350 m, and for three angular separations between paired data (δ = 0°, 30°, and 60°, with a tolerance of 15° in each case), as shown in Table 5.3 and Figure 5.5.

Table 5.3. Parameters for experimental variogram calculations

Azimuth (°)	0
Dip (°)	0
Lag (m)	15
Number of lags	50
δ-angle between data (°)	0, 30, 60
Azimuth tolerance (°)	90
Dip tolerance (°)	90
Lag tolerance (m)	7.5
δ-angle tolerance (°)	15

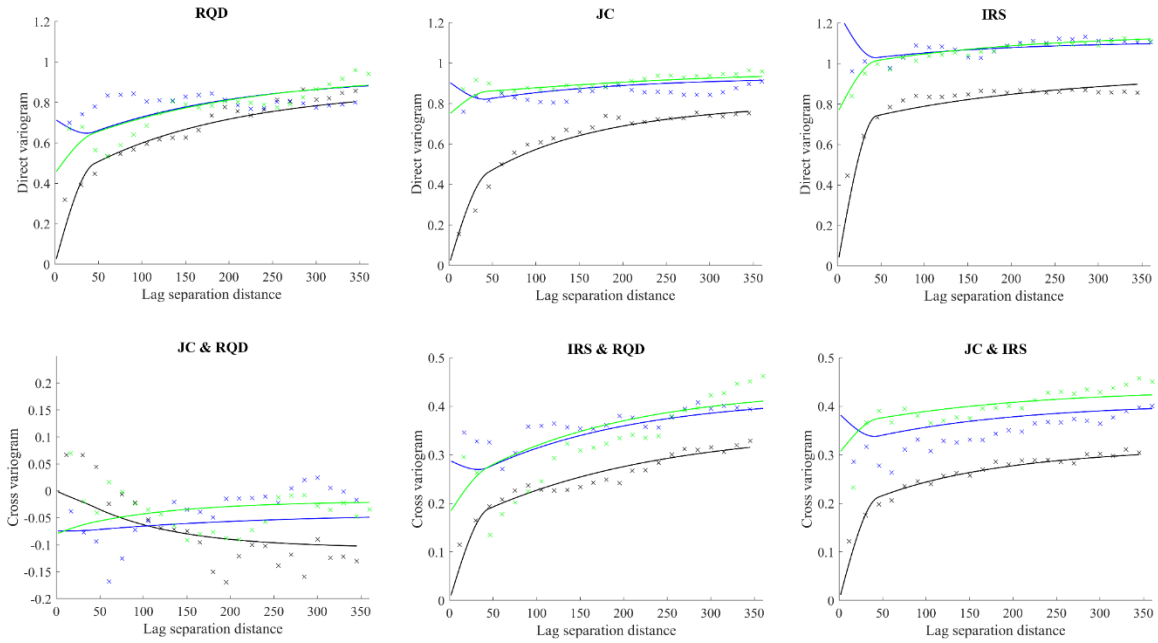

Figure 5.5. Experimental (crosses) and modeled (solid lines) direct and cross-variograms for the normal scores data of RQD, JC and IRS. Calculations are omnidirectional in the geographic space, and associated with an angular separation of 0° (black), 30° (blue) or 60° (green) between paired data

Since the problem is trivariate, direct and cross-variograms are calculated to account for the spatial dependencies between variables, totalizing six variograms (three direct variograms, each related to a single variable, and three cross-variograms, each related to a pair of variables). The fitted model comprises five nested structures (Table 5.4), each one being the product of a geographical component (an exponential or a spherical covariance) and an angular component (a Legendre polynomial covariance), see Sánchez et al. (2019) for mathematical details. The variogram model for the 5D regionalized data fits quite well the calculated experimental points for all the different geographical and angular

separations between paired data (Figure 5.5). The use of a zonal anisotropy (basic exponential covariance with an infinite range) and the fact that the Legendre polynomial changes from positive to negative values as the angular separation increases allow modeling the increase in the variogram sill with the angular separation (see Table 5.4).

Table 5.4. Fitted direct and cross-variograms with their respective structures and parameters

Geographical component: structure Type	Angular component: degree of Legendre polynomial	Geographical range (m)	Sill matrix			
Spherical	6	45		RQD	JC	IRS
			RQD	0.413	0.079	0.181
			JC	0.079	0.297	0.184
			IRS	0.181	0.184	0.739
Exponential	4	100		RQD	JC	IRS
			RQD	0.051	-0.118	-0.027
			JC	-0.118	0.274	0.065
			IRS	-0.027	0.065	0.017
Exponential	0	180		RQD	JC	IRS
			RQD	0.325	-0.048	0.150
			JC	-0.048	0.167	0.077
			IRS	0.150	0.077	0.141
Exponential	6	315		RQD	JC	IRS
			RQD	0.109	-0.076	0.022
			JC	-0.076	0.103	-0.033
			IRS	0.022	-0.033	0.012
Exponential	4	∞		RQD	JC	IRS
			RQD	0.049	0.072	0.070
			JC	0.072	0.108	0.101
			IRS	0.070	0.101	0.175

5.4.4. Conditional simulation of RQD, JC and IRS

The Gaussian random fields associated with the three variables (RQD, JC, IRS) are jointly simulated and conditioned to the normal scores data (Section 5.3.3), then are back-transformed in order to recover the original scale of each variable RQD, JC or IRS. A total of one hundred realizations (i.e., outcomes) are generated on a 3D geographical grid with a mesh of 5 m x 5 m x 5 m with an east-west extension of 1050 m, a north-south extension of 2100 m and a vertical extension of 75 m, for 121 directions covering the 2D angular space. Each realization is finally block-averaged in the geographical space to blocks with size 15 m x 15 m x 15 m (Figure 5.6).

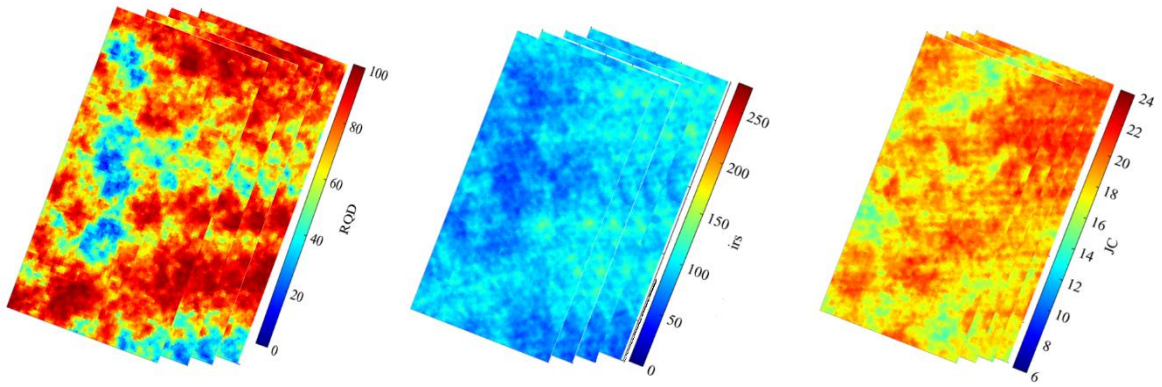

Figure 5.6. One realization of RQD, IRS and JC at four different layers from z=950m to z=1010 m in the geographical space, for a particular direction (vertical) in the angular space

5.4.5. SMR calculation

The results of the RQD simulation are used to derive the spacing between fractures (JS), through Eq. 3, allowing the calculation of the basic RMR (Eq. 1), i.e., without considering the discontinuities parallelism, the probability that the plane of weakness will outcrop the slope, or the dependence on the mining method. At this stage, all the variables (RQD, IRS, JC and basic RMR) are regionalized in the five-dimensional space, so that the results are available for 49,000 blocks in the 3D geographical space and 121 directions in the 2D angular space (Figure 5.7, top panel). Following Sánchez et al. (2021), to characterize each block by a single basic RMR value (instead of a set of 121 directional values), the minimum RMR over all the directions is considered, i.e., one retains the basic RMR measured along the most

unfavorable direction (which may vary from block to block and from realization to realization).

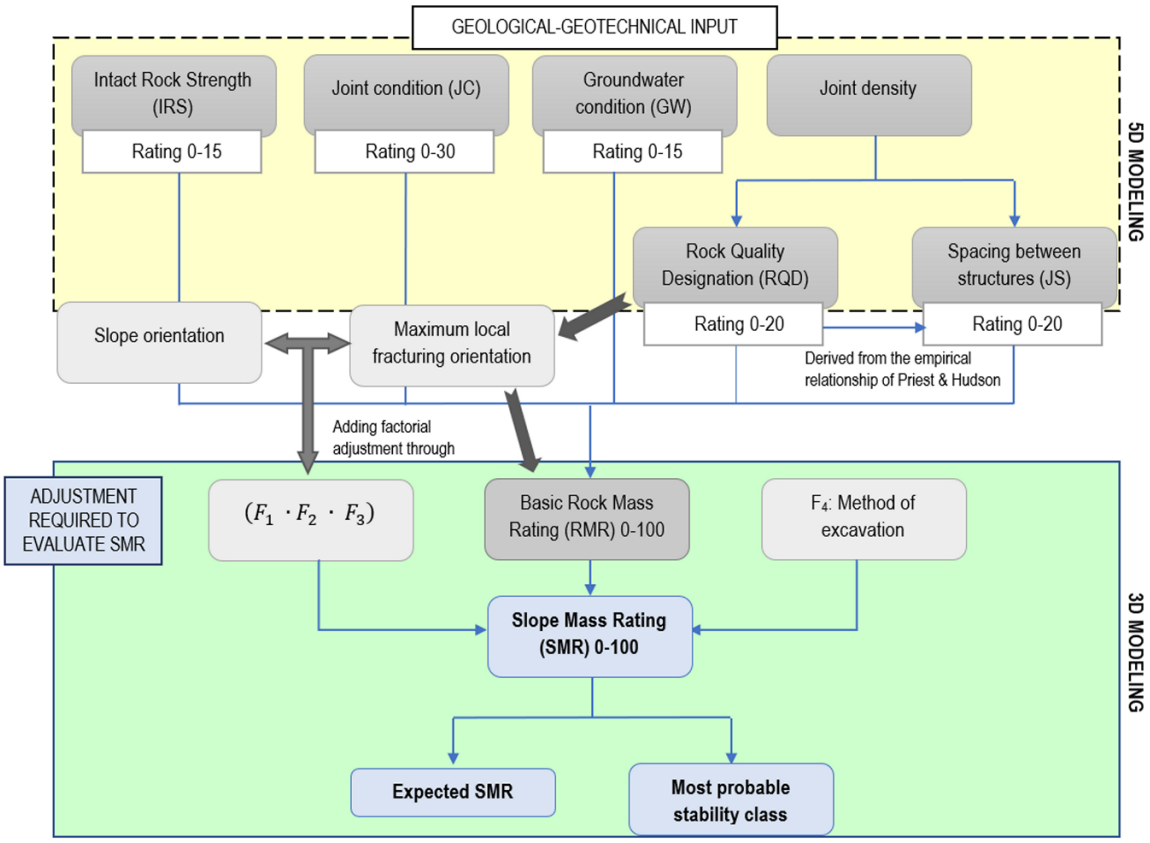

Figure 5.7. Workflow involved in evaluating SMR

To estimate SMR from RMR, one must consider three correction factors depending on the direction of the main structural systems and select the most unfavorable, which considers only the directional behavior at a regional scale, where stability is controlled by both the rock mass properties and large geological features (Grenon and Hadjigeorgiou, 2010). However, the traditional guideline will not allow a realistic geotechnical model for stability analysis given the structural complexity of the study area to the general level. Instead, we can take advantage of the results of our 5D modeling to derive this directional information at a local scale. Indeed, RQD also allows to determine the direction of maximum fracturing since greater fracturing implies lower RQD. That is, the minimum RQD is expected to occur along the direction perpendicular to the fracture plane, as indicated on the Terzaghi concept to the existence of preferential fracturing directions. Then, the fracturing direction

appears associated with RQD, which is one of the primary variables in the study that has been simulated at a block-by-block scale in the geographical space and along multiple directions in the angular space.

To summarize, SMR is calculated from the basic RMR along the direction of maximum fracturing, by adding the product of three factors (described in Section 5.2.2) that depend on the relative orientation of this direction of maximum fracturing (direction of minimum RQD) and the slope orientation, plus the adjustment factor based on the qualified excavation method in +10 (presplitting) (Figure 5.7, bottom panel). To define the maximum angle of the slope, we use the circular failure graph of Hoek and Bray (1981) considering a material density of 2.7 g/cm^3, a conservative work safety factor of 1.5, a completely drained slope, an angle of friction of 27° and a cohesion of 1.85 MPa. The slope dip was set to 70°, an interramps height was 140 m, and the ramp width was 32 m. The resulting interramp angle is 48° and the global angle is 45°, which agrees with the values used in the operation.

Our pit design (a synthetic case) considers a truncated cone whose mining bench height has the vertical block length (15 m), as it is done in the operation, and an inclination angle (dip) of 70° (see Figure 5.8). Also, as the angular convention, we consider the right-hand rule where we have a dip direction of 0° at the north, east 90°, south 180°, and west 270°. The dip direction of the slope for each block varies according to the wall of the pit in which it is located, directly affecting the accuracy of the evaluation of the favorability of the discontinuities. To consider the change in the dip direction in the calculation of SMR, we consider the angle formed between the central point of the section and the center of the target block. Hence, the changes in the dip direction on either a bench-scale may imply potential instability associated with the different modes of slope failure (planar, wedge, circular and toppling failure) that allow outcrops of planes or zones that are significantly weaker than the remaining rock mass on the slope face in the different domains.

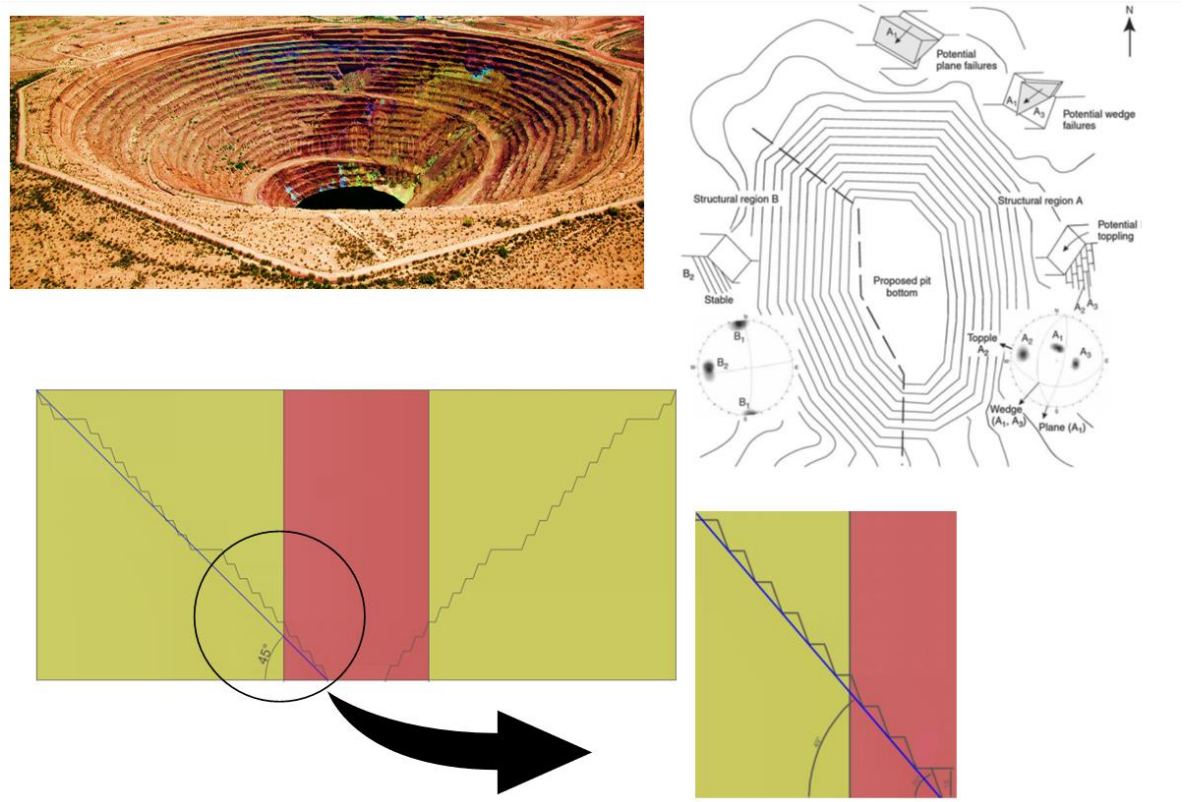

Figure 5.8. Open pit slopes design scales and schematic preliminary evaluation of slope stability of proposed open pit mine from Wylie and Mah, 2004.

5.4.6. Results

- **Expected SMR and kinematic analysis**

SMR can deliver an indication of the different types of failure expected in each block (see Table 5.5) and of the measures to be implemented. The adjustment factors to derive SMR from basic RMR depend on the angle formed by the relation between the orientation of set of discontinuities and the slope face angle, so its value varies depending on the position in space and angle of the bench (dip direction depending on the wall of the pit where the target block is located) and the direction of maximum fracturing or jointing (direction of minimum RQD, among the 121 directions considered for simulation). Indeed, the stability of the selected slopes is determined by potential instability associated with a planar, wedge, circular and toppling failure modes that are structurally controlled by local geological structures. As explained earlier, our determination of SMR does not consider the dip and dip direction of the

main structural systems that affect the rock mass as indicated in the traditional guideline, given that it corresponds to regional geological features that do not allow evaluating the stability of the slope at a local level (bench-scale).

Table 5.5. SMR values by each failure mode (Romana et al. 2003)

Failure modes	SMR value	Description
Plane Failure	SMR > 60	None
	60 > SMR > 40	Majors
	40 > SMR > 15	Very big
Wedge failure	SMR > 75	Very few
	75 > SMR > 49	Some
	55 > SMR > 40	Many
Toppling	SMR > 65	None
	65 > SMR > 50	Minors
	40 > SMR > 30	Majors
Mass failure	SMR > 30	None
	30 > SMR > 10	Possible

On average over the 100 realizations, the SMR exhibits lower values on the western and northwestern sides (Figure 5.9), where the pre-failure overall slope angles are assumed to be quite high (70°), and the SMR scores indicate that absolute failures (all structurally controlled failures) are likely to occur. The expected SMR in relation to the direction of maximum fracturing is fair (approximately 50), seen as partially stable, and presents some joints that can form many wedges requiring systematic support. In the northeastern and southwestern sectors, there are small areas with a slightly higher rock mass quality.

The results of the expected SMR rating allow distinguishing the probability that a type of failure will occur, facilitating kinematic analyses. In particular, the western sector requires important corrective support or even re-excavation due to completely unstable to unstable areas. It is possible to associate the behavior of the rock mass in the west area with the outcrop of the Corina System on the slope, whose orientation is the most unfavorable for the construction of the pit. The western sector exhibits a higher probability of failure mechanisms of big planar, big wedges, or soil-like that can point out a local failure (like a single bench).

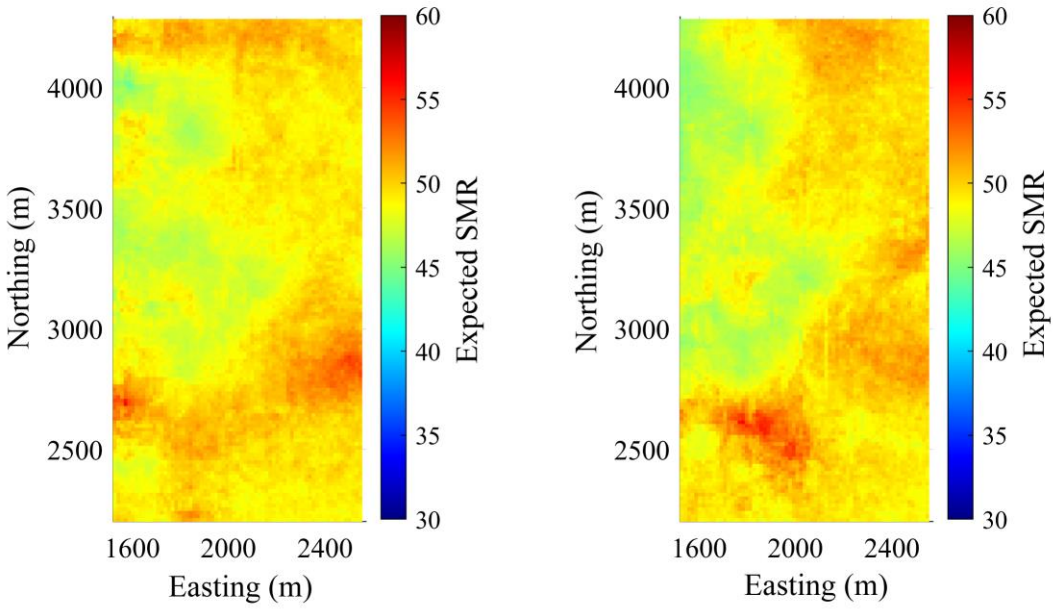

Figure 5.9. Average SMR over 100 realizations considering the direction of maximum fracturing (minimum RQD) to calculate the factorial adjustment (horizontal projection view) for the benches with elevations [950,695] m (left) and [1010,1025] m (right).

According to Table 5.5, an important to a very large plane failure occurring in the study area, i.e., dip discontinuity in the same direction of the slope, is probable for 41% of the blocks in the area under study. For the wedge failure mode to analyze the relationship between the line of maximum slope and the wedge dips in the same direction (otherwise it would dip towards the interior of the wedge), one has that 55% of the blocks can present some or many wedges' failures. Toppling failure occurs when the discontinuity dips against the slope face; according to SMR values, 23% of the blocks can have minor to major toppling. Slope instability dominated by circular failure is an important risk and slope and discontinuity orientations are not sufficient to predict such mechanically complex behavior, but 10% of the blocks may present a mass (or circular) failure. All these results based on the direction of maximum fracturing (minimum RQD) are conservative, obtaining that the blocks present some wedges, major plane reaching very big plane in the western sector at depth, some blocks classify as possible mass or circular at the west, and minor toppling in blocks in the southeast sector (25%) and major toppling in the west, increasing the number of blocks at greater depths.

- **Stability classification**

Followed by the prediction of structurally controlled failures, we continue to the determination of the stability classes according to SMR (Romana, 1985). For each block and each realization, the simulated SMR is assigned one of five classes (very good, good, fair, bad, very bad), then the class that most frequently appears across the 100 realizations is retained as the final classification of the block. The rock mass classification using the SMR score has low variability, with poorer quality sectors closer to the surface mainly in the northwest, then attenuates in northwest-southeast direction, where one has very bad to bad ratings following what is seen in Figure 5.9. The classification of the rock mass finds that most blocks are classified as fair quality (41 -60), 2% of the blocks located at the west and southwest are classified as very bad to bad, and less than a dozen blocks are classified as good at a greater depth of the rock mass (see Table 5.6). All benchs identified with SMR values below 20 fail very quickly, which is mandatory to revise the different remedial measures that can be implemented to support a unstable slope.

Table 5.6. Most frequent stability class according to simulated SMR

Class of SMR	
Very bad	1.28%
Bad	0.77%
Fair	97.92%
Good	0.02%
Very good	0.00%

- **Sensitivity analysis of slope performance**

The simulated SMR allowed obtaining a preliminary kinematic analysis that determines that the structural domains, in their majority, allow supporting a bench face angle of 70°. However, the western sector does not accept this situation due to a large number of blocks with a probable major toppling, possible mass (or circular), and very large plane failure, so the bench angle must be decreased in this western sector to mitigate the consequences of expected slope failure modes. Figure 5.10 shows how the value of the minimum expected SMR is quasi-constantly below 52°, so it establishes this value for the western sector. Reducing the bench face angle

from 70° to 52° generates a transition from very bad/bad quality graded blocks to fair quality that is close to 6%, as illustrated in Figure 5.10 and Table 5.7. In this case, to solve the problem of an unstable formation of zones due to the parallelism between the discontinuities (structures) and the bench, and/or that the dips of the structure are opposite to the orientation of the bench face on the west wall, it is recommended to reduce the bench face angle in this sector to 52°. This measure would avoid the formation of possible ruptures or, in the case of contemplating the occurrence of this failure within the design, tolerate them because they involve less removal of material, and the slope slip can be stopped by the lower benches. To analyze the influence of the angle of the face of the bench in the geographical space, an adrift graph (see Figure 5.11) is used on the Y-axis (North), where between 2500 - 2900 m the angle of 70° presents an expected value of SMR similar to the angles with a lower inclination, which would allow maintaining the initial angle in this section to optimize mining recovery. While between 2900 and 3500 m with an angle of 30°, a considerable improvement in the expected values of SMR is observed, so it is a sector to be subjected to more exhaustive analysis and monitoring.

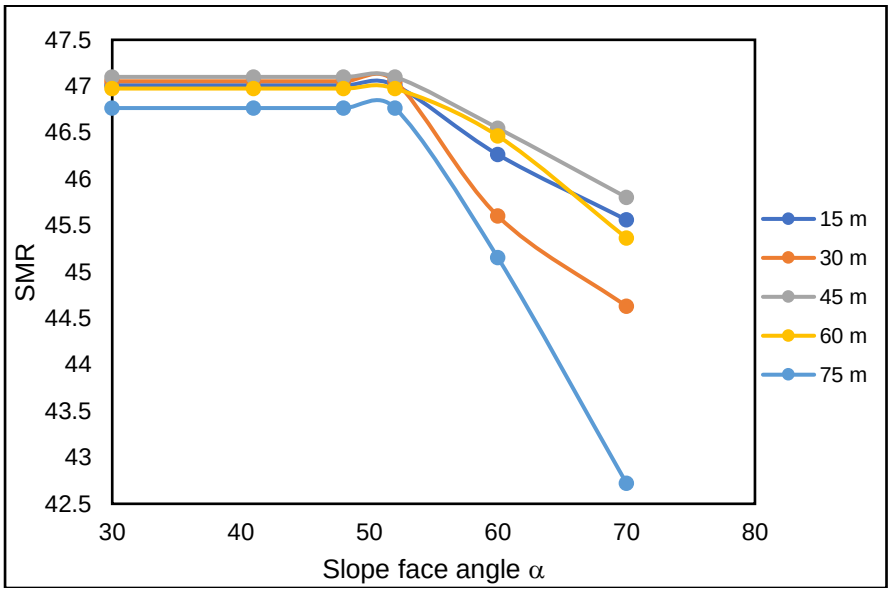

Figure 5.10. Expected SMR according to slope face angle and depth for the western sector

Table 5.7. Stability class of western sector according to slope face angle

	α= 70°	α= 60°	α= 52°	α= 48°	α= 41°	α= 30°
Very bad	3.66%	1.63%	0.05%	0.05%	0.05%	0.05%
Bad	2.26%	1.61%	0.00%	0.00%	0.00%	0.00%
Fair	94.05%	98.04%	99.89%	99.89%	99.89%	99.89%
Good	0.03%	0.03%	0.06%	0.06%	0.06%	0.06%
Very good	0.00%	0.00%	0.00%	0.00%	0.00%	0.00%

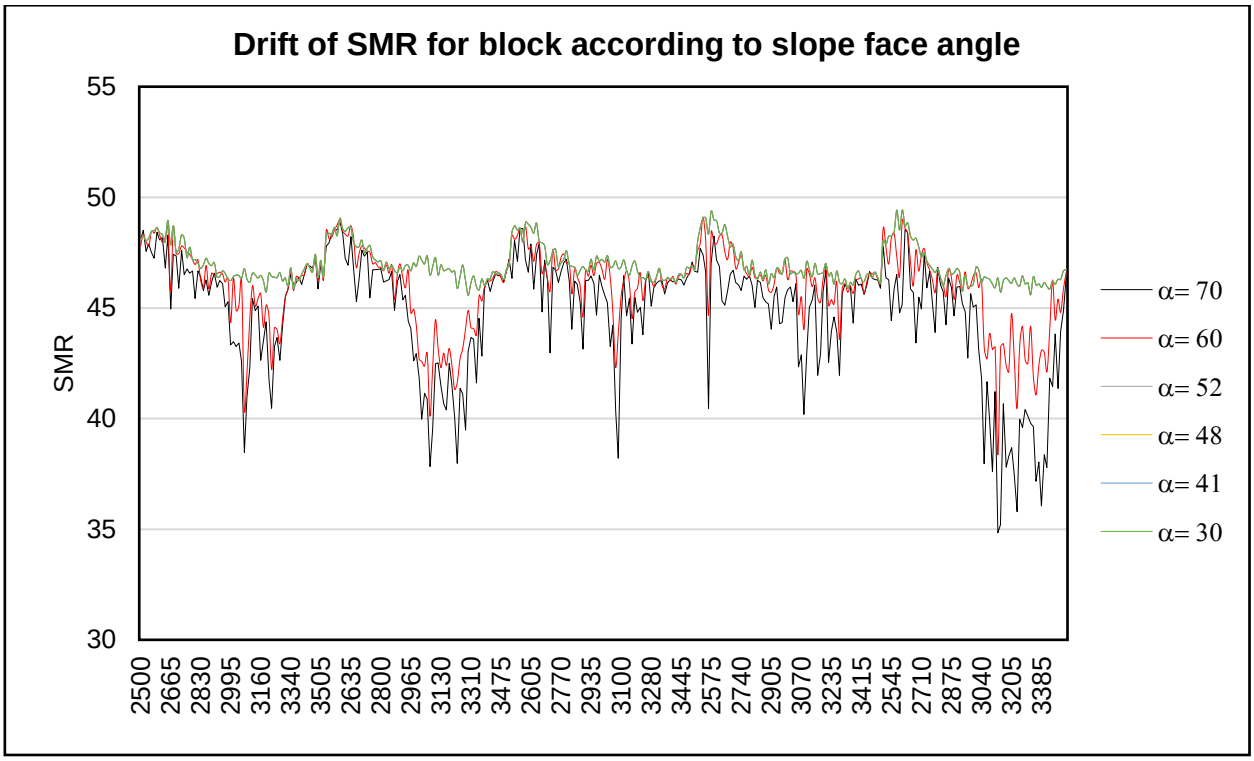

Figure 5.11. Drift of expected SMR according to slope face angle in Y-axis for the western sector

5.4.7. Discussion

In contrast to many geotechnical studies based on global average values that do not provide enough detailed information, in this study the geotechnical parameters are regionalized in the geographical space and in an angular space, i.e., their values depend on the easting, northing, elevation, azimuth and dip of the core sample under consideration. Additionally, geostatistical simulations allow generating multiple realizations (outcomes) that quantify the uncertainty in the values for any unsampled

location and any direction of interest, hence the interest in its application in geotechnics.

The process of logging drill holes in areas affected by core crushing is an additional source of uncertainty, and it is a challenge to interpret the fracture continuity, their large-scale geometry, and their orientation, since the rock mass cannot be seen in 3D on a large scale. The use of RQD as a parameter in Bieniawski's RMR and derived SMR systems presents some problems, in particular, biases due to the orientation of the drill hole with respect to the joint orientation, an issue that is circumvented in our 5D modeling approach. Another drawback of the SMR system classification is to not consider in an explicit manner the slope height as part of the failure mechanism analysis.

Figure 5.10 seeks to establish a slope design acceptance criterion that considers the slope height and the geotechnical characteristics (spatial and angular behavior) of the area under study to obtain results adapted to the rock mass, thus improving Bieniawski's original chart that relies on historical case studies in metallic mines, quarries, and dams. For preliminary design purpose, a slope performance chart can be considered as an enhanced slope stability analysis using the results obtained in our 5D space. Nevertheless, this does not aim to replace the analytical solutions or numerical methods, such as the stability slope charts proposed by Hoek and Bray (1981) that work well in the initial stage of a preliminary slope stability investigation. The Mohr-Coulomb shear strength model is more effective to investigate a circular failure mechanism, where the slope and discontinuity orientations are not sufficient to predict such mechanically complex behavior. However, the determination of shear strength parameters requires numerous mechanical tests and technical interpretations by experts, which are not available since the study area is not within the exploitation area.

5.5. Conclusions

The recovery of low-grade mineral deposits requires the construction of large scale open-pit mines for which rock engineers face new challenges to design slopes. One objective in geotechnical analysis and designs of excavation in rock is to collect the minimum number of orientation data (dip/dip direction) to reach targeted levels of confidence and different degrees of precision. However, a rock mass comprises blocks of intact rock separated by discontinuities such as faults, shear zones, bedding planes and joints, making it hard to predict in space.

The proposed methodology accounts for (1) the inherent nature of geotechnical parameters (namely, their directional dependence) through a regionalization of RQD, JC and IRS in the geographical space crossed with an angular space, and (2) their uncertainty at unsampled locations by the recourse to geostatistical simulations, reproducing better the geographical and directional heterogeneity and the real nature of the rock mass, thus delivering a more reliable geotechnical model for stability analysis.

The failure of the rock mass is mostly governed by discontinuities and occurs according to surfaces formed by one or more joints, involving sliding on multiple discontinuity sets as well as tensile and shear failure of rock bridges and intact rock blocks. In this research, we used SMR classification as the tool for potential structurally controlled failure detection, correcting the basic RMR by four factors that depend on the slope and discontinuity orientations. Also, since the studied mineral deposit is structurally complex, considering the large structures to establish these SMR adjustment factors, as suggested by the traditional approach, would not be representative of the local rock mass behavior. Instead, a directional approach has been chosen, where SMR is derived by considering the direction of minimum RQD (corresponding to the most unfavorable direction of fracturing, i.e., the worst-case scenario). The product of the correction factors $F_1 \times F_2 \times F_3$ can therefore be

regionalized with less fieldwork and gives an excellent indication of slopes stability risk.

The simulation of SMR makes it possible to map the geomechanical quality of the slope, differentiating through a kinematic analysis the different types of failure compatible with the slope-discontinuity relationship, finding blocks compatible with complex mechanisms or faults such as soil, the presence of large plane failures and wedges in the western sector of the area under study.

The SMR system provides an estimate of the behavior of the rock mass and quantitatively defines correction factors, allowing to differentiate the types of failure kinematically compatible with the geometry of the slope and the discontinuity in each block. In the study area, the angle values (for the bench) used in the slope stability evaluation in the western sector may be too steep, which could result in a slope design that is too optimistic for pit stability and the recommendation is to reduce this angle from 70° to 52°. Though, the safety factor and the probability of failure of a slope are not, in themselves, the unique basis for judging the acceptability of a slope design. The decision should also include a consideration of the costs of cleanup and limitation of access versus the cost of remedial action such as changing the slope geometry to reduce the probability of failure. The outcomes of the developed methodology would allow to evaluate stability constraints for various geometric configurations of the pit at the mine planning stage, into an integrated approach with the pit design tools, providing immediate and accurate insight into the economic implications of multiple design scenarios.

As a perspective for future works, we propose to analyze the quality of the approximations (linear discontinuity frequency vs. RQD) and to determine measures of how closely the discontinuity spacing values follow a negative exponential distribution in each location.

CHAPTER VI.

GENERAL DISCUSSION

- **Data collection and preparation**

Geotechnical models play a vital role in the optimization of mine planning and design as they contribute to understanding the spatial variability of rock mass engineering properties and improving the prediction of the rock mass behavior during excavation and during comminution, thus beneficiating the safety of the mine and its personnel, the mining process and the mineral processing process. The geostatistical approaches require a sufficient amount of data for statistical inference, but cost-efficiency and other practical considerations limit the number of boreholes drilled for an exploratory campaign, prevailing the uncertainty in the real spatial continuity of rock mass engineering properties. Therefore, geotechnical information is often scattered or widely dispersed in the area of study, added to a significant degree of subjectivity in the data collection during the site investigation (coming from the subjective definitions of some geotechnical properties), which can make difficult to apply geostatistical approximation techniques properly. Nowadays, drillings are being scanned, so that the fracture counting can be automatic and not restricted to portions of boreholes being logged by geologists; also, instead of using a rock quality designation (RQD) associated with 10 cm, complete information on the fragment size distribution on linear supports can be obtained, allowing an improved modeling of the fracturing density and fragment sizes. In underground operations, something similar is done with the scanning of drift heading, where the geological strength index (GSI) or other similar variables can be inferred. However, these advanced technologies and equipment are used in different periods of time and can cause the inhomogeneity of the geotechnical data in time and space used for modeling.

- **Direction dependence**

The values of geotechnical properties logged in the process of core logging may change significantly, depending upon the borehole or scanline orientation. In other words, the measured value depends not only on the in-situ geographic coordinates of the sample but also on the in-situ borehole direction. Interpolating such geotechnical variables in space without accounting for their directional dependence may produce misleading results, insofar as the interpolated values are representative of the rock mass properties in the sampling directions and not necessarily in other directions. An ideal solution to this issue is to collect logging information using the boreholes/scanline in various orientations to allow for better detection of rock mass directional behavior. In practice, this may not always be possible because the exploration boreholes are generally oriented preferentially in the direction in which the orebody extends. The key proposal of this thesis is to regionalize the geotechnical variables in a five-dimensional space, consisting of the Cartesian product of the three-dimensional Euclidean space and the unit two-dimensional sphere, in order to account for both their geographic and directional variations. Spatial correlation analysis can be performed easily under an assumption of stationarity in the three-dimensional Euclidean space and isotropy on the sphere, so that the covariance or the variogram between two data only depends on their geographic and angular separations. The fitting of nested separable covariance functions eases the search for a valid spatial correlation model and for algorithms to simulate the geotechnical variables in the above-defined five-dimensional space.

The anisotropy indicator defined in Chapter 3 can be an important input for new post-blast P80 fragmentation models, as well as rock mass property scaling using RQD, JC, FF as input, and even mineral resources models. Drill-induced damage from a natural joint to an open fracture must identify or separate its mechanically induced breaks from natural breaks, before analyzing the in-situ anisotropy of geotechnical variables such as RMR, given its influence on the block and rock mass strength.

- **Additivity and change support (upscaling)**

The application of geostatistical techniques in geotechnics has a challenge in that some variables, such as the rock mass rating (RMR), present a non-linear scale and cannot be block-averaged to represent the behavior of a rock mass. Thus, the calculation of the average value in supports more voluminous than the measurements may not have a physical sense, i.e., the variable is non-additive. This fact agrees with the concept of size effect in rock masses, where the characteristics of rock masses may change gradually when increasing the sample size until this size is larger than a critical value (Representative Volume Element or RVE) and the characteristic values remain unchanged.

As an exception, some variables (like the fracture frequency FF or the rock quality designation RQD) are additive when they are measured along the same direction, i.e., the variables are directionally additive. In such a case, the five-dimensional regionalization proposed in this thesis allows the prediction or simulation accounting for a change of support. As for the point-support variable, the regularized (block-averaged) variable is still direction-dependent. Thus, it is necessary to define a rule to derive a single representative value of a block volume from the set of directional values. In the case of FF and RQD, the ‘worst case’ (direction along which the maximum FF or minimum RQD is reached) reflects the maximum fracturing of the rock mass and can be used to define a non-directional block value. This change of support proposal is general, and applicable even if the fracture network is not a set of parallel planes.

- **Stationarity and isotropy assumptions**

In practice, some simplifying assumptions are necessary to infer and model the spatial correlation of regionalized data. In the case of geotechnical data, we considered second-order stationarity in the Euclidean space and isotropy on the sphere, so that the correlation structure only depends on the geographic and angular separations between paired data. If these two assumptions are not taken into account, the non-stationary and anisotropic experimental function (variogram or

covariance) will depend on ten parameters (X, Y, Z, azimuth, and dip of each paired data). So, it would be hardly possible to identify the spatio-angular correlation structure of the regionalized variable with a limited number of experimental data: The ten-dimensional parameter space is too large for inferring the experimental covariance or variogram function. Under the stationarity and isotropy assumptions, one gets a function that only depends on four parameters (projections **h**x, **h**y, **h**z of the geographic separation upon the coordinate axes, and angular separation δ). The representation of the phenomenon in R^3 x S^2 is better than the traditional representation in R^3, as it captures the directional behavior of the variable under study with a minimal increase of the parameter space.

To broaden the scope of application of the presented proposal, future works in 5D geostatistical modeling should include the design of variogram models and simulation algorithms using non-separable covariance functions (e.g., Alegría et al., 2021), or anisotropic covariances on the sphere (e.g., Emery and Alegría, 2020), together with exploratory tools to identify preferred directions of anisotropy on the sphere based on sampling information.

- **Computational requirements**

The traditional approach (3D) achieves a prediction that is generally cheap in terms of computational requirements and pre-processing time but may be locally biased as per the drilling directions of the available samples. The directional approach (5D) is more demanding in terms of modeling and computational capacity (the developments shown in Chapters 3, 4 and 5 use 121 directions to discretize the sphere, i.e., the computational time is multiplied by two orders of magnitude with respect to the 3D case) but provides information on the directional behavior of the variables under study and predictions that are unbiased. This is valuable for geotechnical zoning and decision-making as the predicted or simulated values reflect the inherent nature of the geotechnical parameters (their directional dependence) and can give an insight into the geometry of the rock fragments when combined with other direction-dependent parameters such as the fracture frequency.

- **Stages of Project Mining**

The directional approach is helpful in any stage of a geotechnical project. At the exploratory or early stages, it is suggested to use adaptive geometries in the block model: the size of the block to predict or to simulate will depend on the variability of the geotechnical parameter in the sector and on the available information, i.e., the less amount of available information (and the more variability of geotechnical parameter), the larger the block size. At the development and production stages, it is possible to model the geotechnical parameters in a direction that is parallel or perpendicular to the advance of the construction of the rock excavation. One way to optimize the analysis is to use adaptive geometries in the block model in further developments, giving a higher resolution (smaller block size) in areas with a higher anisotropy index or vice versa.

CHAPTER VII.

CONCLUSIONS AND FUTURE WORKS

Identifying the geomechanical and hydraulic properties of a rock mass is a crucial task for the economic development of underground and open pit mining, in the petroleum industry, tailings tanks, geothermal reservoirs, groundwater resources, underground nuclear waste, among others. Geological phenomena have spatial heterogeneities evidencing a high strength and rigidity contrast on a small scale, making it more challenging to predict the mechanical behavior of the rock mass. Geostatistics allows spatial prediction and uncertainty quantification accounting for such heterogeneities. However, its application to geotechnics faces specific difficulties or limitations, in particular due to the fact that most variables are direction-dependent and are defined on a line support, which raises the question on how to upscale them to a block support.

The thesis addressed the problem of modeling direction-dependent geotechnical variables in the context of mineral resources evaluation, mine design or mine planning. The proposed solution is to regionalize these variables in a five-dimensional space: 3D geographical space × 2D sphere. The geostatistical modeling and simulation can be realized in a simple way by assuming stationarity in the 3D space and isotropy on the sphere and by using separable nested structures, from the viewpoints of the calculation of an experimental covariance or variogram and the fitting of a theoretical model. The main idea is to decompose the covariance functions of the direction-dependent variables as the sum of products of non-directional and directional components. Conditional simulation can be performed via spectral or turning bands algorithms, providing results for any geographic location and any target direction. Upscaling can be done by block-averaging the values associated with the same direction.

Three applications have been developed throughout the thesis. The first application set the theoretical basis of the spatial correlation modeling, proposed a novel algorithm for conditional simulation, and demonstrated the applicability of the

tools and algorithms with a case study on the modeling of the discontinuity frequency in the El Teniente copper deposit (central Chile), where attention was paid to the checking of the model assumptions and the cross-validation of the simulation results. The second application, presented through a case study on a polymetallic deposit, tackled the directional bias characteristic of one-dimensional measurements (boreholes and scanlines) and their extension to volumetric supports like selective mining units, considering the maximum fracturing direction and defining an anisotropy index that quantifies how much a variable is likely to vary, at the same geographic location, when changing the measurement direction. The last application presented the extension of the covariance models in the 3D space crossed with the 2D sphere to the multivariate setting, as well as the adaptation of tools and algorithms to co-simulation, with an application to an open pit mine (Radomiro Tomic, northern Chile), seeking to establish an acceptable slope design criterion for the open pit based on a chart considering SMR and height design to predict a safe slope angle. These applications provide elements to geologists, geotechnicians, and engineers for decision-making in rock mass characterization and classification and in mine design.

As a general result, the tools and methods that are usually used in the traditional geostatistics in Euclidean spaces (in particular, variogram analysis, multivariate modeling, and simulation) have been extended to the 3D space crossed with a 2D sphere, which makes the concepts fully applicable to practitioners, although the computational cost still remains expensive for large-scale problems. This new paradigm allows geotechnical variables to be interpolated at any place in the geographic space for any direction. In practice however, most of the boreholes are often close to vertical, some are horizontal, and very few are inclined, so it may be difficult to characterize the geotechnical parameters along any direction using only borehole information. Another limitation is that two assumptions were considered to model the geotechnical variables: the parent random field is stationary in the 3D space, and isotropic on the 2D sphere. Future work includes the design of random field models and simulation algorithms using non-separable covariances or anisotropic covariances in the sphere, together with exploratory tools to identify preferred directions of anisotropy on the sphere based on sampling information.

In general, quantitative fracture network characterization has traditionally been investigated using 1D scanline or borehole data but recent advances in fracture network data acquisition (e.g., remote sensing, microseismic) have made it possible to examine the spatial attributes of fracture networks reducing the uncertainty and considering the directional dependence using all the potential of 5D geostatistics. The spatial variability of the fracture intensity and intersection density are proxies for secondary porosity and permeability and, as such, are indicators of the efficiency of fluid storage and flow through fractured rock masses, so it can be used to improve the calculations of cave ability, water drainage, roof stability, fragmentation, flow gravity, slope stability, blast ability, and in-situ leaching. The understanding of fracture systems is a critical factor, given that fractures reduce the structural integrity of materials and create conduits and barriers that can enhance or impede subsurface fluid flow. This has a wide range of industrial applications not only limited to mining operations but also such as tailing dam disposal, modeling of oil/gas reservoirs (fractured reservoirs and unconventional reservoirs) or geothermal reservoirs, groundwater resources management, underground nuclear wastes disposal, between other.

In addition, the tools and methodologies developed in the thesis can be useful to several other application domains in the geosciences and environmental, atmospheric, or oceanographic sciences, in which one also deals with direction-dependent variables, such as the hydraulic conductivity or permeability, electromagnetic radiation, wind velocity, ocean current velocity, temperature gradient or gravity gradient.

BIBLIOGRAPHY

[1] Abdideh, M., Mahmoudi, N., Moghadasi, J., 2014. Geostatistical analysis of the uniaxial compressive strength (UCS) of reservoir rock by petrophysical information. Energy Sources, Part A: Recovery, Utilization, and Environmental Effects 36(21): 2320–2327.

[2] Abramowitz, M., & Stegun, I. A., 1970: Handbook of Mathematical Functions, Dover Publications, Inc., New York.

[3] Alegría, A., Emery, X., & Lantuéjoul, C., 2020. The turning arcs: a computationally efficient algorithm to simulate isotropic vector-valued Gaussian random fields on the d-sphere. Statistics and Computing, 30(5), 1403-1418.

[4] Arfken, G., Weber, H.J., 2005. Mathematical Methods for Physicists, 6th ed. Elsevier Academic Press, Amsterdam.

[5] Alegría, A., Porcu, E., Furrer, R., & Mateu, J., 2019. Covariance functions for multivariate Gaussian fields evolving temporally over planet earth. Stochastic Environmental Research and Risk Assessment, 33(8-9), 1593-1608.

[6] Anh, V. V., Broadbridge, P., Olenko, A., & Wang, Y. G., 2018. On approximation for fractional stochastic partial differential equations on the sphere. Stochastic environmental research and risk assessment, 32(9), 2585-2603.

[7] Azimian, A., 2016. A new method for improving the RQD determination of rock core in borehole. Rock Mechanics and Rock Engineering, 49(4), 1559-1566.

[8] Bandis, S., Lumsden, A.C., Barton, N.R., 1981. Experimental studies of scale effects on the shear behaviour of rock joints. International Journal of Rock Mechanics and Mining Sciences & Geomechanics Abstracts, 18(1), 1–21.

[9] Barton, N., 1990. Scale effects or sampling bias? In Proceedings of the 1st International Workshop Scale Effects in Rock Masses, Loen, Norway, 7–8 June 1990; Balkema: Rotterdam, The Netherlands; pp. 31–55.

[10] Barton, N., Reidar, L., Lunde, J., 1974. Engineering classification of rock masses for the design of tunnel support. Rock mechanics 6(4), 189–236.

[11] Bertuzzi, R., Douglas, K., Mostyn, G., 2016. Comparison of quantified and chart GSI for four rock masses. Engineering Geology, 202, 24–35.

[12] Bieniawski, Z.T., 1968. The effect of specimen size on compressive strength of coal. International Journal of Rock Mechanics and Mining Sciences & Geomechanics Abstracts, 5(4), 325–326.

[13] Bieniawski, Z.T., 1973. Engineering classification of jointed rock masses. Civil Engineer in South Africa, 15(12), 335–353.

[14] Bieniawski, Z.T., 1976. Rock mass classification in rock engineering applications. In Proceedings of a Symposium on Exploration for Rock Engineering, 1976 (Vol. 1, pp. 97-106). Balkema, Cape Town.

[15] Bieniawski, Z.T., 1979. The geomechanics classification in rock engineering applications. In Proceedings of 4th Congress of International Society of Rock Mechanics, Montreux, vol. 2, pp. 41–48. Balkema, Rotterdam.

[16] Bieniawski, Z. T.,1989. Engineering rock mass classifications: a complete manual for engineers and geologists in mining, civil, and petroleum engineering. John Wiley & Sons.

[17] Bonnet, E., Bour, O., Odling, N. E., Davy, P., Main, I., Cowie, P., & Berkowitz, B., 2001. Scaling of fracture systems in geological media. Reviews of geophysics, 39(3), 347-383.

[18] Boyd, D.L., Walton, G., Trainor-Guitton, W., 2019. Quantifying spatial uncertainty in rock through geostatistical integration of borehole data and a geologist's cross-section. Engineering Geology, 260, 105246.

[19] Brzovic, A., Villaescusa, E., 2007. Rock mass characterization and assessment of block-forming geological discontinuities during caving of primary copper ore at the El Teniente mine, Chile. International Journal of Rock Mechanics and Mining Sciences & Geomechanics Abstracts 44: 565–583.

[20] Brzovic, A., 2009. Rock mass strength and seismicity during caving propagation at the El Teniente Mine, Chile. In: Tan, C.A. (ed.), 7th International Symposium on Rockbursts and Seismicity in Mines (RaSiM7). Rinton Press, New York, pp. 838–852.

[21] Cai, M., 2011. Rock mass characterization and rock property variability considerations for tunnel and cavern design. Rock mechanics and rock engineering, 44(4), 379-399.

[22] Cannell, J., Cooke, D., Walshe, J.L., Stein, H., 2005. Geology, mineralization, alteration, and structural evolution of the El Teniente porphyry Cu-Mo deposit. Economic Geology 100: 979–1005.

[23] Carrasco, P., Chilès, J. P., and Séguret, S., 2008. Additivity, metallurgical recovery, and grade. In: Ortiz, J. M., and Emery, X. (eds.) Proceedings of the Eighth International Geostatistics Congress. Gecamin Ltda, Santiago, pp. 237-246.

[24] Chen, J.Q., Li, X.J., Zhu, H.H., Rubin, Y., 2017. Geostatistical method for inferring RMR ahead of tunnel face excavation using dynamically exposed geological information. Engineering Geology, 228, 214-223.

[25] Chilès, J.P., 2005. Stochastic modeling of natural fractured media: a review. In: Leuangthong, O., Deutsch, C.V. (Eds.), Geostatistics Banff' 2004. Springer, Dordrecht, pp. 285–294.

[26] Chilès, J. P., Wackernagel, H., Beucher, H., Lantuéjoul, C. and Elion, P., 2008. Estimating fracture density from a linear or areal survey. In: Ortiz, J.M., Emery, X. (eds.), Proceedings of the Eighth International Geostatistics Congress. Gecamin Ltda, Santiago, pp. 535–544.

[27] Chilès, J.P., Delfiner, P., 2012. Geostatistics: Modeling Spatial Uncertainty. Wiley, New York, pp. 699.

[28] Choi, S.Y., Park, H.D., 2002. Comparison among different criteria of RMR and Q-system for rock mass classification for tunnelling in Korea. Tunnelling and Underground Space Technology 17(4): 391–401.

[29] Choi, S.Y., Park, H.D., 2004. Variation of rock quality designation (RQD) with scanline orientation and length: a case study in Korea. International Journal of Rock Mechanics and Mining Sciences, 41(2), 207-221.

[30] Choi, Y., Yoon, S.Y., Park, H.D., 2009. Tunneling Analyst: a 3D GIS extension for rock mass classification and fault zone analysis in tunneling. Computers & Geosciences 35(6): 1322–1333.

[31] Chowdhury, R., Flentje, P., Bhattacharya, G., 2012. Geotechnics in the 21st century, uncertainties and other challenges, with particular references to

landslide hazard and risk assessment. J. Life Cycle Reliab. Saf. Eng., 1, 27–43.

[32] Christian, J. T. and Baecher, G. B., 2003. Reliability and Statistics in Geotechnical Engineering, John Wiley & Sons Ltd, 618 p.

[33] Cuisiat, F.D., Haimson, B.C., 1992. Scale effects in rock mass stress measurements. International Journal of Rock Mechanics and Mining Sciences & Geomechanics Abstracts, 29(2), 99-117.

[34] Cunha, A.P.,1990. Scale effects in rock mechanics. In proocedings of the first International workshop on scale effect in rock masses, Loen, 7-8 June, 3-31.

[35] Cundall, P. A., Pierce, M. E., & Mas Ivars, D., 2008, September. Quantifying the size effect of rock mass strength. In Proceedings of the 1st Southern Hemisphere International Rock Mechanics Symposium (Vol. 2, pp. 3-15). Australian Centre for Geomechanics (ACG).

[36] Daley DJ, Porcu E, 2014. Dimension walks and Schoenberg spectral measures. Proceedings of the American Mathematical Society 142(5):1813–1824

[37] Deere, D.U., Hendron Jr, A.J., Patton, F.D., Cording, E.J., 1967. Design of surface and near-surface construction in rock. In: Failure and Breakage of Rock, Proceedings of the 8th Symposium on Rock Mechanics, American Institute of Mining and Metallurgical Engineers (pp. 273-303).

[38] Deere, D.U., 1989. Rock quality designation (RQD) after 20 years. US Army Corps Engrs. Contract Report GL-89-1. Waterways Experimental Station, Vicksburg, MS.

[39] Deisman, N., Khajeh, M., Chalaturnyk, R.J., 2013. Using geological strength index (GSI) to model uncertainty in rock mass properties of coal for CBM/ECBM reservoir geomechanics. International Journal of Coal Geology 112: 76–86.

[40] Deutsch, C.V., 1997. Direct assessment of local accuracy and precision. In: Baafi, E.Y., Schofield, N.A. (Eds.), Geostatistics Wollongong' 96. Kluwer Academic, Dordrecht, pp. 115–125.

[41] Dershowitz, W.S., 1984. Rock joint systems, Ph.D. thesis, MIT, Cambridge, Mass., 764 p.

[42] Dershowitz, W. S., P. R. La Pointe, and T. W. Doe. "Advances in discrete fracture network modeling." Proceedings of the US EPA/NGWA fractured rock conference, Portland. 2004.

[43] Doostmohammadi, M., Jafari, A., Asghari, O., 2015. Geostatistical modeling of uniaxial compressive strength along the axis of the Behesht-Abad tunnel in Central Iran. Bulletin of Engineering Geology and the Environment 74(3): 789–802.

[44] Dowd, P.A., Xu, C., Mardia, K.V., Fowell, R.J., 2007. A comparison of methods for the stochastic simulation of rock fractures. Mathematical Geology 39(7): 697–714.

[45] Edelbro, C., 2004. Evaluation of rock mass strength criteria (Doctoral dissertation, Luleå tekniska universitet).

[46] Egaña, M., Ortiz, J., 2013. Assessment of RMR and its uncertainty by using geostatistical simulation in a mining project. Journal of GeoEngineering 8(3): 83–90.

[47] Egaña, M. J., 2008. Geoestadística Aplicada a Parámetros Geotécnicos. Memoria de Ingeniería Civil de Minas, Universidad de Chile.

[48] Ellefmo, S.L., Eidsvik, J., 2009. Local and spatial joint frequency uncertainty and its application to rock mass characterisation. Rock Mechanics and Rock Engineering 42(4): 667–688.

[49] Elsayed, A.E., Sen, Z., 1991. Probabilistic simulation of rock quality designation (RQD). Bulletin of the International Association of Engineering Geology-Bulletin de l'Association Internationale de Géologie de l'Ingénieur, 43(1), 31-40.

[50] Emery, X., 2005. Variograms of order □: a tool to validate a bivariate distribution model. Mathematical Geology 37(2): 163–181.

[51] Emery, X., Lantuéjoul, C., 2006. TBSIM: A computer program for conditional simulation of three-dimensional Gaussian random fields via the turning bands method. Computers & Geosciences 32(10): 1615–1628.

[52] Emery, X., Ortiz, J. M. and Cáceres, A. M., 2008. Geostatistical modelling of rock type domains with spatially varying proportions: application to a porphyry copper deposit. Journal of the Southern African Institute of Mining and Metallurgy, 108, 284-292.

[53] Emery, X., & Peláez, M., 2011. Assessing the accuracy of sequential Gaussian simulation and cosimulation. Computational Geosciences, 15(4), 673-689.

[54] Emery, X., Furrer, R., Porcu, E., 2019.a. A turning bands method for simulating isotropic Gaussian random fields on the sphere. Statistics and Probability Letters 144: 9–15.

[55] Emery, X., Porcu, E., & Bissiri, P. G., 2019.b. A semiparametric class of axially symmetric random fields on the sphere. Stochastic Environmental Research and Risk Assessment, 33(10), 1863-1874.

[56] Emery, X., & Porcu, E., 2019. Simulating isotropic vector-valued Gaussian random fields on the sphere through finite harmonics approximations. Stochastic Environmental Research and Risk Assessment, 33(8-9), 1659-1667.

[57] Emery, X., Séguret, S.A., 2020. Geostatistics for the Mining Industry - Applications to Porphyry Copper Deposits. CRC Press, Boca Raton, 247 pp.

[58] Emery, X., & Alegría, A., 2020. A spectral algorithm to simulate nonstationary random fields on spheres and multifractal star-shaped random sets. Stochastic Environmental Research and Risk Assessment, 34(12), 2301-2311.

[59] Emery, X., Alegría, A., & Arroyo, D., 2021. Covariance models and simulation algorithm for stationary vector random fields on spheres crossed with Euclidean spaces. SIAM Journal on Scientific Computing, 43(5), A3114-A3134.

[60] Emery, X., Arroyo, D., & Mery, N., 2022. Twenty-two families of multivariate covariance kernels on spheres, with their spectral representations and sufficient validity conditions. Stochastic Environmental Research and Risk Assessment, 36(5), 1447-1467.

[61] Esmaieli, K., Hadjigeorgiou, J., & Grenon, M., 2010. Estimating geometrical and mechanical REV based on synthetic rock mass models at Brunswick Mine. International Journal of Rock Mechanics and Mining Sciences, 47(6), 915-926.

[62] Etminan, A. H. and Seifi, A., 2008. An improved model for geostatistical simulation of fracture parameters and their effect on static and dynamic models. The Open Petroleum Engineering Journal 1: 47-57.

[63] Exadaktylos, G., Stavropoulou, M., 2008. A specific upscaling theory of rock mass parameters exhibiting spatial variability: Analytical relations and computational scheme. International Journal of Rock Mechanics and Mining Sciences 45(7): 1102–1125.

[64] Fenton, G. A., 1997. Probabilistic methods in geotechnical engineering. In: Workshop presented at ASCE GeoLogan'97 conference, Logan, Utah.

[65] Ferrari, F., Apuani, T., Giani, G.P., 2014. Rock Mass Rating spatial estimation by geostatistical analysis. International Journal of Rock Mechanics and Mining Sciences 70: 162–176.

[66] Fillion, M. H., 2018. Optimizing Geotechnical Data Collection Campaigns in Open Pit Mines (Doctoral dissertation, University of Toronto (Canada)).

[67] Gao, X., Yan, E.C., Yeh, T.C.J., Cai, J.S., Liang, Y., Wang, M., 2018. A geostatistical inverse approach to characterize the spatial distribution of deformability and shear strength of rock mass around an unlined rock cavern. Engineering Geology, 245, 106–119.

[68] Gneiting, T., 1999. Correlation functions for atmospheric data analysis. Quaterly Journal of the Royal Meteorological Society, Part A, 125(559): 2449-2464.

[69] Gneiting, T., 2013. Strictly and non-strictly positive definite functions on spheres. Bernoulli 19(4): 1327-1349.

[70] Goovaerts, P., 2001. Geostatistical modelling of uncertainty in soil science. Geoderma 103: 3–26.

[71] Goulard, M., & Voltz, M., 1992. Linear coregionalization model: tools for estimation and choice of cross-variogram matrix. Mathematical Geology, 24(3), 269-286.

[72] Grenon, M., Hadjigeorgiou, J., 2010. Integrated structural stability analysis for preliminary open pit design. International Journal of Rock Mechanics and Mining Sciences, 47(3), 450-460.

[73] Hadjigeorgiou, J., & Harrison, J. P., 2011, January. Uncertainty and sources of error in rock engineering. In 12th ISRM Congress. International Society for Rock Mechanics and Rock Engineering.

[74] Haftani, M., Chehreh, H.A., Mehinrad, A., Binazadeh, K., 2016. Practical investigations on use of weighted joint density to decrease the limitations of RQD measurements. Rock Mechanics and Rock Engineering, 49(4), 1551-1558.

[75] Hekmatnejad, A, Emery, X., Brzovic, A., Schachter, P., Vallejos, J.A., 2017. Spatial modeling of discontinuity intensity from borehole observations at El Teniente mine, Chile. Engineering Geology 228: 97–106.

[76] Hekmatnejad, A., Emery, X., Brzovic, A., Vallejos, J., 2016. Spatial prediction of fracture intensity based on drill hole observations. In: Proceedings of the 2016 SME Annual Conference and Expo: The Future for Mining in a Data-Driven World. Society for Mining, Metallurgy & Exploration, Englewood, Colorado, pp. 282-286.

[77] Hoek, E., & Brown, E. T., 1980. Underground excavations in rock. Inst. Mining and Metallurgy, London, 156.

[78] Hoek, E., Bray, J., 1981 Rock Slope Engineering. London: Institute of Mining and Metallurgy.

[79] Hoek, E., 1983. Strength of jointed rock masses. Geotechnique, 33(3), 187-223.

[80] Hoek, E., 1994. Strength of rock and rock masses. ISRM News Journal, 2, 4-16.

[81] Hoek, E., 2006. Practical Rock Engineering. Rocscience: Rock mass classification

[82] Hoek, E., Carter, T.G., Diederichs, M.S., 2013. Quantification of the geological strength index chart. In 47th US rock mechanics/geomechanics symposium. American Rock Mechanics Association.

[83] Huang, C., H. Zhang, and S. M. Robeson, 2011. On the validity of covariance and variogram functions on the sphere. Mathematical Geosciences 43(6): 721-733.

[84] Hudson, J., 2012. Design methodology for the safety of underground rock engineering. Journal Rock Mechanics and Geotechnical Engineering, 4, 205–214.

[85] Hyman, J.D., Karra, S., Makedonska, N., Gable, C.W., Painter, S.L., Viswanathan, H.S., 2015. DFNWORKS: A discrete fracture network framework for modeling subsurface flow and transport. Computers & Geosciences 84: 10–19.

[86] Jeon, S., Hong, C., You, K., 2009. Design of tunnel supporting system using geostatistical methods. In: Ng, C.W.W., Huang, H.W., Liu, G.B. (Eds.), Geotechnical Aspects of Underground Construction in Soft Ground. CRC Press, Boca Raton, pp. 781–784.

[87] Jing, L., 2003. A review of techniques, advances and outstanding issues in numerical modelling for rock mechanics and rock engineering. International Journal of Rock Mechanics and Mining Sciences, 40(3), 283-353.

[88] Jones, R. H., 1963. Stochastic processes on a sphere. The Annals of mathematical statistics, 34(1), 213-218.

[89] Journel, A.G., 1983. Non-parametric estimation of spatial distributions. Mathematical Geology 15(3): 445–468.

[90] Jun, M., and M. L. Stein, 2008. Nonstationary covariance models for global data. The Annals of Applied Statistics 2(4): 1271-1289.

[91] Kloppenburg, A., Alzate, J. C., & Rodríguez, G., 2003. Building a discrete fracture network based on the deformation history: a case study from the Guaduas Field, Colombia. In 8th Simposio Bolivariano-Exploracion Petrolera en las Cuencas Subandinas.

[92] Lang, A., & Schwab, C., 2015. Isotropic Gaussian random fields on the sphere: regularity, fast simulation and stochastic partial differential equations. The Annals of Applied Probability, 25(6), 3047-3094.

[93] Lantuéjoul, C., 2002. Geostatistical Simulation, Models and Algorithms. Springer, Berlin, pp. 256.

[94] Lantuéjoul, C., Freulon, X., & Renard, D., 2019. Spectral simulation of isotropic Gaussian random fields on a sphere. Mathematical Geosciences, 51(8), 999-1020.

[95] Lato, M., Kemeny, J., Harrap, R.M., Bevan, G., 2013. Rock bench: establishing common repository and standards for assessing rockmass characteristics using LiDAR and photogrammetry. Computers & Geosciences 50: 106-114.

[96] Le Gia, Q.T., Sloan, I.H., Womersley, R.S., Wang, Y.G., 2019. Isotropic sparse regularization for spherical harmonic representations of random fields on the sphere. Applied and Computational Harmonic Analysis, in press. https://doi.org/10.1016/j.acha.2019.01.005

[97] Le Goc, R., Darcel, C., Davy, P., Pierce, M. and Brossault, M. A., 2014. Effective elastic properties of 3D fractured systems. In: Proceedings of the 1st International Conference on Discrete Fracture Network Engineering, Paper ID 142, Vancouver, Canada

[98] Madani, N. and Asghari, O., 2013. Fault detection in 3D by sequential Gaussian simulation of Rock Quality Designation (RQD). Arabian Journal of Geosciences 12(10): 3737-3747

[99] Maerten, L., Pollard, D. D., & Karpuz, R., 2000. How to constrain 3-D fault continuity and linkage using reflection seismic data: a geomechanical approach. AAPG bulletin, 84(9), 1311-1324.

[100] Maksaev, V., Tomlinson, A.J., & Blanco, N., 1994. Estudio geológico de la franja longitudinal comprendida entre Quebrada Blanca y Chuquicamata SERNAGEOMIN-CODELCO, internal report: 72 p.

[101] Mao, S. and Journel, A., 1999. Generation of a reference petrophysical/seismic data set: the Stanford V reservoir. 12th Annual Report Stanford Center for Reservoir Forecasting, Stanford USA.

[102] Marinucci, D. & Peccati, G., 2011. Random Fields on the Sphere, Representation, Limit Theorems and Cosmological Applications. New York: Cambridge.

[103] Marinos, V.I.I.I., Marinos, P., Hoek, E., 2005. The geological strength index: applications and limitations. Bulletin of Engineering Geology and the Environment, 64(1), 55-65.

[104] Marinos, V., Carter, T.G., 2018. Maintaining geological reality in application of GSI for design of engineering structures in rock. Engineering Geology, 239, 282-297.

[105] Matheron, G., 1971. The Theory of Regionalized Variables and its Applications. Paris School of Mines, Paris.

[106] Matheron, G., 1973. The intrinsic random functions and their applications. Advances in applied probability, 5(3), 439-468.

[107] Matonti, C., Guglielmi, Y., Viseur, S., Bruna, P. O., Borgomano, J., Dahl, C., Marié, L., 2015. Heterogeneities and diagenetic control on the spatial distribution of carbonate rocks acoustic properties at the outcrop scale. Tectonophysics, 638, 94-111.

[108] Milne, D., Hadjigeorgiou, J., & Pakalnis, R., 1998. Rock mass characterization for underground hard rock mines. Tunnelling and underground space technology, 13(4), 383-391.

[109] National Research Council, 2006. Geological and geotechnical engineering in the new millennium: opportunities for research and technological innovation. National Academy Press, Washington, DC.

[110] Oh, S., Chung, H., Kee Lee, D., 2004. Geostatistical integration of MT and boreholes data for RMR evaluation. Environmental Geology 46: 1070–1078.

[111] Ozturk, C.A., Nasuf, E., 2002. Geostatistical assessment of rock zones for tunneling. Tunnelling and Underground Space Technology 17: 275–285.

[112] Ozturk, C.A., Simdi, E., 2014. Geostatistical investigation of geotechnical and constructional properties in Kadikoy–Kartal subway, Turkey. Tunnelling and Underground Space Technology 4: 35–45.

[113] Palmström, A., 1982 The volumetric joint counted useful and simple measure of the degree of rock mass jointing. In: Proceedings of the 4th Congress of International Association of Engineering Geology, pp. 221e8. New Delhi.

[114] Palmstrom, A., 2005. Measurements of and correlations between block size and rock quality designation (RQD). Tunnelling and Underground Space Technology, 20(4), 362-377

[115] Pinheiro, M., Emery, X., Miranda, T. and Vallejos, J., 2016a. Truncated Gaussian Simulation to Map the Spatial Heterogeneity of Rock Mass Rating. Rock Mechanics and Rock Engineering 49(8): 1-6.

[116] Pinheiro, M., Vallejos, J., Miranda, T. and Emery, X., 2016b. Geostatistical simulation to map the spatial heterogeneity of geomechanical parameters: A case study with rock mass rating. Engineering Geology 205: 93-103.

[117] Peron, A., Porcu, E., & Emery, X., 2018. Admissible nested covariance models over spheres cross time. Stochastic environmental research and risk assessment, 32(11), 3053-3066.

[118] Popescu, R., Deodatis, G. and Nobahar, A., 2005. Effects of random heterogeneity of soil properties on bearing capacity. Probabilistic Engineering Mechanics 20: 324-341.

[119] Porcu, E., Bevilacqua, M., Genton, M.G., 2016. Spatio-temporal covariance and cross-covariance functions of the great circle distance on a sphere. Journal of the American Statistical Association 111(514): 888–898.

[120] Porcu, E., Alegria, A., & Furrer, R., 2018. Modeling temporally evolving and spatially globally dependent data. International Statistical Review, 86(2), 344-377.

[121] Porcu, E., Castruccio, S., Alegria, A., & Crippa, P., 2019. Axially symmetric models for global data: a journey between geostatistics and stochastic generators. Environmetrics, 30(1), e2555.

[122] Pratt, H.R., Black, A.D., Brown, W.S., Brace, W.F., 1972. The effect of speciment size on the mechanical properties of unjointed diorite. International Journal of Rock Mechanics and Mining Sciences & Geomechanics Abstracts, 9(4), 513-516.

[123] Priest, S. D. and J. A. Hudson., 1976. Discontinuity spacing in rock. International Journal of Rock Mechanics and Mining Sciences & Geomechanics Abstracts 13(5): 135-148.

[124] Priest, S.D., 1985. Hemispherical projection methods in rock mechanics. Allen & Unwin.

[125] Rocha, M., 1974. Present possibilities of studying foundations of concrete dams, Advances in rock mechanics, National Academy of Sciences, Washington, D.C.

[126] Rojas, R., 2021. Modelamiento de fallas principales en yacimiento Radomiro Tomic, Distrito Chuquicamata. In proceedings of the 7th International Conference on Geology and Mine Planning, Santiago, Chile.

[127] Romana, M., 1985. New adjustment ratings for application of Bieniawski classification to slopes. In Proceedings of the International Symposium on Role of Rock Mechanics, Zacatecas, Mexico (pp. 49-53).

[128] Rosenbaum, M.S., Rosen, L. and Gustafson, G., 1997. Probabilistic models for estimating lithology. Engineering and Geology 47: 43–55.

[129] Ryu, D. W., Kim, T. K. and Heo, J. S., 2003. A study on geostatistical simulation technique for the uncertainty modelling of RMR. Tunnel and Underground 13: 87–99.

[130] Sánchez, L.K., Emery, X., Séguret, S.A., 2019. 5D geostatistics for directional variables: Application in geotechnics to the simulation of the linear discontinuity frequency. Computers & Geosciences, 133, 104325.

[131] Sánchez, L. K., Emery, X., Séguret, S. A., 2021. Geostatistical modeling of Rock Quality Designation (RQD) and geotechnical zoning accounting for directional dependence and scale effect. Engineering Geology, 293, 106338.

[132] Santos, V., Da Silva, P.F., Brito, M.G., 2018. Estimating RMR values for underground excavations in a rock mass. Minerals 8(3): 78.

[133] Schoenberg, I.J., 1942. Positive definite functions on spheres. Duke Mathematics Journal, 9(1): 96–108.

[134] Schultz, R. A., 1996. Relative scale and the strength and deformability of rock masses. Journal of Structural Geology, 18(9), 1139-1149.

[135] Séguret, S.A., Guajardo, C., Freire, R., 2014. Geostatistical evaluation of fracture frequency and crushing. In: Castro, R. (Ed.), Proceedings of the 3rd International Symposium on Block and Sublevel Caving. Universidad de Chile, Santiago, pp. 280–288.

[136] Séguret, S.A., Guajardo, C., 2015. Geostatistical evaluation of rock quality designation & its link with linear fracture. In: Schaeben, H., Tolosana Delgado, R., van den Boogaart, K.G., van den Boogaart, R. (Eds.) Proceedings of IAMG 2015 - 17th Annual Conference of the International

Association for Mathematical Geosciences. Curran Associates, Red Hook, NY, pp. 1043–1051.

[137] Séguret, S.A., 2016. Fracturing, crushing, and directional concentration. Mathematical Geosciences, 48(6), 663-685.

[138] Séguret, S., Emery, X., 2019. Géostatistique de Gisements de Cuivre Chiliens – 35 Années de Recherche Appliquée. Presses des Mines: Paris, France, 266pp. [in French].

[139] Sen, Z., Kazi, A., 1984. Discontinuity spacing and RQD estimates from finite length scanlines. International Journal of Rock Mechanics and Mining Sciences & Geomechanics Abstracts, 21(4), 203-212.

[140] Singh, B., Goel, R., 1999. Slope mass rating (SMR). In: Rock mass classification: a practical approach in civil engineering. Elsevier science, Oxford, pp 171–183

[141] Skewes, M.A., Arevalo, A., Floody, R., Zuñiga, P., Stern, C.R., 2002. The giant El Teniente breccia deposit: hypogene copper distribution and emplacement. In: Goldfarb, R. (ed.), Global Exploration 2002 - Integrated Methods of Discovery. Society of Economic Geologist Special Publication, vol. 9, pp. 299–332.

[142] Skewes, M.A., Arevalo, A., Floody, R., Zuniga, P., Stern, C.R., 2006. The El Teniente megabreccia deposit, the world's largest deposit. In: Porter, T.M. (ed.), Super Porphyry Copper and Gold Deposits – A Global Perspective. Porter Geoscience Consultancy Publishing, Adelaide, Australia, pp. 83–113.

[143] Song, K.I., Cho, G.C., Lee, S.W., 2011. Effects of spatially variable weathered rock properties on tunnel behavior. Probabilistic Engineering Mechanics, 26(3), 413-426.

[144] Stavropoulou, M., Exadaktylos, G. and Saratsis, G., 2007. A combined three-dimensional geological/geostatistical numerical model of underground excavations in rock. Rock Mechanics and Rock Engineering 40(3): 213-243.

[145] Stein, M. L., 2007. Spatial variation of total column ozone on a global scale. The Annals of Applied Statistics, 1(1), 191-210.

[146] Terzaghi RD, 1965. Sources of error in joint surveys. Geotechnique 15(3): 287-304.

[147] Tomlinson, A.J., Blanco, N., 1997. Structural evolution and displacement history of the West Fault system, Precordillera, Chile: part II, Postmineral history. In Congreso Geológico Chileno No. 8, Actas 3.

[148] Tomlinson, A.J., Blanco, N., Dilles, J.H., Maksaev, V., Ladino, M., 2018. Carta Calama, Región de Antofagasta. Servicio Nacional de Geología y Minería, Carta Geológica de Chile, Serie Geología Básica No. 199: XX p., 1 mapa escala 1:100.000. Santiago.

[149] Vatcher, J., McKinnon, S.D., Sjöberg, J., 2016. Developing 3-D mine-scale geomechanical models in complex geological environments, as applied to the Kiirunavaara Mine. Engineering Geology, 203, 140-150.

[150] Wackernagel, H., 2003. Multivariate Geostatistics – An Introduction with Applications. Springer, Berlin, 387 pp.

[151] Wyllie, D. C., Mah, C., 2004. Rock Slope Engineering. CRC Press.

[152] Yardimci, A.G., Karpuz, C., 2018 Fuzzy approach for preliminary design of weak rock slopes in lignite mines. Bull Eng Geol Environ 77, 253–264.

[153] Xu, C.S., Dowd, P., 2010. A new computer code for discrete fracture network modelling. Computers & Geosciences 36(3): 292–301.

[154] Yadrenko, M. I., & Balakrishnan, A. V., 1983. Spectral Theory of Random Fields (Spektral'naja Teorija Sluchajnykh Polej). Optimization Software, Publications Division.

[155] Yaglom, A., 1987. Correlation Theory of Stationary and Related Random Functions, Vol. I: Basic Results; Vol. II: Supplementary Notes and References. Springer, New York.

[156] You, K. H., 2003. An estimation technique of rock mass classes for a tunnel design. Geotechnical Engineering 19: 319–326 (in Korean with English abstract).

[157] Zhang, L., Einstein, H.H., 2004. Using RQD to estimate the deformation modulus of rock masses. International Journal of Rock Mechanics and Mining Sciences, 41(2), 337-341.

[158] Zhang, W., Chen, J. P., Liu, C., Huang, R., Li, M., & Zhang, Y., 2012. Determination of geometrical and structural representative volume elements at the Baihetan dam site. Rock Mechanics and Rock Engineering, 45(3), 409-419.

[159] Zhang, L., 2016. Determination and applications of rock quality designation (RQD). Journal of Rock Mechanics and Geotechnical Engineering, 8(3), 389-397.

[160] Zhang, L., Xia, L., & Yu, Q., 2017. Determining the REV for Fracture Rock Mass Based on Seepage Theory. Geofluids, 2017.

[161] Zheng, J., Yang, X., Lü, Q., Zhao, Y., Deng, J., Ding, Z., 2018. A new perspective for the directivity of Rock Quality Designation (RQD) and an anisotropy index of jointing degree for rock masses. Engineering Geology, 240, 81-94.